

## TARGETED MOLECULAR IMAGING: A GUIDE TO COMBINATION THERAPY

APPROVED BY SUPERVISORY COMMITTEE

---

Orhan K. Öz, M.D., Ph.D. (Mentor)

---

Jer-Tsong Hsieh, Ph.D.

---

Padmakar Kulkarni, Ph.D.

---

Xiankai Sun, Ph.D.

---

Peter P. Antich, Ph.D. (Chairman)

## DEDICATION

I would like to acknowledge all the people who love me, support me and help me.

This has been a wonderful journey. Thanks to the Graduate Program in Radiological Sciences directed by Dr. Peter P. Antich for giving me such an opportunity to taste science, to pursue the dream of becoming a scientist. Thanks to my supervisor, Dr. Orhan K. Öz, for all the things I learned from you, from how to design and perform a simple experiment, to more importantly, how to think and work as a physician scientist. Thanks to Dr. Jer-Tsong Hsieh for his serious scientific attitude, patient advice and kind help, all of which will be beneficial my whole life. Thanks to Drs. Padmakar Kulkarni and Xiankai Sun as my committee members, thanks to Drs. Roderick (Roddy) McColl and Anca Constantinescu, and thanks to all the people I worked together with in Dr. Öz lab and Dr. Hsieh's lab for their help and support. Thanks to Ms. Beverley Huet for the help with statistics. Thanks to Ms. Kay Emerson, Ms. Jocelyn Chafouleas and Ms. Dorothy Smith for their help with my dissertation preparation. Thanks to Celeste Roney, Robert Bollinger, and Lan Jiang as my classmates. Thanks to Mai Lin for helpful discussions. Thanks to my sisters Hong Ren, Qin Ren and their families for all the support to myself and my parents. Without any of these, this mission would have been impossible. This work belongs to each who've ever helped me and supported me.

Finally, I wish to dedicate this dissertation to my love Peiying Liu and my parents, for the unselfish endless love and support.

TARGETED MOLECULAR IMAGING: A GUIDE TO COMBINATION THERAPY

by

GANG REN

DISSERTATION

Presented to the Faculty of the Graduate School of Biomedical Sciences

The University of Texas Southwestern Medical Center at Dallas

In Partial Fulfillment of the Requirements

For the Degree of

DOCTOR OF PHILOSOPHY

The University of Texas Southwestern Medical Center at Dallas

Dallas, Texas

December, 2006

Copyright

by

Gang Ren, 2006

All Rights Reserved

## TARGETED MOLECULAR IMAGING: A GUIDE TO COMBINATION THERAPY

Publication No. \_\_\_\_\_

Gang Ren, M.D., Ph.D.

The University of Texas Southwestern Medical Center at Dallas  
Graduation Year 2006

Supervising Professor: Orhan K. Öz, M.D., Ph.D.

Recombinant adenovirus is widely used to deliver genes for cancer gene therapy. Coxsackie and Adenovirus' Receptor (CAR) is the primary receptor for recombinant adenovirus. Little attention has been paid to determine CAR protein expression and promoter activity *in vivo*. This study tested the hypothesis that targeted molecular imaging of CAR could predict the tissue receptivity to viral infection and the response to treatment with histone deacetylases inhibitor (HDACi). To image CAR protein expression, human prostate cancer xenografts were established in nu/nu mice. The ability of iodinated anti-CAR intact, F(ab')<sub>2</sub> fragments and control F(ab')<sub>2</sub> fragments to distinguish CAR (+) tumors was tested by biodistribution, gamma camera scintigraphy and validated by western blot. Tumor susceptibility to infection

was tested with adenoviruses carrying the reporter  $\beta$ -galactosidase. To assess CAR promoter activity, a sodium iodide symporter (NIS) reporter construct containing the NIS open reading frame driven by the CAR promoter (CAR-NIS), was constructed by directional cloning. Tumor cell lines stably expressing CAR-NIS or empty vector were established. NIS protein function was assessed by intracellular accumulation of  $^{99m}\text{TcO}_4^-$  and mRNA level was tested by RT-PCR. The inductivity of the CAR promoter by HDACi *in vivo* was tested by imaging CAR-NIS tumors after administration of  $^{99m}\text{TcO}_4^-$  using a gamma camera. A replication-deficient recombinant adenovirus coding CAR-NIS was constructed to deliver the reporter construct to cells and tumors to permit radionuclide imaging. Radiolabeled anti-CAR F(ab')<sub>2</sub> fragments more effectively distinguished CAR(+) from CAR(-) tumors at early time points. Tumors with greater retention of radiolabeled anti-CAR showed higher levels of CAR protein expression by western blot and  $\beta$ -galactosidase activity after adenoviral infection. Stable CAR-NIS transfectants showed 16-fold to 180-fold increase of  $^{99m}\text{TcO}_4^-$  accumulation after HDACi treatment in PC3 prostate cancer cells or TCC bladder cancer cells, respectively ( $p < 0.001$ ). Ad-CAR-NIS effectively delivered the HDACi inducible CAR-NIS into target cells in a dose dependent manner. The transgene CAR-NIS expression was imaged *in vivo* using gamma camera scintigraphy. Molecular imaging approaches to image CAR protein expression and assess CAR promoter activity *in vivo* can predict tissue receptivity to adenoviral infection and have potential to direct combination of gene delivery and chemotherapy.

## TABLE OF CONTENTS

PRIOR PUBLICATIONS .....	x
LIST OF FIGURES .....	xii
LIST OF TABLES .....	xiii
LIST OF APPENDICES .....	xiv
CHAPTER ONE	
INTRODUCTION .....	1
1.1 Prostate Cancer and Bladder Transitional Cell Carcinoma .....	1
1.2 Gene Therapy .....	2
1.3 Epigenetic Control of CAR by HDAC Inhibitor .....	5
1.4 Molecular Imaging and Cancer Gene Therapy .....	8
1.5 Human Sodium Iodide Symporter (hNIS) .....	11
1.6 Radiotracers and Radionuclide Imaging Modalities .....	12
CHAPTER TWO	
IMAGING OF CAR PROTEIN EXPRESSION .....	15
2.1 Antibody Preparation .....	15
2.2 FACS Studies .....	18
2.3 Animal Model Establishment .....	19
2.4 Radioiodination and Quality Assurance (QA) .....	22
2.4.1 Radioiodination .....	23
2.4.2 Quality Assurance .....	25
2.5 Biodistribution Studies .....	33

2.6 Radionuclide Imaging of CAR Protein Expression .....	41
2.7 <i>In Vitro</i> Validation of Anti-CAR Imaging Studies .....	44
2.8 Detection of Tissue Receptivity to Adenovirus of <i>In Vivo</i> Tumor .....	45
CHAPTER THREE	
IMAGING OF CAR PROMOTER ACTIVITY .....	48
3.1 Directional Cloning (Construction of Reporter Molecule CAR-NIS).....	48
3.2 Transfection .....	50
3.3 HNIS Functional Assay .....	51
3.4 Drug Screening .....	55
3.5 Single Clone Screening.....	56
3.6 Animal Model Establishment .....	56
3.7 <i>In Vivo</i> Reporter Gene Imaging .....	56
3.8 <i>In Vitro</i> Validation of Reporter Gene Imaging .....	61
CHAPTER FOUR	
TARGETED RADIONUCLIDE IMAGING OF ADENOVIRUS DELIVERY (TRIAD) ...	63
4.1 Construction of Recombinant Adenovirus.....	63
4.1.1 Clone CAR-NIS into Shuttle Vector .....	63
4.1.2 Recombinant Adenovirus Construction.....	65
4.1.3 Recombinants Identification by PCR.....	66
4.2 Virus Amplification and Purification.....	66
4.3 Plaque Forming Assay .....	67
4.4 Functional Assay after Adenoviral Gene Delivery .....	68



4.5 Molecular Imaging of Adenoviral Delivery <i>In Vivo</i> .....	71
4.6 <i>In Vitro</i> Validation of TRIAD .....	76
4.7 <i>In Vitro</i> Combination Therapy .....	78
CHAPTER FIVE	
SUMMARY, CONCLUSIONS AND FUTURE DIRECTIONS .....	80
5.1 Imaging CAR Protein Expression .....	80
5.2 Imaging CAR Promoter Activity .....	81
5.3 Targeted Molecular Imaging of Adenoviral Delivery .....	82
APPENDIX A Abbreviations .....	86
APPENDIX B Additional Data for Imaging CAR Protein Expression .....	88
APPENDIX C Additional Data for Imaging CAR Promoter Activity .....	92
APPENDIX D Additional Data for TRIAD .....	94
Bibliography .....	97
Vitae	

## PRIOR PUBLICATIONS

Dwaine Braasch, Zain Paroo, Anca Constantinescu, Gang Ren, Orhan Öz, Ralph Mason and David Corey. “Biodistribution of phosphodiester and phosphorothioate siRNA” *“Bioorganic & Medicinal Chemistry Letter”*, Volume 14, Issue 5, 8 March 2004, Pages 1139-1143

Gang Ren, Padmakar Kulkarni, Rey-Cheng Pong, Mohammad Qurashi, Jer-Tsong Hsieh and Orhan K. Öz et al. “Molecular Imaging of CAR Protein Expression: Prediction of Tumor Sensitivity to Adenoviral Infection and Transgene Expression” *Submitted to Molecular Imaging and Biology, December, 2006.*

Padmakar V Kulkarni, Michael Bennett, Anca Constantinescu, Veera Arora, Mohammed Qureshi, Gang Ren, George Jacob, Peter P Antich, Ralph P Mason, Robert Parkey, and Orhan K Öz “Imaging lung clearance of  $^{99m}\text{Tc}$  YAC-1 tumor cells to assess natural killer (NK) cell function in mice” *Submitted to “Nuclear Medicine and Biology”, December, 2006.*

Gang Ren, Mohammad Qureshi, Xiankai Sun, Jer-Tsong Hsieh and Orhan K. Öz “Imaging Induction of CAR Promoter Activity” *Manuscript in Preparation, December, 2006.*

Abstracts:

G. Ren, A. Constantinescu., R. Pong, D. Xie, JT. Hsieh, O.K. Öz, *In Vivo* Imaging of Gene Therapy. *Mol Imaging and Biology*, 2004. 6(2): p. 82.

G. Ren, A. Constantinescu., M. Qureshi, P Kulkarni, R.P.Mason, R.W. Parkey, JT. Hsieh, O.K. Öz, Molecular Imaging Guided Urogenital Cancer Therapy. *J Nucl Med*, 2005. 46, Supple 2: p. 199.

G. Ren, A. Constantinescu., M. Qureshi, P Kulkarni, R.W.Parkey, JT.Hsieh, O.K. Öz, Targeted Imaging in Urogenital Cancer. *Mol Imaging*, 2005. 4(3): p.284-5.

## LIST OF FIGURES

Figure 1. <i>Histone Acetylation and Deacetylation</i> .....	6
Figure 2. <i>Schematic Diagram of IgG Structure</i> .....	16
Figure 3. <i>Antibody Preparations Anti-CAR vs. Control IgG1</i> .....	18
Figure 4. <i>FACS Analysis of CAR Expression</i> .....	19
Figure 5. <i>PC3 Growth Study</i> .....	21
Figure 6. <i>Animal Model</i> .....	22
Figure 7. <i>ITLC Strip</i> .....	26
Figure 8. <i>Autoradiograph of Labeled Purified Anti-CAR and Control Antibody</i> .....	28
Figure 9. <i>HPLC (Waters)</i> .....	29
Figure 10. <i>Immunoreactivity of <sup>125</sup>I labeled Anti-CAR F(ab')<sub>2</sub></i> .....	32
Figure 11. <i>Biodistribution of Radiolabeled Intact Anti-CAR</i> .....	34
Figure 12. <i>Biodistribution of Radiolabeled Anti-CAR F(ab')<sub>2</sub></i> .....	35
Figure 13. <i>Biodistribution of Radiolabeled Control F(ab')<sub>2</sub></i> .....	36
Figure 14. <i>Tumor/Blood for Radiolabeled Anti-CAR and Control Antibodies</i> .....	37
Figure 15. <i>Specificity of Radiolabeled Anti-CAR and Control Antibody Tumor Targeting</i> ...	37
Figure 16. <i>Representative In Vivo Anti-CAR Images</i> .....	42
Figure 17. <i>Representative Western Blot Detection of CAR</i> .....	45
Figure 18. <i>Western Blot Detection of CAR and <math>\beta</math>-galactosidase</i> .....	46
Figure 19. <i>In Vivo Transduction of Tumors According to CAR Expression Status</i> .....	46
Figure 20. <i>Schematic Diagram of pcDNA3 (A) and pBluescript II (B)</i> .....	49
Figure 21. <i>hNIS Functional Assay after HDACi (FK228) Treatment in PC3-CAR-NIS</i> .....	52
Figure 22. <i>hNIS Functional Assay after HDACi (FK228) Treatment in TCC-CAR-NIS</i> .....	53
Figure 23. <i>hNIS Functional Assay of HDACi Treatment</i> .....	55
Figure 24. <i>Representative Image of Reporter Gene Imaging</i> .....	59
Figure 25. <i>Transient Expression Assay</i> .....	65
Figure 26. <i>Plaque Forming Assay</i> .....	68
Figure 27. <i>Ad-CAR-NIS Infection (DU-145)</i> .....	69
Figure 28. <i>Representative Radionuclide Images of Local Ad-CAR-NIS Delivery</i> .....	72
Figure 29. <i>Representative Radionuclide Imaging of Systemic Ad-CAR-NIS Delivery</i> .....	74
Figure 30. <i>Images of Ad-CAR-NIS Delivery to HDACi Pretreated Tumor Bearing Mice</i> .....	76

## LIST OF TABLES

Table 1. <i>Comparison of Common Vectors</i> .....	3
Table 2. <i>Comparison of Molecular Imaging Modalities</i> .....	13
Table 3. <i>Properties of Different Targeting Antibodies</i> .....	17
Table 4. <i>Characteristics of Commonly Used Radioiodines</i> .....	23
Table 5. <i>ROI of Ad-CAR-NIS Delivery</i> .....	73

## LIST OF APPENDICES

APPENDIX A .....	86
APPENDIX B .....	88
APPENDIX C .....	92
APPENDIX D .....	94

# **CHAPTER ONE**

## **INTRODUCTION**

### **1.1 Prostate Cancer and Bladder Transitional Cell Carcinoma**

Prostate cancer (PCa) is the leading cause of cancer and the second leading cause of cancer-related death annually in men in the United States and Europe [1, 2]. Transitional cell carcinoma of the bladder (TCC) is the second most common malignancy of all male genitourinary cancers and the second leading cause of death of all the urinary cancer [1, 2]. Early prevention, detection and early treatment are goals for cancer management while advanced invasive and metastatic PCa and recurrent TCC still remain challenging [3-8]. No single treatment is effective for cure of both diseases and aggressive treatment of localized diseases does not necessarily improve survival, or improve the quality of life. Gene therapy is an alternative experimental approach for patients who are inoperable or unwilling to have surgery. PCa and TCC are both ideal types of diseases for gene therapy because of the regional anatomy of prostate and bladder, the existence of sensitive tumor diagnostic and prognostic markers such as PSA and PSMA, and the known genetic and epigenetic alterations in genes and gene expression associated with the progressions of PCa and TCC [9-13]. Together with other traditional therapies such as chemotherapy and radiation therapy, individualized combination strategies could improve the treatment efficacy of refractory urogenital cancer [3-23].

## 1.2 Gene Therapy

Human gene therapy is defined as the transfer of genetic material into target cells of a patient that will result in a therapeutic effect [24]. In cancer gene therapy, the goal is to effectively eliminate most cancer cells or sensitize cancer cells to therapies without doing serious damage to normal tissues and cells. In order to attain this goal, we need to deliver therapeutic genes efficiently and specifically to targets by using different vectors. What makes an ideal vector? An ideal vector system for use in cancer gene therapy would target only the desired cells within the target tissue. It would allow expression of a therapeutic amount of transgenic products for a certain time and ideally, the transgene expression could be regulated. So far viral and non-viral vectors have been used to introduce the therapeutic genes into specific human cell populations where the therapeutic product is required. Generally viral vectors have higher transduction efficiency than non-viral vectors. However, no single vector system seems to be optimal for all potential gene therapy applications [9, 24-29]. Currently, a number of gene therapy clinical trials for hormone refractory prostate cancer are undergoing Phase I/II clinical trial ([www.clinicaltrials.gov](http://www.clinicaltrials.gov)). One challenge we are facing now is how to achieve efficient and specific target gene delivery. Current viral vectors used for prostate cancer gene therapy are summarized in Table 1 [9, 29].



**Table 1. Comparison of Common Vectors**

<b>Vector</b>	<b>Advantages</b>	<b>Disadvantages</b>	<b>Insert Size</b>
Adenovirus	High transduction efficiency; Infect dividing and nondividing cells; High viral titers; High transgene expression; No insertional mutagenesis.	Transient transgene expression; Local tissue inflammation; Immunogenicity.	7.5 kb
Herpes Virus	Infects nondividing cells; No insertion mutagenesis; Moderate transduction efficiency;	Potential pathogenicity; Short duration of transgene expression;	10-100 kb
Adeno-associated Virus (AAV)	High transduction efficiency; Infects nondividing cells; No immunogenicity.	Needs helper Ad; Limited insert size; Potential insertional mutagenesis;	2-4.5 kb
Retrovirus (RVs)	Potentially long term transgene expression; Infects dividing cells; No immunogenicity.	Relative low transduction efficiency; Potential insertional mutagenesis;	6-8 kb
Lentivirus	Long term transgene expression; Infect nondividing cells;	Potential insertional mutagenesis; Low titers;	6-8 kb
Naked DNA	Easy preparations; non-toxic;	Poor efficiency.	Unlimited
Liposomes	Large insert size; non-toxic;	Poor efficiency; prone to degradation;	50 kb
DNA-protein complex	Large insert size; non-toxic;	Poor efficiency; short expression	50 kb

Adenoviruses are non-enveloped icosahedral viruses containing a 36 kb double-stranded DNA genome. Of 51 serotypes of adenoviruses [30], serotypes 2 and 5 have been most widely used as gene delivery vectors. Adenoviral vectors are among the most commonly used viral vectors for gene therapy, second only to retroviral vectors. Several characteristics make the adenoviral vector well suited for gene therapy: 1) It is ubiquitous; 2) It can enter both dividing and non-dividing cells and it tends to yield high levels of gene transfer; 3) It has low pathogenicity in humans; and 4) It will not be integrated into the host genome and will not cause any insertional mutagenesis. The major disadvantages of adenovirus are: 1) It has limited insert size; 2) It may stimulate a severe host immune response, especially when

administered repeatedly; and 3) It has transient transgene expression since it does not integrate into the host chromosome [9, 25, 31].

Adenoviral vectors are especially suitable for PCa and TCC since they are preferably taken up by carcinoma cells [9, 11-13, 32-34]. Their local use in prostate cancer has shown promising results in phase I clinical trials [14, 35, 36] and their systemic use in preclinical models of PCa has shown systemic efficacy and good safety [37-39]. However, one critical question for adenoviral gene therapy that remains to be addressed is how to evaluate the potential efficacy of therapy before and after initiation of gene delivery using noninvasive and real-time approaches, especially before the initiation of adenoviral gene delivery. By monitoring adenoviral gene delivery efficiency at real time not only can we predict a successful adenoviral gene delivery before the initiation of a gene therapy trial but also evaluate and improve the transduction efficiency, direct therapeutic strategy and avoid unnecessary host immune response caused by adenovirus mediated gene delivery.

There are two key steps for adenoviral infection: binding and internalization [32]. Vector binding to specific receptor on cells in target tissue is a rate-limiting step. The initial high affinity binding of adenovirus to the primary cellular receptor, Coxsackie and Adenovirus' Receptor (CAR) occurs via the globular knob domain of the trimeric fiber capsid protein. Subsequently, the interaction of Arg-Gly-Asp (RGD) peptide sequences in the penton base protein with secondary relatively low affinity host cell receptors integrins  $\alpha_v\beta_3$  and  $\alpha_v\beta_5$  allows receptor-mediated endocytosis of the virus. The virion then escapes from the endosome and localizes to the nuclear pore where its genome is translocated to the nucleus. It has been shown that the cDNA of receptor CAR encodes a typical immunoglobulin (Ig)-like

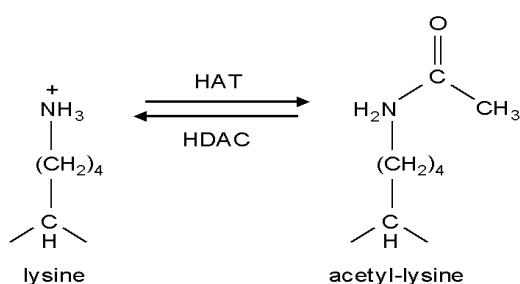
membrane protein with two Ig domains that interact with adenovirus fiber protein. In addition to the extracellular domain that is of most importance to the biology of CAR protein [40], CAR cDNA encodes a 22-amino acid transmembrane domain and a 107-amino acid intracellular (cytoplasmic) domain that has a putative tyrosine phosphorylation site that may be involved in its role as a cell adhesion molecule but not essential for adenovirus infection [41-43]. CAR is normally expressed in human brain, liver, lung, colon, small intestine, kidney, pancreas, colon, prostate and testis [26]. CAR has drawn a lot of attention because of its unique role in adenoviral gene delivery [44, 45]. Examination of CAR expression has been the subject of several studies. Most of these studies were done by using *in vitro* approaches such as RT-PCR and western blot. It was reported that CAR is differentially expressed with respect to tumor types or different grades of same tumor. It can inhibit tumor growth and it may be used to predict adenoviral gene therapy efficacy in cardiac diseases and cancers [31, 42, 46-51]. However, what is lacking is a noninvasive, real-time approach to assess this primary receptor CAR expression for adenoviral gene delivery *in vivo*. My research interest is to apply noninvasive approaches to qualitatively and quantitatively monitor the expression level of this potential marker for tissue receptivity of adenoviral gene delivery at both the protein and promoter activity levels in urogenital cancers *in vivo*. The accomplishment of the project will help to direct gene therapy at the interface of molecular imaging and viral gene therapy for solid tumors.

### **1.3 Epigenetic Control of CAR by HDAC Inhibitor**

It has been found that histone deacetylases inhibitor (HDACi) could effectively increase tissue receptivity to adenoviral gene delivery by epigenetically regulate CAR expression [52-

55]. During the development of cells of a multi-cellular organism, many genes are expressed in a specific spatiotemporal manner because the structures of gene are differentially regulated. The term "epigenetic" refers to the modification of gene structures leading to heritable changes in the expression of gene that do not involve mutations of the DNA sequence [56, 57]. Histone modification (acetylation or deacetylation) is one of basic molecular mechanisms that mediate epigenetic phenomena; the other is DNA methylation. It is closely related to chromatin structure which is important to many cellular processes such as transcriptional control in eukaryotes [58]. The fundamental structural unit of chromatin is nucleosome, which is composed of a histone octamer core (2 H2A, 2 H2B, 2 H3 and 2 H4) and bound DNA. The folding of DNA within the nucleosome can either promote or impede transcription depending on the structural context. Histone-histone and histone-DNA interactions are important for the initiation of transcription. The condensed chromatin structure can be changed to accessible structure which allows the initiation of transcription by inhibition of histone deacetylation. Figure 1 shows the histone acetyltransferases (HAT) and histone deacetylases (HDAC) control the histone modification.

**Figure 1. Histone Acetylation and Deacetylation**



Histone acetyltransferases (HAT) transfer an acetyl group to lysine to form  $\epsilon$ -N-acetyl lysine. Histone deacetylases (HDAC) mediate the reverse reaction.

The acetylation of the lysine residues in the histone tails alters the strength of the bond between the histone and DNA and loosens the contact between them because the acetylation neutralizes the positive charge on histone, which initiates the binding of RNA polymerase and transcriptional factors to the promoter region of any given gene thereby stimulating the initiation of transcription [59]. HDAC catalyses the reverse reaction and therefore suppresses gene transcription. HDACi inhibits the HDAC activity, which results in an increase in HAT activity leading to gene transcription. HDACis have shown their anti-tumor potential due to their ability to modulate transcription of certain tumor suppressor genes and to induce differentiation and apoptosis [60-63]. In addition, they may also suppress tumor progression, in part by inhibition of neovascularization [64, 65].

There are different categories of HDACis. Their chemical structures can be short chain fatty acid, hydroxamates, cyclic tetrapeptides or benzamides and their inhibition efficacies are different too [66]. Of them, FK228 is a fermentation product isolated from *Chromobacterium violaceum* [67]. It shows the most potent ability in terms of *in vivo* inhibitory effect on tumor growth of a prostate cancer xenograft model [68]. It also effectively increases tissue receptivity to adenoviral gene delivery by up-regulating CAR expression [52-55]. The combination of HDACis and other drugs such as ipriflavone could further induce CAR expression in bladder cancer [53].

In this project, prior to initiation of gene therapy, I proposed to use molecular imaging approaches to assess the CAR protein expression level and CAR promoter activity responding to the HDACi treatment *in vivo*. There have been no previous studies using an imaging approach to evaluate CAR expression at the transcriptional, translational or

functional level to predict the adenoviral delivery efficiency before initiation of adenoviral gene therapy. Since more and more studies have shown that epigenetic gene silencing plays an important role in all stages of different cancers including prostate tumorigenesis [52, 69-71], this approach may contribute to high throughput drug screening for suitable HDACi which has potential to reverse epigenetically silenced genes in prostate cancer. Additionally, this approach could also help to direct the combination of HDACi and other drugs for increasing adenoviral gene therapy efficacy in urogenital cancers by assessing CAR promoter activity and finally contribute to targeted molecular imaging guided combination therapy for urogenital cancer.

#### **1.4 Molecular Imaging and Cancer Gene Therapy**

Molecular imaging is different from traditional anatomical imaging. It is broadly defined as *in vivo* characterizations and measurements of biological events at cellular and molecular levels by using reconstructed images acquired from living animals [72-75]. Merging different disciplines such as cellular and molecular biology, genetics, biochemistry, biophysics and powerful imaging modalities, molecular imaging can be used to monitor the location, magnitude, and duration of specific gene expression, as well as to assess molecular events happening inside the body. The ultimate benefits are to clarify disease occurrence and mechanisms, direct therapeutics and predict prognosis *in vivo* at the cellular and molecular levels [76-82].

Cancer gene therapy is an experimental approach to introduce genetic materials into cancer cells in order to replace the defective genes, to stimulate immune response, to sensitize chemotherapy or radiation therapy, to pro-apoptosis or anti-angiogenesis. Molecular imaging

could play an important role in directing gene therapy by noninvasively imaging the gene delivery, the transgene expression, the regulation of transgene and the therapeutic effects produced by transgene expression at real time [37, 39, 83-86].

In this project, both antibody imaging (imaging the CAR protein expression) and reporter gene imaging (imaging the CAR promoter activity) were utilized to address current problems in urogenital cancer management and adenoviral gene delivery. The antibody imaging is straightforward. It could be used for imaging of protein expression. The limitations of antibody imaging include that the detectable signal could be limited by the expression level of target protein and each specific protein expression would need a specific antibody. An alternative approach to solve these is to image the target protein at the transcriptional level, in other words, imaging the promoter activity using reporter genes imaging approaches. Coupling different promoters and different reporter genes, reporter gene imaging can target different molecular events at the transcriptional level. The versatility of reporter gene largely broadens the choices of imaging modalities and imaging probes. The second half of this project focused on *in vivo* reporter gene imaging, to image CAR promoter activity.

The term reporter gene is referred as a gene with a readily measurable expression or activity that can be distinguished easily over the background of any given cells or tissues [72, 87]. In the field of *in vivo* molecular imaging, reporter gene imaging is based upon two major approaches. One is an intracellular enzyme based approach such as using herpes simplex virus type 1 thymidine kinase (HSV1-TK) or luciferase (LUC). The other is cell membrane receptor or transporter based reporter gene imaging, such as using human dopamine 2 receptor (hD<sub>2</sub>R) or human sodium iodide symporter (hNIS) [72, 78, 88, 89]. For an ideal

imaging reporter gene, specificity, sensitivity, dynamic range (half life), and a reliable assay are all important. Particularly for this project, the characteristics of an ideal reporter gene are: 1) It must be nontoxic; 2) It should not stimulate immune responses; and 3) The size of the reporter molecule should be small enough to fit into a delivery vehicle. For imaging the expression of this reporter gene, the contrast between target and background is the key while the image signal should correlate well with gene expression in both qualitative and quantitative ways. The choice of the promoter that drives the transcription of the reporter gene is also important. The choice of promoter will allow different transcriptional control over the expression of the reporter gene. Ideally, the use of tissue-specific promoters provides a way of selectively targeting the tumor cells and potentially maximizes tissue or tumor-specific radionuclide imaging and radionuclide therapy.

Studies have shown the feasibility of the PSA promoter to direct targeted prostate cancer therapy or the CEA promoter to drive human sodium iodide symporter (hNIS) expression and attain therapeutic effect in prostate cancer and colon cancer [90-93]. The CAR promoter was chosen for this project because reduced CAR promoter activity correlates well with CAR protein expression [71] and CAR promoter activity can be epigenetically upregulated by HDACi in urogenital cancer [53, 71]. Therefore, CAR promoter activity can be used to predict CAR protein expression level for potential adenoviral gene delivery efficiency and the response of HDACi treatment and combination therapy.



## 1.5 Human Sodium Iodide Symporter (hNIS)

HNIS was chosen as the reporter gene since it has many advantages that make it an excellent candidate. It was first found on the normal human thyroid follicular cell membrane [94]. Researchers also found hNIS expression in normal extra-thyroid tissues: salivary gland, gastric mucosa, choroids plexus, lactating breast tissue and placenta. hNIS can proportionally transport a variety of anions such as iodine radioisotopes and pertechnetate *in vivo* [89, 95, 96]. Using Tc-99m-pertechnetate ( $^{99m}\text{TcO}_4^-$ ) or radioiodine ( $^{131}\text{I}$ ,  $^{125}\text{I}$  or  $^{123}\text{I}$ ), gamma camera scintigraphy has been widely used to assess thyroid function and direct radioiodine therapy in the clinic. With the cloning of cDNA of human NIS and rat NIS, the molecular characterization and function of NIS have become clear [94, 97-99]. hNIS has been used for studying human telomerase promoter activity and endogenous p53-mediated transcription at transcription level [100, 101]. hNIS also has great potential in stem cell trafficking, *in vivo* monitoring of epigenetic regulation and transgenic animal models [102, 103]. Besides its imaging potential, hNIS has potential in therapy because of its ability to cause a cell to accumulate toxic radioisotopes such as  $^{131}\text{I}$ ,  $^{188}\text{Re}$  and  $^{211}\text{At}$ . Therefore, it may act as a "suicide gene". Both imaging potential and therapeutic effects after hNIS expression and radionuclide treatment have been shown in many different tumor cell lines, such as the thyroid cancer, prostate cancer, colon cancer, lung cancer, glioma, hepatoma, gastrointestinal and pancreatic neuroendocrine cancer, melanoma, breast cancer and ovarian cancer [38, 86, 104-117]. However, none of the studies have used hNIS as a reporter gene to screen HDACis' potency and finally use hNIS to develop a therapeutic strategy combining adenoviral gene delivery, chemotherapy and radionuclide therapy together.

In general, compared with other reporter genes, hNIS has a lot advantages as a gene reporter.

1) It is naturally and physiologically expressed; 2) It has widely available and inexpensive reporter probes such as  $^{99m}\text{TcO}_4^-$  and radioiodine that are already approved for clinical use by FDA; 3) Its function can be monitored by different modalities of imaging including planar gamma camera imaging, SPECT or PET ( $^{94m}\text{Tc}$ ,  $^{124}\text{I}$ ,  $^{76}\text{Br}$ ); and 4) Its potential for targeted radionuclide therapy, together with its suitable size for adenoviral delivery makes combination of gene therapy, radionuclide therapy, immunotherapy and chemotherapy possible. The proposed reporter molecule, hNIS driven by the CAR promoter, has its novelty in that it is inducible by HDACis and its potential for prognostic evaluation of combination of chemotherapy, radionuclide therapy and gene therapy. The proposed targeted imaging approaches, including the anti-CAR imaging and reporter gene CAR-NIS imaging, will provide a novel potential noninvasive assay system that permits evaluation of gene therapy efficacy and identification of promising drug candidates with clinically relevant anticancer activity. The ultimate goal is to extend these imaging approaches to direct combination therapy in cancer research.

## 1.6 Radiotracers and Radionuclide Imaging Modalities

Tracer techniques refer to utilization of radioisotopes for the purpose of detection of location and area where the isotope that is retained. The use of a radiotracer allows the detection of the administered radiolabeled agents at the pico-molar level (i.e. a single gamma ray can be detected), whereas CT and MRI are able to depict change in attenuation or signal intensity, respectively from administered agents at milli-molar (mM) or micro-molar ( $\mu\text{M}$ ) levels. Thus, the radionuclide techniques provide opportunities to probe biochemical events that are

not available to traditional radiological methods. In the clinic, short-lived radiopharmaceuticals are injected into a patient's blood stream in amounts of pico-molar concentrations thus having minimum effect on the process being studied. The half-life of these materials is between minutes to weeks. The camera then takes a time-exposure image of the pharmaceutical as it enters and concentrates in tissues or regions.

A gamma camera is an imaging device detecting the gamma rays emitted by radionuclide. It is the basis of more advanced modalities including Single Photo Emission Computed Tomography (SPECT) and Positron Emission Tomography (PET) [72, 74, 118]. The gamma camera is often equipped with collimators which are devices to allow only those rays traveled in a specified direction to be detected while others will be filtered.

Current commonly used molecular imaging modalities are compared in Table 2 [72].

**Table 2. Comparison of Molecular Imaging Modalities**

Modality	Imaging Sources	Spatial Resolution	Depth	Temporal Resolution	Sensitivity
PET	Gamma Ray (511 keV)	1-2 mm	No limit	10 <sup>sec</sup> -minutes	10 <sup>-11</sup> -10 <sup>-12</sup> M
SPECT	Gamma Ray	1-2 mm	No limit	minutes	10 <sup>-10</sup> -10 <sup>-11</sup> M
Optical Imaging (Bioluminescence)	Visible Light	3-5 mm	1-2 mm	seconds-minutes	10 <sup>-15</sup> -10 <sup>-17</sup> M
Optical Imaging (Fluorescence)	Visible Light or Near Infrared	2-3 mm	<1 mm	seconds-minutes	10 <sup>-9</sup> -10 <sup>-12</sup> M
MRI	Radiowaves	25-100 $\mu$ m	No limit	minutes to hours	10 <sup>-3</sup> -10 <sup>-5</sup> M
CT	X-ray	50-200 $\mu$ m	No limit	minutes	-
Ultrasound	Ultrasound	50-500 $\mu$ m	mm-cm	seconds-minutes	-

MRI, optical imaging and nuclear medicine (PET, SPECT and planar scintigraphy) techniques have been used to study endogenous and exogenous gene expression *in vivo* [72, 83, 87]. They differ in spatial resolution, temporal resolution, tissue penetration and

sensitivity. In order to image molecular events at cellular and molecular levels, more sensitive modalities are preferred. Optical imaging techniques are limited in tissue penetration which limits their translational ability from small animals to big animals to human. To image CAR protein expression and imaging CAR promoter activity by means of imaging hNIS function, we chose gamma camera planar scintigraphy since the planar images could be easily acquired in a short time and clinical gamma camera was widely available. The planar images can be acquired in a high throughput fashion while at the cost of detailed anatomical information and accuracy of quantification [72]. However, planar imaging could provide "proof of principle" images. The planar images can be easily extended to tomographic images with the help of dedicated SPECT and PET scanners, both of which could display more anatomical and functional information in both qualitative and quantitative fashions but take much more time for image acquisition.

## **CHAPTER TWO**

### **IMAGING OF CAR PROTEIN EXPRESSION**

Direct imaging of protein expression is to image the target protein by using an imaging probe that can be retained specifically and proportionally at the expression location of target proteins. Using radiolabeled monoclonal antibodies is a traditional way of direct imaging protein (antigen) expression. Since the approval of CEA scan by FDA in 1996 [119], many others have been approved such as Myoscint, Verluma, Proscint, Rituxan, Herceptin, Erbitux and Avastin for diagnostic or therapeutic purposes [120-127]. The success of radiolabeled RmcB (monoclonal anti-CAR antibody) may exert its role as an indicator for adenoviral gene delivery efficiency. The hypothesis of this part was that molecular imaging of CAR protein expression could be used to predict the adenoviral gene delivery efficiency.

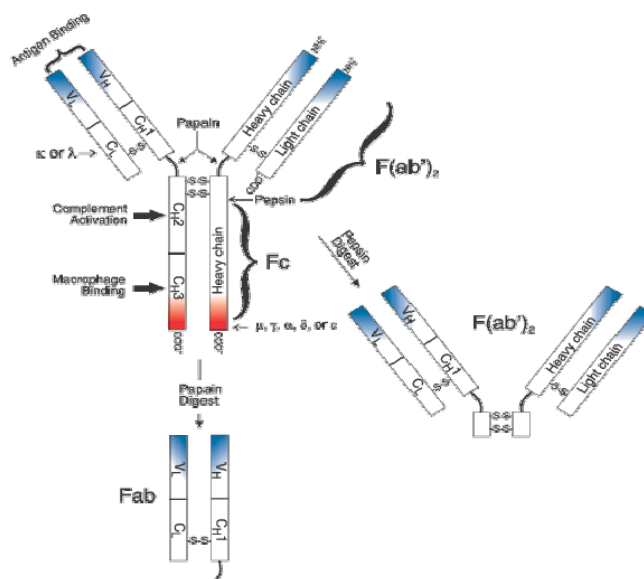
Many factors affect the detection of target protein in antibody imaging, such as the choices of targeting agents (intact or fragments of antibody), the properties of antibodies and antigens, the choices of radiolabel and radiolabeling procedures, the route and dosage of targeting agents administration, the time of imaging, and the processing of imaging data. Each is important in the optimization of direct antibody imaging. The details of preparation of radiolabeled anti-CAR were addressed as follows.

#### **2.1 Antibody Preparation**

For the antibody, antibody fragmentation provides diverse molecules for radiolabeling and subsequent studies. Antibody fragments are produced by enzymatic digestion of intact

antibody. They always have a shorter circulating half-life than the intact antibody does. Due to their smaller molecular weight, they can be filtered and excreted in increased amounts by the kidney; they can diffuse faster and deeper into tumors [128-130]. More importantly, the loss of Fc fragment also reduces binding by the Fc-receptor on hemopoietic cell surface. RmCB [131] is a monoclonal antibody of murine origin, if administered in human, the human anti mouse antibody (HAMA) could occur. HAMA will cause the loss of the target agent (antibody) and an allergic reaction [132, 133]. Most of the HAMA response is directly against the Fc portion of antibody, so the removal of Fc portion further decreases the possibility of occurrence of HAMA. In addition, both human-murine chimeric antibodies and humanized antibodies are undergoing investigation for possible solution to avoid HAMA [134-136] .

**Figure 2. Schematic Diagram of IgG Structure**



Whole (Intact) IgG antibody is composed of two heavy chains (Y shape) and two light chains. They are associated with each other by disulfide bonds. Papain could digest intact antibody into F(ab')<sub>2</sub> or even smaller Fab fragments.

Adapted from <http://www.probes.com/handbook/boxes/0439.html>

The choice of either intact antibody or antibody fragments (for example: F(ab')<sub>2</sub>, F(ab'), diabodies and minibodies) is based upon their own properties and the purpose of the study [129, 137]. F(ab')<sub>2</sub> fragments were chosen because of their relatively longer (compared with smaller fragments) half life and higher tumor uptake (Table 3 [129] ).

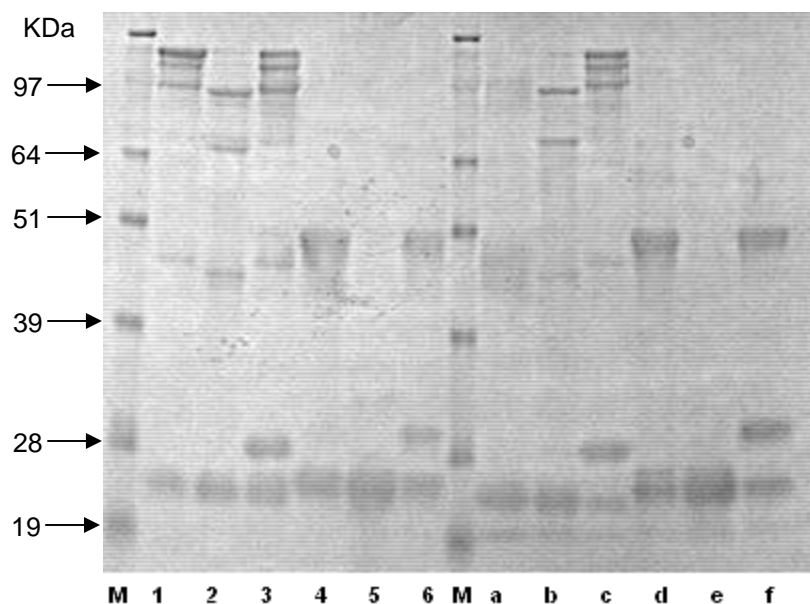
**Table 3. Properties of Different Targeting Antibodies**

	IgG	F(ab') <sub>2</sub>	Fab'	Diabody	scFv
Physical					
Molecular wt	150 K	100 K	50 K	40 K	20 K
Biological					
Immune effector function	Yes	No	No	No	No
t <sub>1/2</sub> , blood	2-3 d	1-2 d	4 h	<4 h	1 h
Target organ	Liver	Liver	Kidney	Kidney	Kidney
Tumor binding					
Uptake					
1 = highest, 4 = lowest	1	2	3	3	4
Duration					
1 = longest, 4 = shortest	1	2	3	3	4
Optimal accretion time	Days	Day	Hours	Hours	Hour

In our experiment, affinity purified RmcB, an anti-CAR monoclonal IgG, was obtained from Harlan (Madison, WI). The anti-CAR in PBS was further dialyzed against water to remove salts and then lyophilized. Five mg of the desalted anti-CAR was used for the preparation of F(ab')<sub>2</sub> fragment following the protocol of the F(ab')<sub>2</sub> Preparation Kit from Pierce (Rockford, IL). In brief, the antibody was resuspended in the elution buffer and then digested with immobilized ficin for 24-48 h at 37°C, depending upon the amount of intact antibody, followed by protein affinity column purification to remove undigested IgG and Fc fragments. The F(ab')<sub>2</sub> fragment, collected in the flow through from the column, was further desalted and concentrated using an Amicon Ultra (MW cut off: 30k) filtering device (Millipore Bedford, MA). For comparison, a control F(ab')<sub>2</sub> was prepared by the same protocol using isotype matched mouse IgG1 (Southern Biotech) which reacts with the hinge region of the heavy chain of human IgG1. The concentrated F(ab')<sub>2</sub> fragments were then applied to SDS

gel electrophoresis under both non-reducing and reducing conditions to confirm the purity before labeling (Figure 3).

**Figure 3. Antibody Preparations Anti-CAR vs. Control IgG1**



Lanes 1-3 Anti-CAR under non-reducing conditions (1 Intact, 2 F(ab')<sub>2</sub>, 3 Undigested Intact).  
 Lanes 4-6 Anti-CAR under reducing conditions (4 Intact, 5 F(ab')<sub>2</sub>, 6 Undigested Intact).  
 Lanes a-c Control IgG1 under non-reducing conditions (a Intact, b F(ab')<sub>2</sub>, c Undigested Intact).  
 Lanes d-f Control IgG1 under reducing conditions (d Intact, e F(ab')<sub>2</sub>, f Undigested Intact).  
 M: Molecular marker (Invitrogen®).

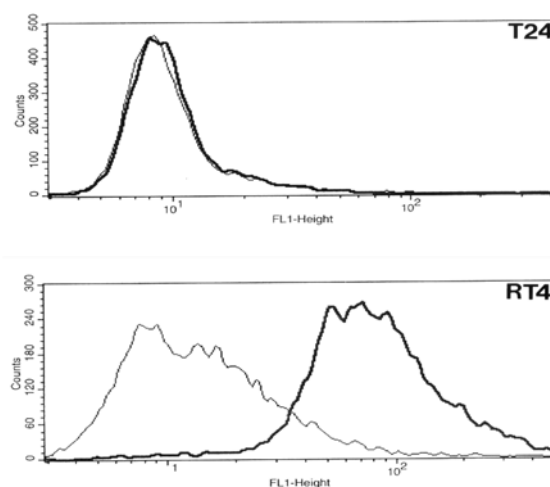
## 2.2 FACS Studies

Fluorescence Activated Cell Sorting (FACS) provides the "demographics" of heterogeneous mixtures of cell suspension and separates them into their different classes based upon intensity of fluorescence they emit when passing through a laser beam. To validate the efficacy of anti-CAR monoclonal antibody, membrane fluorescence staining was performed on a single-cell suspension with the use of anti-CAR monoclonal antibody [131] and fluorescein isothiocyanate (FITC)-conjugated secondary antibodies. Fluorescence-activated



cell scanning was performed with a dual-laser Vantage flow cytometer (Becton Dickinson, Mountain View, CA) delivering 50 mW at 488 nm with an Enterprise<sup>®</sup> air-cooled laser. Analysis was performed using LYSYS<sup>®</sup> II software (Becton Dickinson, Mountain View, CA). The positive population of cells was determined by gating the right-hand tail of the distribution of the negative control sample for each sample for each individual cell line at 1%. This setting was then used to determine the percentage of positive cells for each individual cell line [46, 47]. The anti-CAR antibody was shown to be effectively differentiating high CAR expression cells (RT4) from control cells (T24) shown in Figure 4. The same antibody was used for future studies.

**Figure 4. FACS Analysis of CAR Expression**



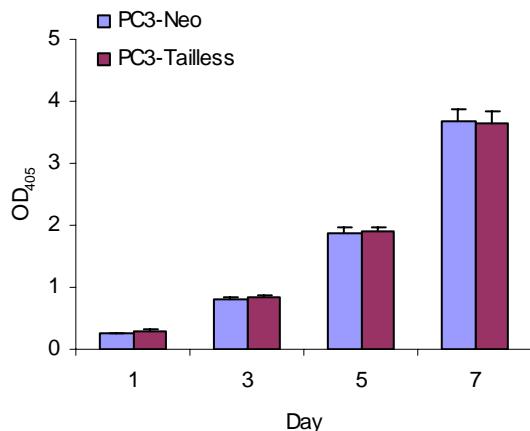
Using anti-CAR monoclonal antibody, the top figure shows no expression level difference between anti-CAR and control in T24 cell line that was proved to be no expression of CAR. The bottom figure shows higher expression of CAR expression in RT4 cell line.

### 2.3 Animal Model Establishment

All animal procedures were approved by and conducted in accordance with guidelines of the UT Southwestern Institutional Animal Care and Research Advisory Committee. To induce

human tumors in nu/nu mice (Harlan),  $1-2 \times 10^6$  cells per site were subcutaneously injected into both flanks of 6 to 8-week-old male hosts, one side with CAR (+) cells (PC3-Tailless), the other with CAR (-) ones (PC3-Neo). The cell lines were chosen because: 1) PC3 is a spontaneously established and commonly used cell line; 2) It represents a group of androgen independent human prostate cancer; 3) It does not secrete PSA which makes the diagnosis and prognosis of this group of PCa very difficult [138]; and 4) PC3-Tailless is CAR (+) cell line. It is a cell line stably transfected with CAR-Tailless, a mutant CAR gene with a deletion of the cytoplasmic domain, which is not essential for adenovirus binding, of CAR cDNA [43, 47, 139].

Prior to injection, an *in vitro* cell growth study was performed to confirm that both cell lines would grow at the same rate (doubling time is approximately 18 h). To do crystal violet cell growth assay [140], equal numbers of PC3-Neo cells and PC3-Tailless cells ( $5 \times 10^3$ /well) were plated in a 12-well plate. After 1, 3, 5, 7 days, cells (quadruplicate wells) were fixed with 1% Glutaraldehyde for 15 minutes and then stained with crystal violet for another 15 minutes. Two hundred  $\mu$ L Sorenson's solution [140] was used to elute the dye from the cells and then read optical density (OD) at 405 nm. The assay showed the two different PC3 derivatives grow at the same rate (Figure 5).

**Figure 5. PC3 Growth Study**

Equal numbers ( $5 \times 10^3$ ) of PC3-Tailless or PC3-Neo cells were plated in a 12-well-dish in quadruplicate. After 1, 3, 5, 7 days, cells were fixed and stained with crystal violet. The dye was eluted and OD was measured at 405 nm.

Subsequently, the same numbers of cells was mixed at 1:1 volume with Matrigel that provides basement membrane extracellular matrix for tumor growth (BD Biosciences) [141]. Once the tumors became palpable, the volume of subcutaneous tumors was measured weekly with a caliper, and tumor volume was calculated ( $\text{volume} = \text{length} \times \text{width} \times \text{height} \times 0.5236$ ) until the tumor volume was around  $30\text{-}40 \text{ mm}^3$ . Only animals with similar size CAR (+) and CAR (-) flank tumors (Figure 6) were used in biodistribution and imaging studies. The mice were subjected to sacrifice if the tumor grew to more than 10% of the body weight or the tumors started to ulcerate.

**Figure 6. Animal Model**



Human xenografts were established in nude mice. One flank bears PC3-Tailless cells, the other flank PC3-Neo cells. Tumors with similar size were chosen for imaging studies.

## 2.4 Radioiodination and Quality Assurance (QA)

The choice of radionuclide is essential for imaging of CAR expression. Ideally, for radiolabeling, the procedure should be simple, reliable and reproducible. For imaging purpose, radionuclides that won't interfere with normal physiology and with appropriate physical and biological half-life are preferred because the background activity is caused by non-specific uptake, normal distribution or metabolism of reporters or probes. Their radiation properties, including the decay mode, half-life, and emission energy, are all important. Currently, there are two major categories of radionuclide commonly used for radiolabeling of monoclonal antibodies: radiohalogens and radiometals. In contrast to radiometals, radioisotopes of iodine have the advantages of easy labeling procedures, well-known chemistry, and rather high specific activities [142-144]. More importantly, the versatility of iodine radioisotopes allows advanced imaging modalities such as SPECT ( $^{123}\text{I}$ ) and PET ( $^{124}\text{I}$ ). Because of the above reasons and their common availability, radioiodines were chosen to label the anti-CAR antibody and its fragments. Specifically,  $^{123}\text{I}$  ( $T_{1/2} = 13.2$  h) was chosen

to image the CAR expression repeatedly because of its preferential imaging properties. No matter what radioisotope is used for radiolabeling, the radiolabeled antibodies should retain their original protein integrity, stability and immunoreactivity.

#### 2.4.1 Radioiodination

Among the radioisotopes of iodine,  $^{125}\text{I}$ ,  $^{123}\text{I}$ , and  $^{131}\text{I}$  (Table 4) have the advantages of easy availability and relatively low cost. Iodination is accomplished by substitution or addition of iodine atoms into organic molecules. Basically there are two procedures to label compounds with radioiodine: 1) *The exchange reaction*. The compounds are initially labeled with non-radioactive (cold) iodine and then exchanged with radioactive iodine (hot) atoms. This procedure yields low specific activity compounds. Normally the compounds are heated to enable the exchange process. Thus, it is not practical for proteins.

**Table 4. Characteristics of Commonly Used Radioiodines**

Isotope	Half Life	Decay Mode	Major Emissions
I-123	13.2 h	EC, $\gamma$	159 keV
I-124	4.2 d	EC, $\beta^+$	690 keV
I-125	60 d	EC, $\gamma$	X-ray (98%)
I-131	8.0 d	$\beta^-$ , $\gamma$	364 keV (80%), 637 keV (9%)

2) *The substitution reaction*. In direct iodination, the substitution reaction takes place on the hydrogen in an aromatic ring of the tyrosine. The radioactive iodine must be oxidized to an eletrophilic reactive species. There are a variety of oxidizing agents with different characteristics such as iodine monochloride, chloramine T (N-choloro-4-methybenzene sulfonamide), IODOGEN<sup>®</sup> and lactoperoxidase. Though chloramine-T is a stronger

oxidizing agent than IODOGEN<sup>®</sup>, it may lead to more degradation to peptides or proteins [143, 145]. Bolton-Hunter agent (Appendix B1) is an indirect iodination method in which Bolton-Hunter reagents [146] are labeled with radioiodine and then attach to  $\epsilon$ -residue on lysine other than residue on tyrosine of the antibody and thus decrease the possibility of *in vivo* dehalogenation which happens on tyrosine. It is extremely useful for proteins without tyrosine group. However it is more time-consuming and has variable incorporation yields [142-145, 147, 148]. IODOGEN<sup>®</sup> (Appendix B1) was chosen for radioiodination of antibodies because 1) IODOGEN<sup>®</sup> is in solid phase; 2) It is stable; 3) It has high incorporation yields; and 4) The labeling procedure is relatively easy.

Briefly, the IODOGEN<sup>®</sup> tubes were prepared by plating on one inner side of 12  $\times$  75 mm glass tubes 20-50  $\mu$ g of IODOGEN<sup>®</sup> (1,3,4,6-tetrachloro-3a, 6a-diphenylglycoluril), from a 1 mg/mL solution in chloroform. After evaporation, the tubes were protected from light, capped and stored in an anhydrous environment at 4°C until use. The iodination of intact antibody or F(ab')<sub>2</sub> fragment was performed by adding on the opposite side of the IODOGEN<sup>®</sup> tube (the other side is IODOGEN<sup>®</sup> in solid phase): 25-50  $\mu$ L of 10 mM PBS pH 7.4, approximately 100  $\mu$ g of protein from a 1 mg/mL solution, and 1-2 mCi of the sodium radioiodine solution. The tube was then rotated for direct contact with the IODOGEN<sup>®</sup> spot, placed on ice, incubated for 4-5 minutes with occasional stirring. Free iodine was separated from the iodinated compound on a Sephadex G25 pre-packed column (Amersham Pharmacia Biotechnology). The desalted protein was eluted with 10 mM PBS. The radiolabeled product was collected as follows: After the void volume (about 2 mL), 10-20 fractions of 200  $\mu$ L each were eluted and collected. The highest activity fractions (labeled

protein) were pooled together (if necessary) for animal injection. Before pooling, the radiochemical purity of each fraction should be measured (addressed in following section). An alternative to purify the iodinated antibodies is to use Centricon (MW cutoff: 30k) from Millipore. Centrifuge was performed at 5,000 rpm (Hermle Z300K) for 60 minutes. 10mM PBS was used to elute the labeled antibodies. Radioactivity was measured with a dose calibrator (model CRC-15R, Capintec). The radiochemical yield, radioactive concentration and specific activity were calculated after radioiodination. The radiolabeled antibodies were also subjected to further quality assurance and then diluted to the desired activity and concentration in 0.1% BSA PBS for biodistribution and imaging studies.

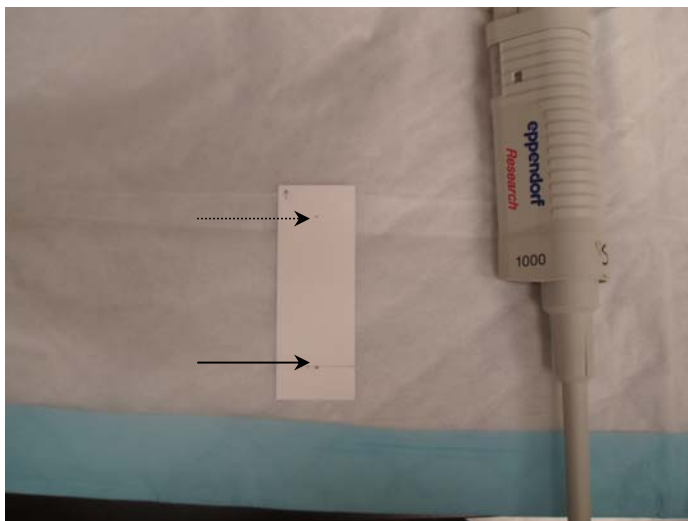
The major disadvantage of radioiodinated antibodies is that the radioiodine label could be rapidly dissociated (deiodination) from the antibodies because of intralysosomal proteolytic digestion caused by deiodinases. The mechanism of *in vivo* deiodination is not clear yet. One possibility is deiodinases may not distinguish radioiodinated tyrosine from thyroxine. The occurrence of dehalogenation may differ in different antibodies and different labeling methods [143, 145, 149]. Alternative approaches to minimize the degree of *in vivo* dehalogenation include to attach iodide to groups other than tyrosine such as Bolton-Hunter moiety as discussed above or to use radiometal labels such as indium-111 ( $^{111}\text{In}$ ), yttrium-90 ( $^{90}\text{Y}$ ) (therapeutic purposes only), rhenium ( $^{188}\text{Re}$ ,  $^{186}\text{Re}$ ) or copper ( $^{67}\text{Cu}$ ,  $^{64}\text{Cu}$ ) [143, 150-152]. These could be addressed in future studies.

#### **2.4.2 Quality Assurance**

The collected labeled intact or fragments of antibody were subjected to quality assurance (QA) using instant thin layer chromatography (ITLC), high-performance liquid

chromatography (HPLC), gel assay and radio-immunoreactivity assay.

**Figure 7. ITLC Strip**



Whatman<sup>®</sup> No.1 Filter Paper. One  $\mu\text{L}$  labeled antibody was spotted onto using pipette at the original point (solid arrow) and ran in 85% methanol until the solvent front reached the end-point shown by the dot arrow.

### ***Radiochemical Purity***

Radiochemical purity refers to the fraction of a given radioisotope (radioiodine) in the desired chemical form (radiolabeled antibody) [153]. It was analyzed by instant thin-layer chromatography (ITLC) using Whatman<sup>®</sup> No. 1 filter paper (Figure 7). The solid phase of ITLC is silica gel and the mobile phase (solvent) is 85% methanol in 10 mM PBS. ITLC strips were cut into pieces after running the strip in solvent and then the radioactivity in each small piece was measured with a  $\gamma$ -counter (Wizard Automatic  $\gamma$ -Counter, Perkin-Elmer). The amount of incorporated radioiodine is determined as follows: Percentage of  $I_{\text{bound}} = 100 \times (\text{activity of lower strip half}) / \text{total activity}$ . Alternatively, radiochemical purity could be analyzed by a radio-TLC scanner (Raytest, Shell). Radiolabeled species move with their unique retention factor ( $R_f$ ) values, defined as the distance traveled by the compound (radiolabeled antibody) divided by the distance traveled by the solvent. For radiolabeled anti-

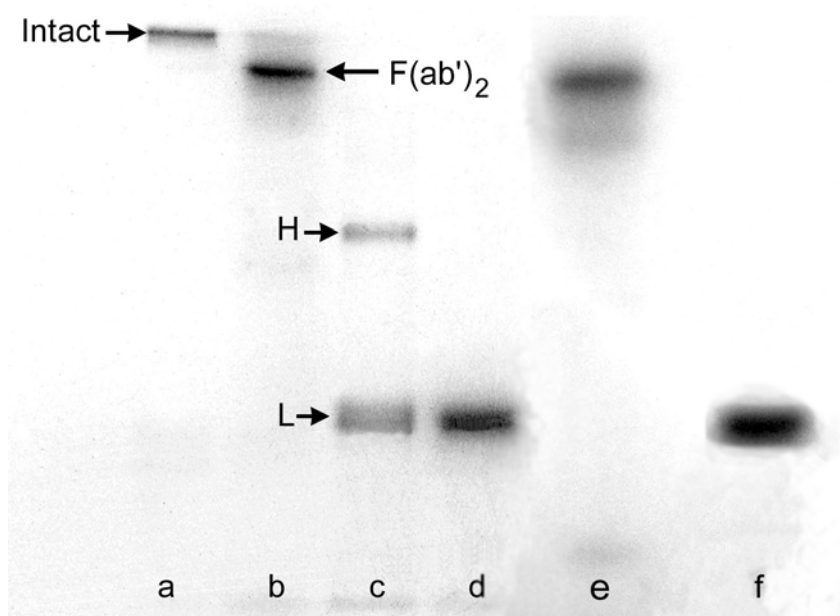


CAR antibodies, the labeled antibodies stayed at the point of application and free iodine migrated to the solvent front. The  $R_f$  value for labeled antibodies in this project was around 0. The radiochemical purity of the antibodies was found to be around 90% before purification and about 99% after purification.

### ***Protein Purity***

Electrophoresis separates proteins by their electrical charge and molecular weight. SDS-PAGE gels (Invitrogen) were run under both reducing and non-reducing conditions to exclude possible property changes of the radiolabeled antibody or antibody fragments (protein purity). The addition of 2-mercaptoethanol (2- $\beta$ ME) as a reducing agent is to break down all disulfide bonds in the antibody structure to generate smaller fragments and separate the fragments by their size (Figure 8).

**Figure 8. Autoradiograph of Labeled Purified Anti-CAR and Control Antibody**



Lanes a, b and e: Labeled proteins under non-reducing conditions. Lanes c, d and f: Labeled proteins under reducing conditions. Lanes a, c: Intact anti-CAR. Lanes b, d: Purified anti-CAR  $F(ab')_2$  fragment. Lanes e, f: Purified control  $F(ab')_2$  fragment. H=heavy chain. L=light chain.

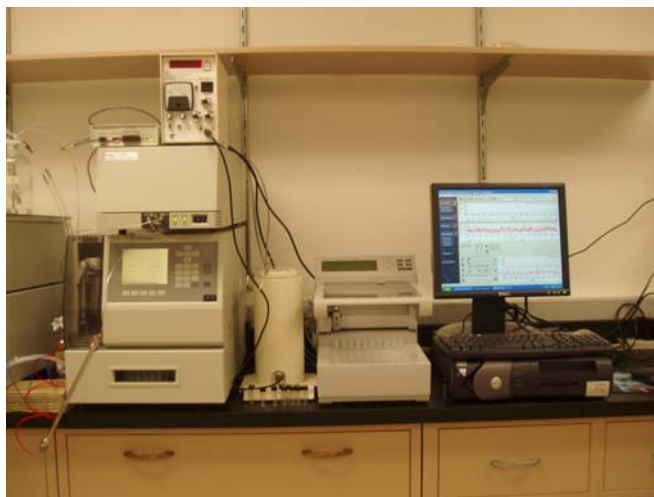
As expected, under non-reducing conditions, intact antibody migrated around 150 kD. The  $F(ab')_2$  fragment migrated around 100 kD and was smaller than the intact antibody (Figure 8 lanes a, b and e, respectively). Under reducing conditions the labeled intact antibody showed 2 bands, the larger being the heavy chain and the smaller faster migrating one, the light chain (Figure 8 lane c). The reduced  $F(ab')_2$  fragments migrated as a single 25 kD band (Figure 8 lane d, f).

### ***Serum Stability***

The serum stability of radioiodinated antibodies was tested by using radio-TLC and size-exclusion high performance liquid chromatography (SE-HPLC). Radio-TLC has been addressed in previous section. For SE-HPLC, 5-10  $\mu$ Ci radiolabeled antibodies were mixed

with 200  $\mu$ L mouse serum (Sigma) and incubated under room temperature and 37°C. At 0, 2, 24 and 48 h after incubation, a 25  $\mu$ L aliquot of serum sample was taken out for SE-HPLC analysis using a BioSuite 450 column (Waters). The HPLC system (Waters, Figure 9) consists of pump control separation module (Model 2690), a programmable photodiode array detector (Model 996), multi-wavelength UV absorbance detector (Model 490), a radio detector (Shell) and an auto- sampler (Model 717).

**Figure 9. HPLC (Waters)**



Samples (20  $\mu$ L) were introduced via an auto-injector with a 20  $\mu$ L loop and the chromatographic methods were carried out at ambient temperature. Data acquisition and analysis were performed using the Empower<sup>®</sup> chromatography software (Waters Association), which communicated with the HPLC equipment. The column was equilibrated for 30 minutes before running each sample. Time point 0 was used as control. Labeled antibodies in PBS, unlabeled antibodies and free iodine-125 ( $\text{Na}^{125}\text{I}$ ) were also used as controls. Fractions were collected every one minute for 30 minutes. Elution conditions were as follows: flow rate = 0.5 mL/min, solvent: 0.1 M Sodium Phosphate Buffer + 0.05%

Sodium Azide, UV detection= 280 nm. The fractions were counted by gamma-counter and the counts per minutes were plotted as a function of retention time. Under these parameters, the retention time of free  $^{125}\text{I}$  was approximately 27 minutes and the  $^{125}\text{I}$  labeled intact anti-CAR and  $\text{F(ab')}_2$  fragments were approximately 19 and 21 minutes respectively. After 48 h incubation at  $37^\circ\text{C}$ , the radiolabeled anti-CAR antibodies were not degraded in mouse serum shown by unchanged retention time as labeled antibodies in PBS. Simultaneously, radio-TLC showed after incubation in mouse serum, the labeled antibodies kept their radiochemical purity around 99%. There was no clear dehalogenation of radioiodinated anti-CAR or its  $\text{F(ab')}_2$  fragments in the mouse serum under  $37^\circ\text{C}$  *in vitro*. However, the stability could be different *in vivo* because the amount of dehalogenase may vary in circulation. This was further discussed in biodistribution studies.

### ***Immunoreactivity***

The measurement of immunoreactivity was tested by Lindmo's assay. This assay is based upon the principle that the fraction of immunoreactive radiolabeled antibody is accurately determined by linear extrapolation to binding at infinite antigen excess. The immunoreactive fraction "r" is determined as the inverse of the intercept value [154]. In following equations, [B] is the concentration of bound antibody; [F] is the concentration of free antigen; [T] is the total concentration of antibody.

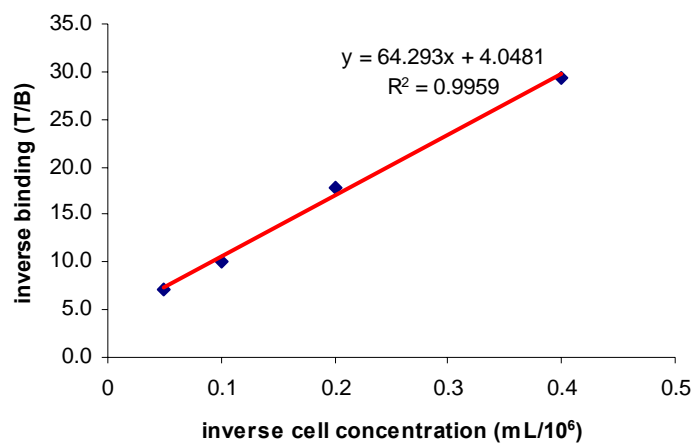
$$[B] = Ka [F][rT - B]$$

$$[T]/[B] = 1/r + 1/rKa[F]$$

To test immunoreactivity, different concentrations of CAR (+) PC3-Tailless or CAR (-) cells PC3-Neo in 1.0 mL of 1% BSA in PBS were incubated (Started with  $2 \times 10^7$  cell/mL, 1:1

serially diluted to  $3.125 \times 10^5$  cell/mL) with labeled ( $^{125}\text{I}$  labeled  $\text{F(ab')}_2$ ) and /or unlabelled antibody. CAR (-) cells were used as controls. Non-labeled Anti-CAR  $\text{F(ab')}_2$  was used for determining the specificity of labeled antibody. The cells were kept in suspension through moderate rotation (50 rpm/min) and incubated at room temperature for 2 h (The time and temperature were determined by a series of separate experiments comparing different temperatures:  $4^\circ\text{C}$ ,  $37^\circ\text{C}$  and room temperature and different incubation times: 1, 2, 4 and 24 h). Cells were harvested by centrifugation followed by 3 washes with media to remove unbound antibody. Supernatant and cell pellets were counted separately for radioactivity using a  $\gamma$ -counter. The specific binding percentage was calculated and the data was plotted using the inverse binding (T/B) versus inverse cell concentration ( $\text{mL}/10^6$ ). The linear extrapolation was used to decide the immunoreactive fraction of radiolabeled anti-CAR  $\text{F(ab')}_2$ . The results showed that the labeled anti-CAR  $\text{F(ab')}_2$  could specifically bind to CAR expressing cells. This was shown by a blocking study (Appendix B2) in which the binding of labeled antibody to cells was blocked when cells were pretreated with unlabeled anti-CAR  $\text{F(ab')}_2$  was blocked. Somewhat disappointingly, the immunoreactive fraction "r" was calculated to be 0.25 (Figure 10).

**Figure 10. Immunoreactivity of  $^{125}\text{I}$  labeled Anti-CAR  $\text{F(ab')}_2$**



Up to  $2 \times 10^7$  PC3-Tailless cells were incubated with anti-CAR  $\text{F(ab')}_2$  under room temperature for 1 hour and then washed with PBS 3 times. Cell pellets were collected and counted to determine the binding ratio between total applied (T) and specific binding (B). Data were then plotted as inverse binding (T/B) vs. inverse cell concentration (mL/10<sup>6</sup>). The intercept of y axis equal=  $1/r$ .  $r=0.25$ .

The reasons could include:

- i. The IODOGEN<sup>®</sup> procedure affected the protein property. Though the SDS-PAGE gel showed good protein integrity, it could be that the integrity of the radiolabeled protein is good but the radiolabel is on critical residues for binding to the antigen. To further exclude this, Lutetium-177 ( $^{177}\text{Lu}$ )-labeled  $\text{F(ab')}_2$  was used to take the place of radioiodine label and test the immunoreactivity since  $^{177}\text{Lu}$  does not label the tyrosine residues. The results showed the "r" was even lower.
- ii. The specific activity is too low? In this case, the unlabeled antibody in the preparation would take over the labeled antibody and saturate most the binding site. In order to exclude this, different radioiodination approaches could be used in order to improve the specific activity.
- iii. "Antigen excess" status had never been attained. This will cause systematic errors in evaluating the immunoreactivity by using Lindmo's assay [155]. Further studies are needed to address the binding sites per cell in order to apply other

mathematical model to calculate the immunoreactivity without attaining “antigen excess” status [155-158].

- iv. Alternative approaches to address immunoreactivity are needed, including using radioiodinated antibodies to perform a FACS study and then compare with the FACS study of unlabeled counterparts.

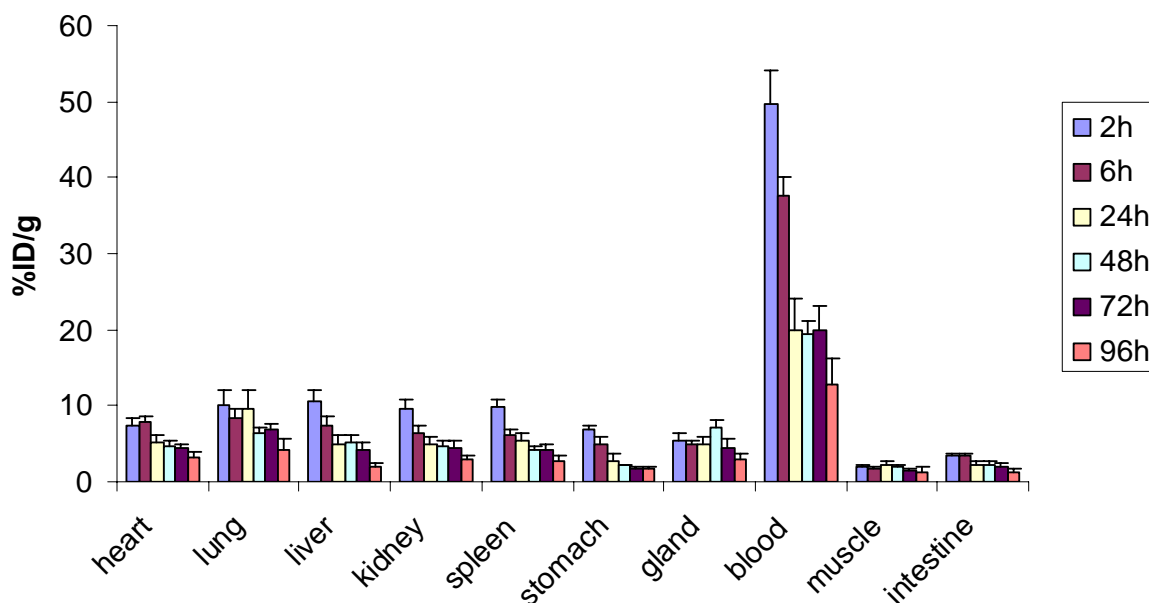
However, since it is true if the immunoreactivity is low, the labeled antibody could behave very differently in targets, low immunoreactive antibodies would suffer from a more rapid clearance from the tumor and much slower clearance rates in non-tumor organs [159]. These could be further proved by biodistribution and imaging studies. To do biodistribution studies, about 5  $\mu\text{Ci}$  of radiolabeled ( $^{125}\text{I}$ ) antibody (either anti-CAR or control antibody) was intravenously administered to each mouse for biodistribution experiments while approximately 100  $\mu\text{Ci}$  of  $^{123}\text{I}$  radiolabeled antibody was administered for imaging. In any particular experiment the dose/animal was the same for each animal.

## 2.5 Biodistribution Studies

Six to eight weeks old athymic mice bearing CAR positive (CAR (+)) and CAR negative (CAR (-)) tumors on either flank were anesthetized with avertin (4.0 mg/10 g) by intraperitoneal injection. Subsequently, labeled intact ( $^{131}\text{I}$ ) and F(ab')<sub>2</sub> fragment ( $^{125}\text{I}$ ) of anti-CAR were intravenously administered simultaneously for a paired biodistribution study which allows the direct comparison of intact and F(ab')<sub>2</sub> fragment in the same animal [160]. At various time points after injection, the blood, major organs, and tumors were harvested, weighed, and activity was counted in a PerkinElmer 1470  $\gamma$ -counter in the appropriate channel. Target to background ratios were calculated as the ratio of tumor activity (%ID/g)

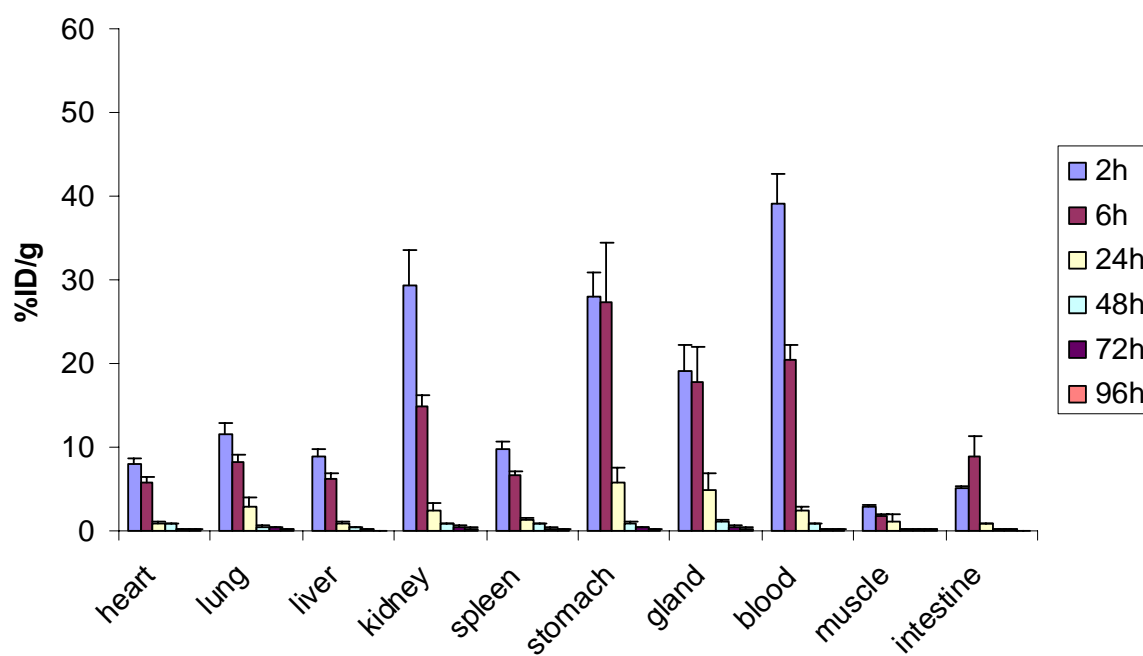
divided by the activity in the blood (%ID/g). The specificity, that is, the ability to discriminate CAR (+) and CAR (-) tumors by the labeled anti-CAR antibody, was quantified as the ratio [%ID/g CAR (+) tumor] / [%ID/g CAR (-) tumor]. For comparison, 5  $\mu$ Ci of labeled F(ab')<sub>2</sub> fragment generated from control mouse IgG1 were injected into 36 mice bearing same tumors and the same organs were collected at the same time points as for labeled anti-CAR biodistribution in a control biodistribution study.

**Figure 11. Biodistribution of Radiolabeled Intact Anti-CAR**



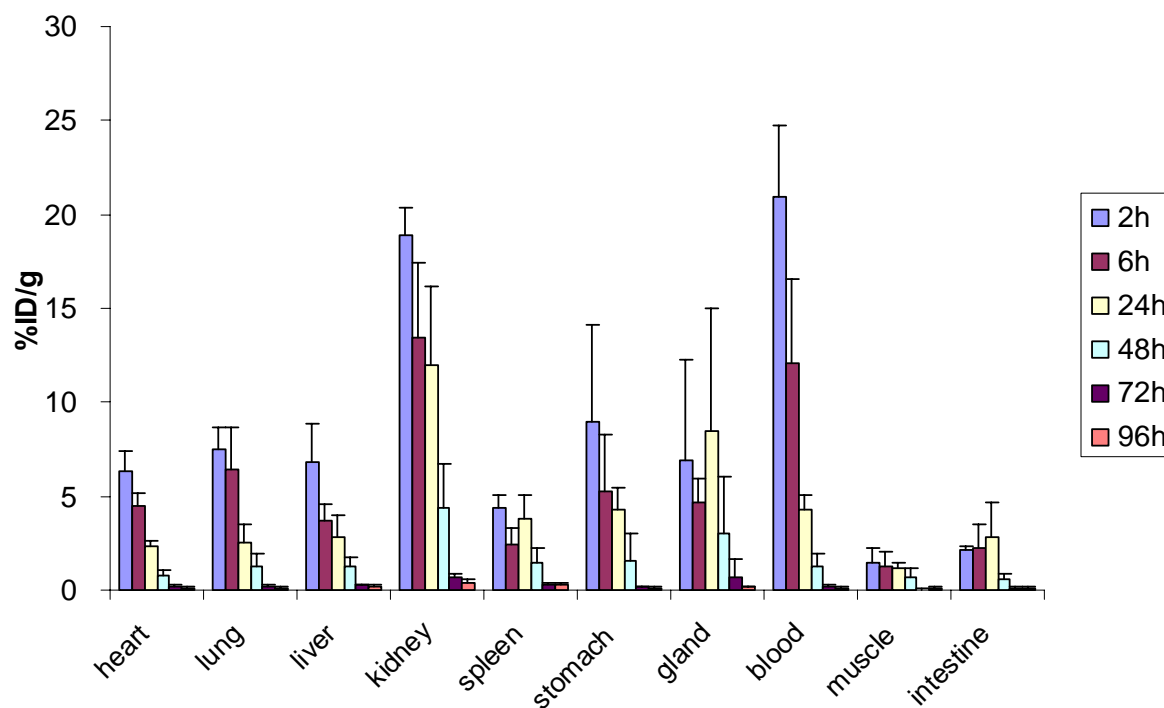
<sup>131</sup>I labeled intact Anti-CAR was i.v. injected and major organs were collected at different time points. Activity was counted and normalized with standard and organ weight for %ID/g.



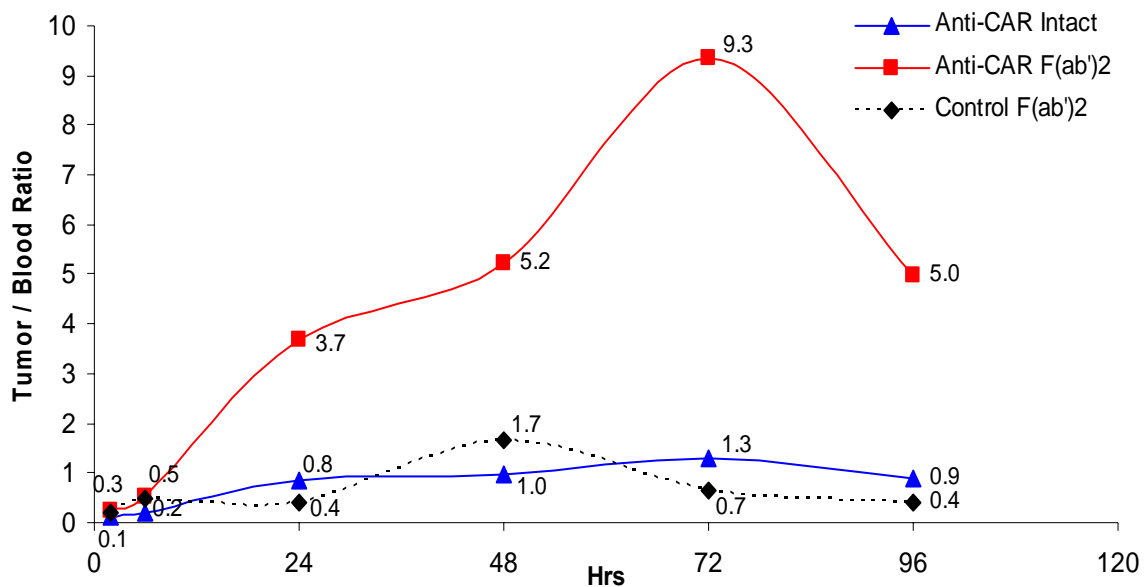
**Figure 12. Biodistribution of Radiolabeled Anti-CAR F(ab')<sub>2</sub>**

<sup>125</sup>I labeled Anti-CAR F(ab')<sub>2</sub> was i.v. injected and major organs were collected at different time points. Activity was counted and normalized with standard and organ weight for %ID/g.

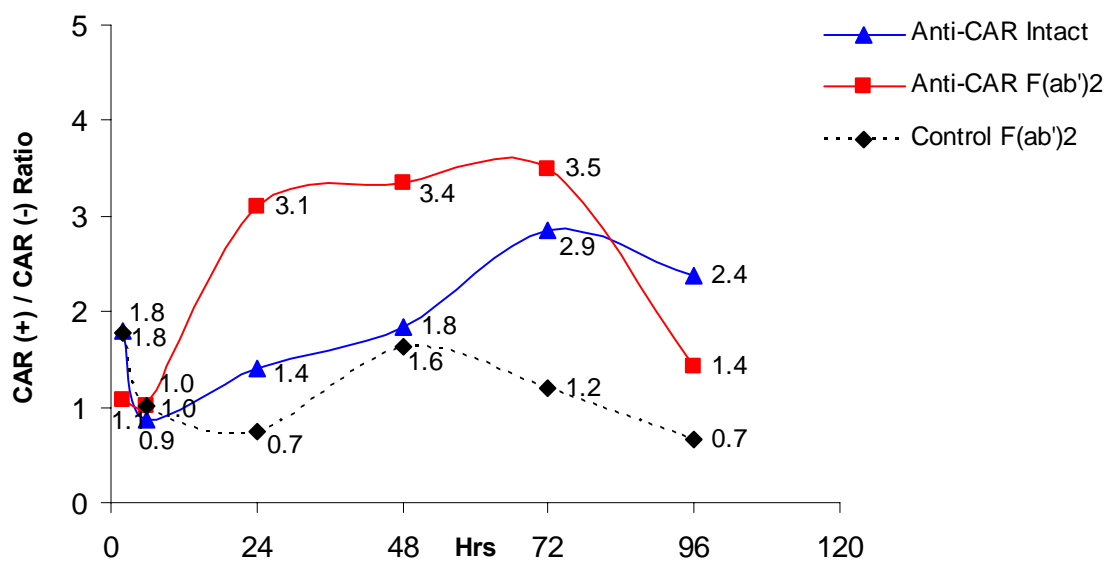
**Figure 13. Biodistribution of Radiolabeled Control  $F(ab')_2$**



$^{125}\text{I}$  labeled control  $F(ab')_2$  was i.v. injected and major organs were collected at different time points. Activity was counted and normalized with standard and organ weight for %ID/g.

**Figure 14. Tumor/Blood for Radiolabeled Anti-CAR and Control Antibodies**

Activity in CAR (+) tumors and blood was determined as a function of time for each form of radiolabeled antibodies. Tumor to blood ratios are shown. Error bars were omitted for clarity.

**Figure 15. Specificity of Radiolabeled Anti-CAR and Control Antibody Tumor Targeting**

Activity in CAR (+) and CAR (-) tumors was determined as a function of time for each form of radiolabeled antibody. The ratio of activity in CAR (+) / CAR (-) are shown. Error bars were omitted for clarity.

The results of biodistribution of intact anti-CAR, its F(ab')<sub>2</sub> fragment are shown in Figure 11-15. The data were analyzed by ANOVA. Based upon these results, intact anti-CAR or its fragments can be used for assessing *in vivo* CAR protein expression but with different pharmacokinetics.

For heart, lung, kidney, stomach, glands (salivary and thyroid glands), liver, a significant interaction between antibody form and time was observed ( $p < 0.0001$  for all organs). This interaction indicates that there is a different time course for each antibody form, pointing to higher activity or slower clearance for the intact form. Both forms of the antibody showed blood pool activity at 2 h and 6 h higher than organs (Figure 11, 12). The radiolabeled intact antibody cleared from the blood pool slower than the labeled fragment (Figure 11, 12, Appendix B3,  $p < 0.0001$  for form vs. time interaction). This higher blood pool activity was also reflected in the higher heart and lung activity. Starting at 24 h post-injection, intratumoral activity, expressed as %ID/g, was higher in CAR (+) tumors irrespective of form of the anti-CAR (Appendix B4). For both intact anti-CAR and anti-CAR F(ab')<sub>2</sub>, the %ID/g in CAR(+) versus CAR (-) was significantly different ( $p < 0.0001$  for fragment,  $p = 0.0002$  for intact, ANOVA).

The ability of radiolabeled antibodies to localize CAR (+) tumors was determined by ratio between target (tumors) and background (blood) (Figure 14). The anti-CAR fragments produced higher target to background (%ID/g tumor to %ID/g blood) ratios at all time points, most strikingly from 24-96 h. For example, at 24 h the ratio was 3 versus only 1 for the radiolabeled intact antibody (Figure 14). The ratio peaked to a value of 9 at 72 h post-

injection. The specificity of radiolabeled antibody localization into CAR (+) tumors was determined using the CAR (-) tumors as controls (Figure 15).

In the biodistribution study of the control Ab, the general pattern of  $^{125}\text{I}$  labeled control antibody  $\text{F(ab')}_2$  was similar to that of anti-CAR  $\text{F(ab')}_2$  as shown by tumor/blood ratio and  $\text{CAR}(+) / \text{CAR}(-)$  (Figure 13-15). There was no statistically significant difference between  $\text{CAR}(+)$  and  $\text{CAR}(-)$  tumors ( $p > 0.05$ ) for %ID/g of this control antibody fragment. The tumor / blood ratio for control  $\text{F(ab')}_2$  fragments peaked at 1.7 at 48 h post-injection and gradually declined. The  $\text{CAR}(+) / \text{CAR}(-)$  ratio was significantly lower than the ratio for anti-CAR  $\text{F(ab')}_2$  ( $p < 0.01$ ) at 24 h post-injection and later.

The tumor targeting ability of different antibodies was compared in biodistribution studies. In the study, the %ID/g of radiolabeled anti-CAR  $\text{F(ab')}_2$  was higher in both  $\text{CAR}(+)$  and  $\text{CAR}(-)$  tumors (Appendix B3). Furthermore,  $\text{F(ab')}_2$  cleared more rapidly than intact (Appendix B4). This more rapid clearance was primarily responsible for the superior (9:1 vs. 1.3:1) tumor / blood ratio at 72 h post-injection observed for  $\text{F(ab')}_2$  fragment of anti-CAR. Actual %ID/g was higher for the intact antibody. Antibody fragments also tend to be cleared more readily by the kidneys and show less hepatic uptake (Figure 12, 13). The constant blood activity in animals injected with labeled intact anti-CAR indicates tumor visualization over background would not change much over this time interval. On the other hand, the lower blood pool activity for radiolabeled anti-CAR fragments is beneficial for imaging using short-lived radioisotopes and for improved conspicuity of lesions. More importantly, the blood levels at 24 h were low enough to permit imaging with  $^{123}\text{I}$  labeled anti-CAR  $\text{F(ab')}_2$  fragments. Taken together, fragments have higher tumor/blood (T/B) ratios than intact

antibody because of rapid clearance from circulation (decreased blood activity) and improved penetration.

The specificity of different antibodies was also compared in above studies. The %ID/g for either CAR (+) or CAR (-) tumors showed the antibody form\*time interaction was significant for anti-CAR, indicating the difference between intact and F(ab')<sub>2</sub> was not the same across time points ( $p < 0.0001$  for both tumor types). For example at 2 h and 6 h, the activity in CAR (+) was higher for F(ab')<sub>2</sub>, but for all other time points the activity was higher for the intact antibody irrespective of tumor type. However, from 24 h to 72 h the %ID/g values of intact anti-CAR for CAR (-) tumors remain nearly constant (Figure 11) suggesting this activity was due to constant blood levels. On the other hand, the %ID/g values increased with time for the CAR (+) tumors, indicating specific localization. Despite the lower %ID/g at the later time points compared with intact antibody, the more rapid blood clearance observed in the case of the anti-CAR F(ab')<sub>2</sub> fragments yielded higher CAR (+)/CAR (-) ratios, indicating this form of anti-CAR may be the superior imaging agent over the time frame of the study. The ability of anti-CAR F(ab')<sub>2</sub> to distinguish CAR (+) from CAR (-) tumor was especially superior to intact anti-CAR at 24 h and 48 h ( $p < 0.001$ ). The ID%/g of control F(ab')<sub>2</sub> was significantly different from anti-CAR F(ab')<sub>2</sub> at all time points (Appendix B3) which indicated the importance of antibody specificity in tumor localization and excluded the possibility that the antibody distribution difference was due to the difference of blood flow in both tumors.

Additionally, in our study at early time points (2 and 6 h), the kidney activity for anti-CAR F(ab')<sub>2</sub> was significantly higher than that for intact antibody ( $p < 0.01$ ), indicating the need for

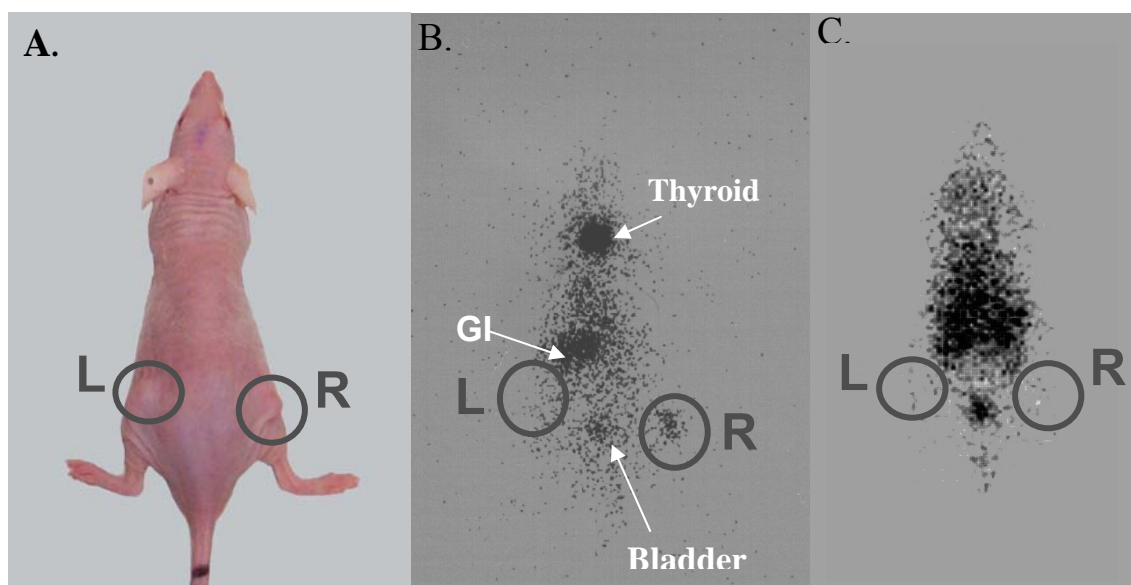
appropriate procedures to accelerate the wash-out from the kidney in order to decrease the renal toxicity for future preclinical studies.

In summary, based upon biodistribution studies, the anti-CAR F(ab')<sub>2</sub> showed superior tumor/blood ratios though actual tumor uptake (%ID/g) was lower than intact anti-CAR. Limited by technical difficulties, the tumor / prostate ratio was not calculated. This could be an important parameter when translating anti-CAR imaging approaches to orthotopic animal models and human studies.

## **2.6 Radionuclide Imaging of CAR Protein Expression**

A gamma camera was used for radionuclide imaging of CAR protein expression. In our study, planar scintigraphic imaging was performed 24 h after injection of <sup>123</sup>I labeled F(ab')<sub>2</sub> of either anti-CAR or control F(ab')<sub>2</sub>. A 20-30-minute image was acquired on one head of a Toshiba 9300 triple head clinical gamma camera equipped with different (depending on radioisotope used) collimators. A 20% window was centered at different energy peak depending on different radioisotopes (159 keV for <sup>123</sup>I). Data were collected in a 256 by 256 matrix; appropriate zooming and orientation were used for better imaging display. The xenografts were excised and counted *ex vivo* by a gamma counter after imaging sessions.

**Figure 16. Representative *In Vivo* Anti-CAR Images**



One hundred  $\mu\text{Ci}$   $^{123}\text{I}$  labeled anti-CAR  $\text{F(ab')}_2$  or control  $\text{F(ab')}_2$  were i.v. injected, mice were anesthetized by avertin and images were acquired for 10 minutes. Panel A shows a nu/nu mice bearing two human prostate cancer tumors. The tumor on the left is CAR (-) while the tumor on the right is CAR (+). Panel B shows a planar image obtained 24h after the intravenous injection of  $^{123}\text{I}$  labeled anti-CAR  $\text{F(ab')}_2$ . Panel C shows a planar image obtained 24h after intravenous injection of  $^{123}\text{I}$  labeled control  $\text{F(ab')}_2$ .

Seven mice were used for anti-CAR imaging and two were used for control imaging studies.

For each mouse, approximately 100  $\mu\text{Ci}$  of  $^{123}\text{I}$  radiolabeled antibody fragments were administered for imaging. As shown in the representative image (Figure 16B), CAR (+) and CAR (-) tumors could be effectively distinguished *in vivo* by direct molecular imaging of CAR protein expression. The pixel intensity in the CAR positive tumor ( $3.9 \pm 1.5$ ,  $n=7$ ) was  $2.2 \pm 0.4$  ( $p < 0.005$ ) times higher than that of CAR negative tumor ( $1.7 \pm 0.6$ ,  $n=7$ ). The *ex vivo* ratio averaged from 3 to 7:1 for CAR (+) vs. CAR (-) ( $n=5$ ). The images obtained after injection of control  $^{123}\text{I}$ - $\text{F(ab')}_2$  is shown in Figure 16C. Using  $^{123}\text{I}$  labeled  $\text{F(ab')}_2$  fragments of either anti-CAR or control IgG1, the anti-CAR could distinguish the CAR expressing



tumor while the control antibody could not. In comparison with traditional *in vitro* methods of monitoring CAR protein, direct antibody imaging can image the protein expression noninvasively *in vivo*.

There were some limitations of this approach. One was though  $^{123}\text{I}$  is the best radiotracer for imaging purpose and the  $\text{F(ab')}_2$  fragments target more efficiently than intact antibody, the image quality was still affected by the iodide uptake of normal thyroid tissue and GI tract because of *in vivo* dehalogenation. Blocking the thyroid, stomach and bladder activity before imaging is necessary to acquire images in which the detector would be counting activity mostly in tumors. To block those unwanted organs, one solution is to treat the animals with saturated potassium iodide (KI) treated water (1:2000) or Lugol's solution for three days before imaging studies based upon acute Wolff-Chaikoff effect [161], i.e. the murine thyroid iodide organification would be blocked when the iodide plasma levels reached a high threshold. Alternatively, instead of radioiodination, one could use a metal radioisotope such as Indium-111 to label the antibody and perform the imaging study [162]. In addition, alternative radioiodination approach such as Bolton Hunter could also help. Finally, use of shielding cover the upper body of the animal so that emissions from the tumor xenografts as mostly detected could optimize the image.

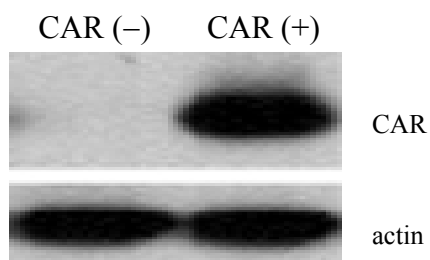
Another limitation for CAR protein imaging was the animal model used here was established using CAR stably transfected cells and the CAR expression may be artificially higher than that in prostate cancer. Although the transfected CAR expressing cells have comparable CAR level as naïve prostate cancer cells such as DU-145 and LNCaP cells [139], for low CAR expression cells such as PC3, a potential solution is to use a chemotherapeutic agent to pre-

treat tumors and induce target CAR expression followed by monitoring it with molecular imaging approaches.

## **2.7 *In Vitro* Validation of Anti-CAR Imaging Studies**

Without confounding blood flow in protein extract, plus the amplification provided by the detection system, western blot could be more sensitive than the *in vivo* approach. The purpose of *in vitro* studies was to confirm the imaging findings. Western blots were used to confirm the CAR protein expression in targets. In detail, cell lysate was prepared by homogenizing tumor specimens in a lysis buffer containing 1% Triton X-100 and 10% glycerol. The supernatant was collected by centrifuging at 12,000 rpm for 1 min at 4 °C. Protein concentration of each sample was determined using the Bradford method (BIO-RAD® Torrance, California). An equal amount (30 µg) of protein from each sample was loaded into to a 10% SDS-polyacrylamide gel and electroblotted to a nitrocellulose membrane. After blocking with 10 mM PBS containing 5% non-fat powdered milk, the membrane was incubated with a polyclonal anti-CAR antibody (1:350) [163] for 1.5 h, followed by incubating with the HRP-conjugated goat anti-rabbit IgG (1:2,500) for 1 h. After an extensive washing with 10mM PBS containing 0.1% Tween 20, the immobilized antibody was visualized using a SuperSignal® West Dura Extended Duration Substrate (Pierce Biotechnology PerBio Rockford, IL). Bio-Image Intelligent Quantifier® software (Bio Image) was used for quantifying the intensity of each protein band. To determine the relative CAR protein levels, the intensity of the CAR protein band was normalized with the intensity of the  $\beta$ -actin protein band from each sample.

**Figure 17. Representative Western Blot Detection of CAR**



Western blot analysis, obtained by using protein extracts from the left and right sided tumor xenografts, shown in Figure 16. Only the tumor identified as CAR (+) on the image shows a band. The membrane was probed with anti-actin to demonstrate equal protein loading.

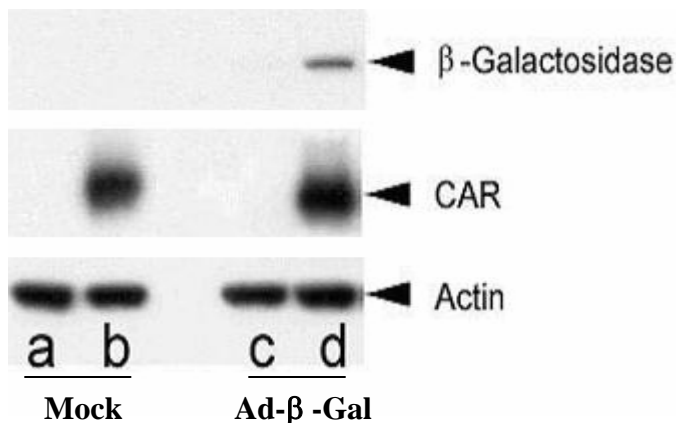
## 2.8 Detection of Tissue Receptivity to Adenovirus of *In Vivo* Tumor

The ultimate goal of imaging CAR expression *in vivo* is to predict the tissue receptivity to adenoviral gene delivery and the transgene expression. To determine the tissue receptivity for tumors with different levels of CAR expression, CAR (+) and CAR (-) tumors, grown in both flanks of nu/nu mice, were directly injected with adenovirus containing a construct encoding  $\beta$ -galactosidase ( $5 \times 10^8$  pfu). Prior to injection and tumor harvest, images were acquired and the tumor with higher visual intratumoral activity was predicted to be CAR (+). In order to compare the CAR expression level with the transgene ( $\beta$ -galactosidase) expression, tumor lysate, either CAR (+) or CAR (-), was probed with both polyclonal anti-CAR (1:350) and anti- $\beta$ -galactosidase (1:3,000) (Promega) and both CAR protein and  $\beta$ -galactosidase protein bands were normalized with loading control as described in section 2.7.

On western blots, only CAR (+) tumor showed  $\beta$ -galactosidase activity after 1-day infection. The intensity of  $\beta$ -galactosidase bands showed a semi-quantitative relationship to CAR expression level (Figure 18). The  $\beta$ -galactosidase enzymatic activity in the tumor homogenates was determined as follows: tumors were excised from animal 24 h or 72 h after virus injection and homogenized with cell lysis buffer as described above. OD<sub>405</sub> was

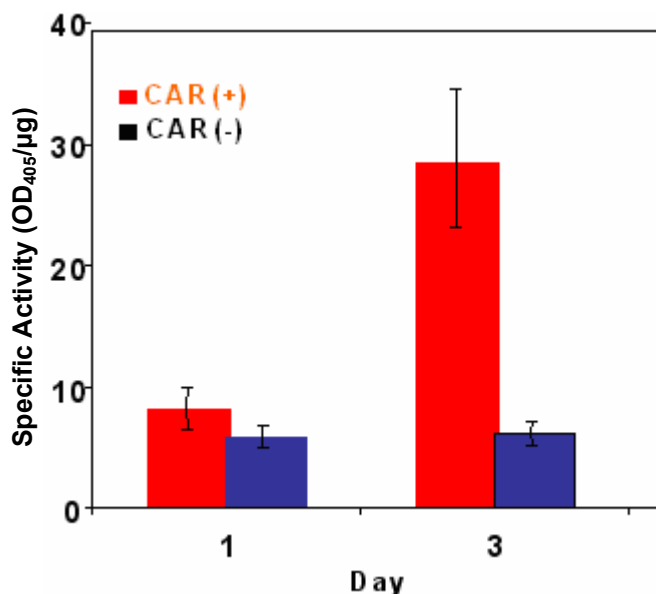
measured using a microplate reader (Bio-Tek Instrument Inc.) and normalized to the protein concentration of each sample. At Day 3, the CAR (+) tumor showed three times more activity than CAR (-) tumor (Figure 19).

**Figure 18. Western Blot Detection of CAR and  $\beta$ -galactosidase**



Tumor homogenates were prepared 1 day after infection with  $\beta$ -galactosidase expressing virus (Lane c, d) or control virus (Lane a, b). Top row autoradiograph after probing with  $\beta$ -galactosidase. Middle row autoradiograph after probing with anti-CAR. Bottom row autoradiograph probing with anti-actin. Lane a-b, mock-infected tumors; Lane c-d, tumors infected with Ad- $\beta$ -galactosidase. Lane a and Lane c: CAR (-) tumors; Lane b and Lane d: CAR (+) tumors.

**Figure 19. In Vivo Transduction of Tumors According to CAR Expression Status**



The  $\beta$ -gal adenovirus was injected into tumors directly then tumors were harvested at the indicated time. Each tumor was homogenized and 200  $\mu$ l of homogenate were subjected to  $\beta$ -gal assay (Invitrogen®) and protein concentration determination. OD values were measured at 405 nm and the specific activity of  $\beta$ -gal was calculated by normalizing  $\beta$ -gal activity with protein concentration of each sample. CAR expression status as determined by anti-CAR molecular imaging.

One limitation of our assay was although the enzymatic activity showed good correlations between CAR expression and transgene expression, the western blot at 3 day after intratumoral Ad- $\beta$ -Gal failed to show correlations (data not shown). The transgene expression in CAR (-) could be detected after 3-day intratumoral injection of Ad- $\beta$ -Gal. Though imaging may be sufficiently quantitative to act as a surrogate for tissue sampling to determine the CAR expression profile when making treatment decisions, knowing when tissue expression is optimal for viral infection, and CAR does play an role in adenoviral delivery to prostate cancer xenografts model, one thing that will need to be kept in mind is there is CAR-independent way for adenoviral delivery which may lead to adenoviral delivered transgene expression even in CAR (-) tumors [164, 165]. In addition, adenoviral delivered transgene expression in our animal model could also be caused by mechanical force formed during intratumoral injection. This should be further addressed by using other administration routes in the future. Thus, the measurement of CAR alone would not be sufficient to predict the adenoviral gene delivery efficiency. Our approach did not directly quantify viral uptake. One direct approach would have been using [ $^3\text{H}$ ]-thymidine labeled adenovirus and measuring the amount of activity in tumor homogenates [163]. In addition, strategies like direct labeling of viral vectors with a gamma emitter for imaging studies to monitor viral uptake for evaluation of viral delivery efficiency will be needed in the future.

## CHAPTER THREE

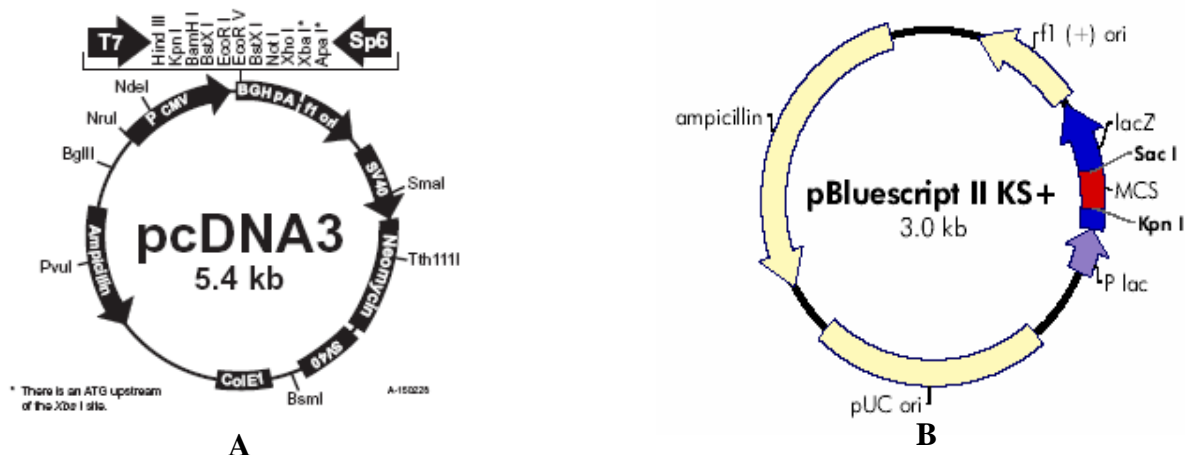
### IMAGING OF CAR PROMOTER ACTIVITY

The hypothesis was *in vivo* reporter gene imaging could be used for noninvasive assessment of the CAR gene promoter activity and developed for drug screening and evaluation of efficacy of combination therapy. In this study, PC3 and TCC were chosen as cell model because they both have very low CAR expression level [139, 163]. As mentioned in previous chapter, for low CAR expressing cells, the anti-CAR imaging approach may not be suitable, therefore methods to induce CAR expression are needed which provides us a platform to image CAR promoter activity *in vivo*.

#### 3.1 Directional Cloning (Construction of Reporter Molecule CAR-NIS)

Directional cloning was used to construct the novel reporter molecule CAR-NIS, i.e. DNA inserts and vector molecules were digested with two different restriction enzymes to create non-complementary cohesive ends at either end of each restriction fragment. This allows the insert to be ligated with the vector in a specific orientation and prevent the vector from self-ligation. The number of false positive clones thereby markedly decreases.

**Figure 20. Schematic Diagram of pcDNA3 (A) and pBluescript II (B)**



Panel A. The schematic diagram of pcDNA3 vector, hNIS cDNA was cloned in the EcoR I site.

Panel B. pBluescript vector, CAR promoter was cloned in multi-clone site (MCS).

The full-length hNIS plasmid (2.3 kb, cloned into pcDNA3 expression vector (Figure 20A) at EcoR I site) was kindly provided by Dr. Sissy. M. Jhiang, Ohio State University, Columbus, OH. To construct hNIS under the control of CAR promoter, the first step was to remove the CMV promoter that controls the constitutive expression of hNIS [166, 167]. The CMV promoter was cut out by using restriction enzyme Hind III and Nru I. The promoter of CAR was sub-cloned from a human genomic library and then cloned into pBS-bluescript vector (Stratagene, Figure 20B). The CAR promoter (1.2 kb) was removed from the vector by digestion with Sac I and Kpn I and then ligated by T4 DNA ligase with the no-CMV-pcDNA3 vector (linearized with Kpn I). The plasmid was then used to transform *E. Coli* XLI blue competent cells followed by selection with ampicillin. A single clone was selected based on ampicillin resistance. The CAR-NIS plasmid was purified by QIAGEN mini-prep. The insert was verified by both diagnostic enzyme digestion using Kpn I and Not I and DNA

sequencing with designed primers (SP6: GATTTAGGTGACACTATAG; 21D: GCTCTATCCCTACCAGAGATG; 41U: CATCTCTGGTAGGGATAGAGC). The enzymatic digestion yield the correct size insert of 3.7 kb and the insert sequence was confirmed by DNA sequencing. After confirmation, the CAR-NIS plasmid was amplified by a Sigma<sup>®</sup> maxi-prep for future use. The final stock of DNA concentration was 0.12 µg/µL and  $A_{260}: A_{280} = 1.8$ .

### 3.2 Transfection

Transfection is a technique originally developed to allow viral infection of animal cells by uptake of purified viral DNA rather than by intact virus particles. It has been developed to allow entry of foreign DNA into target cells using different approaches. For transient transfection, the transgene is not incorporated into the genome and is carried as an episome that can be lost. This means that expression levels will not be constant over time, and will eventually fade away. For stable transfection, the transgene is incorporated into the genome. It thus provides stable, long-term expression at the cost of being more difficult to produce. The prostate cancer cell line PC3 or bladder cancer cell line TCC was maintained in T-medium supplemented with 5% fetal bovine serum. These cells were routinely cultured in a humidified incubator at 37 °C with 5% CO<sub>2</sub>. In each transfection experiment, 1 µg of CAR-NIS or pcDNA3 plasmid DNA (Empty vector for negative control) was added into each cell line ( $4 \times 10^5$  cells/well) using LipofectAMINE<sup>®</sup> Plus (Invitrogen) according to manufacturer's protocol (Life Technology). For stable transfection, G418 (400 mg/mL) (Stratagene) was added 24 h later after transfection and the stable transfectants were selected

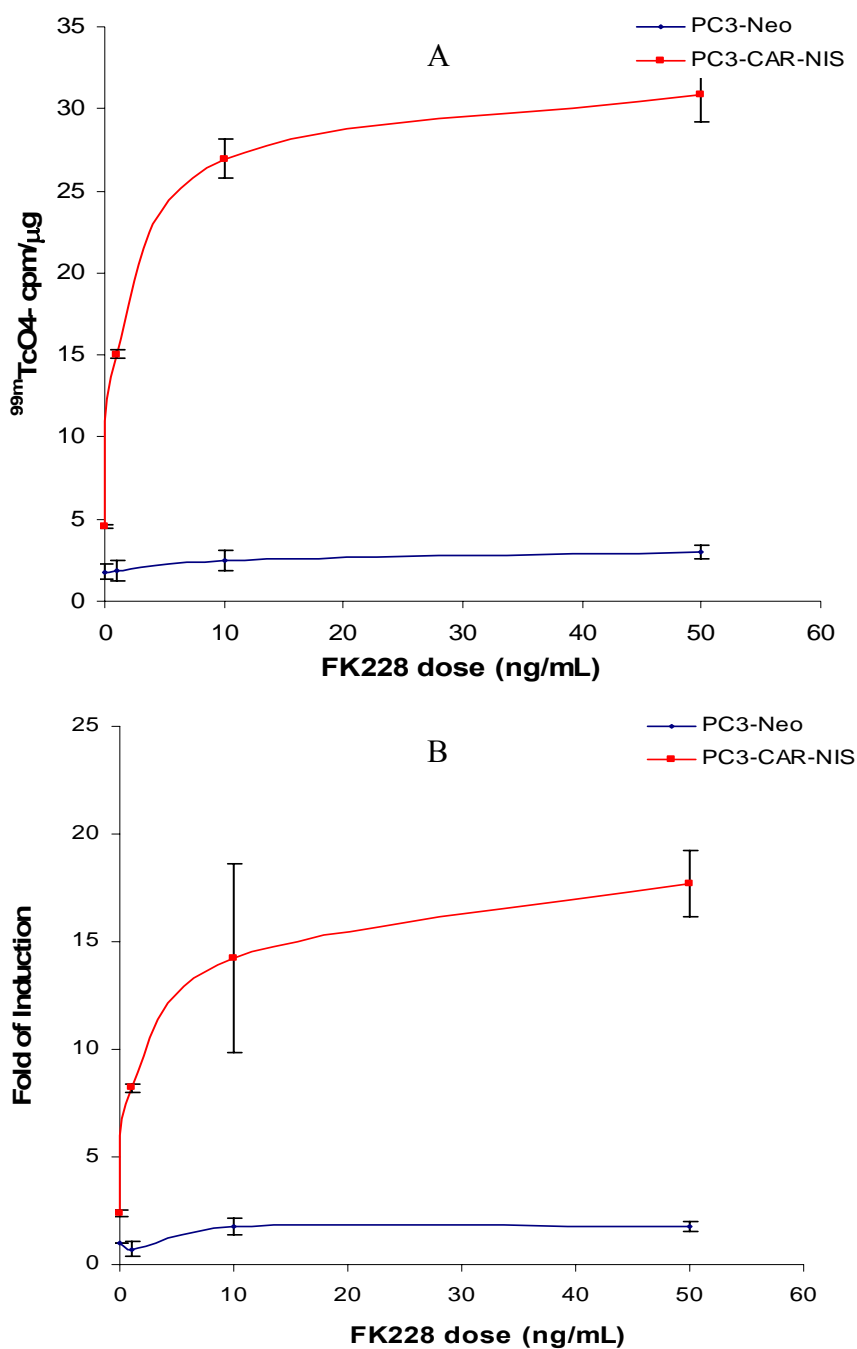


for neomycin resistance for 4 weeks with increasing doses of G418 (up to 800 mg/mL). PC3-CAR-NIS and TCC-CAR-NIS were generated based upon above methods. PC3-Neo and TCC-Neo were used as controls.

### 3.3 HNIS Functional Assay

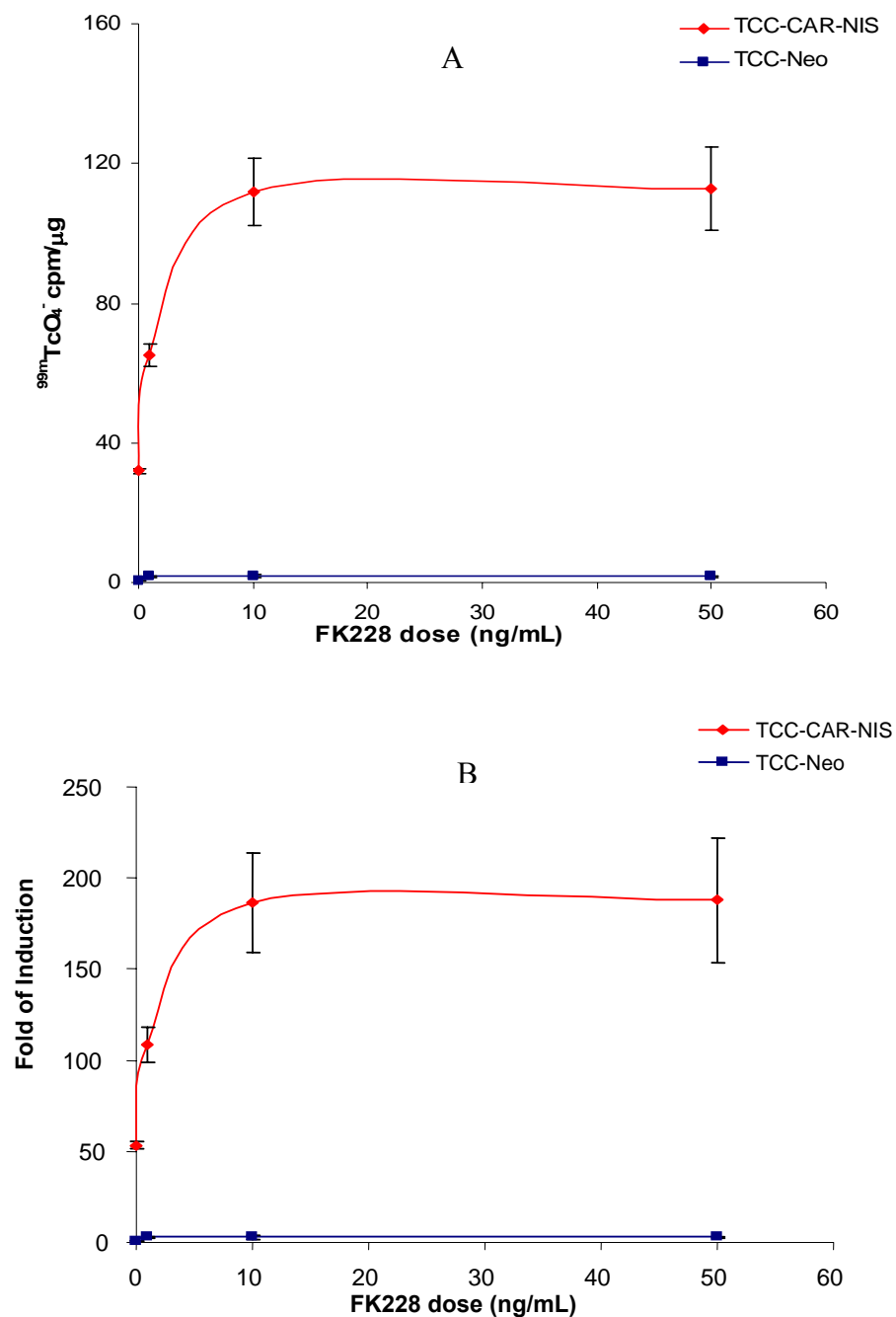
Transfected PC3 cells ( $4 \times 10^5$  / well) or TCC cells ( $5 \times 10^5$  / well) were seeded into 6-well plates in 2.5 mL T medium supplemented with 5% fetal bovine serum. CMV-hNIS transfected cells were used as a positive control. After 24 h incubation at 37°C with 5% CO<sub>2</sub>, the medium was aspirated and fresh medium was added containing different concentrations (0, 1, 10, 50 ng/mL) of FK228 (Tujisawa Pharmaceutical Co. Osaka, Japan.). Another 24 h later,  $^{99m}\text{TcO}_4^-$  uptake was initiated by adding 2.5 mL serum free T medium containing about 7.5  $\mu\text{Ci}$   $^{99m}\text{TcO}_4^-$  per well. Incubation was performed for an hour. Reactions were rapidly terminated by removing radioactive medium and washing cells with ice-cold phosphate buffered saline (10 mM PBS) three times. A phosphor plate was exposed by placing the multi-well dish upon petri-dish for an hour and subjected to process using a Cyclone<sup>®</sup> Phosphor System (PerkinElmer) [168]. During the phosphor imaging process, the energy from the radioisotopes ionizes the photostimulable crystals on the phosphor plate and leads to release of detectable photons by a photomultiplier tube (PMT). After imaging, cells were lysed using 500  $\mu\text{L}$  0.5 N sodium hydroxide and accumulated  $^{99m}\text{TcO}_4^-$  was measured by a gamma counter (Wizard Automatic  $\gamma$ -Counter Perkin-Elmer). The cell lysate was subjected to protein concentration measurement using the Bradford methods. Activity was normalized to protein concentration.

**Figure 21. *hNIS* Functional Assay after HDACi (FK228) Treatment in PC3-CAR-NIS**



A. Equal numbers of PC3-Neo or PC3-CARNIS were treated with the HDACi FK228 at different doses for 24h. NIS function was tested by accumulation of  $^{99m}\text{TcO}_4^-$ . The counts per minute (cpm) was normalized by  $\mu\text{g}$  cell lysate protein. Data is expressed as mean  $\pm$  SD. B. Fold of induction was calculated by each sample's cpm/ $\mu\text{g}$  compared with baseline TCC-Neo. At FK228 dose of 10 ng/mL, the induction leveled off.

**Figure 22. *hNIS* Functional Assay after HDACi (FK228) Treatment in TCC-CAR-NIS**



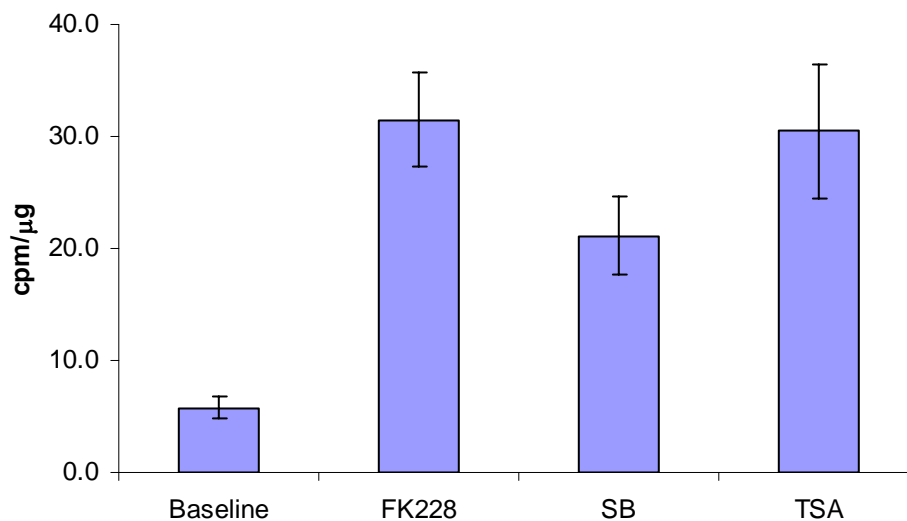
A. Equal numbers of TCC-Neo or TCC-CAR-NIS were treated with the HDACi FK228 at different doses for 24h. NIS function was tested by accumulation of  $^{99m}\text{TcO}_4^-$ . The counts per minute (cpm) was normalized by per  $\mu\text{g}$  cell lysate protein. Data was expressed as mean $\pm$ SD. B. Fold of induction was calculated by each sample's cpm/ $\mu\text{g}$  compared with baseline TCC-Neo. At FK228 dose of 10 ng/mL, the induction leveled off.

For the PC3 transfectant, the basal level of radioisotope ( $^{99m}\text{TcO}_4^-$ ) in PC3-CAR-NIS ( $4.6 \pm 0.1$  cpm/ $\mu\text{g}$ ) cell was 2.5 fold greater than that of PC3-Neo. After treated cells with FK228 50 ng/mL, PC3-CAR-NIS uptake increased to  $30.8 \pm 1.6$  cpm/ $\mu\text{g}$  (16 fold compared with basal line PC3-Neo) while PC3-Neo increased to  $3 \pm 0.2$  cpm/ $\mu\text{g}$  (Figure 21A, B). For the TCC transfectant, TCC-CAR-NIS uptake increased to  $112.8 \pm 11.9$  cpm/ $\mu\text{g}$ , TCC-Neo increased to  $1.7 \pm 0.2$  cpm/ $\mu\text{g}$  compared with basal line  $0.6 \pm 0.2$  cpm/ $\mu\text{g}$  (Figure 22A, B). The induction was shown to be dose dependent in above experiments. When cells were treated with FK228 at 100 ng/mL, the fold of induction went down and more cell death appeared (data not shown). FK228 treatment time was extended to 36 h or 48 h, while no additional induction was found, there was more cell death. In order to decide the optimal timing and dosage of FK228 induction of CAR-NIS, the above experiments were repeated more than ten times, each time each cell sample was at least triplicate. Figures 21 and 22 were the representative results of one set of experiment. At the transcriptional level, real-time PCR showed the CAR-NIS expression could increase by 360 fold when TCC-CAR-NIS cells were treated with 10 ng/mL FK228 for 24 h (Appendix C2). The PCR results (mRNA level) matched well with NIS functional assay ( $^{99m}\text{TcO}_4^-$  uptake) results. Taken together, the new reporter gene CAR-NIS was successfully stably transfected into both PC3 and TCC cells. In the CAR-NIS expressing cells, the CAR-NIS gene expression was inducible with HDACi FK228. In order to develop the approach for the purpose of drug screening or drug assay, the induction of CAR promoter activity by other HDACis was tested.

### 3.4 Drug Screening

The hNIS functional assay has potential to be used for screening suitable compounds for combination therapy. In order to compare their ability for inducing the CAR promoter, the PC3-CAR-NIS cells were plated and subjected to 24 h HDACi treatment, including FK228 (10 ng/mL), SB (Sodium Butyrate 10 nM), TSA (Tricostatin A 50 nM). After treatment, the cells were incubated with medium containing about 7.5  $\mu\text{Ci}$   $^{99\text{m}}\text{TcO}_4^-$  in 3 mL 5% T medium per well for 2 h and then cells were lysed and activities were counted as described in section 3.3. The results are shown in Figure 23. Compared with SB 10 nM ( $p < 0.001$ ), FK228 10 ng/mL and TSA 50 nM showed more potent effect in terms of induction of CAR promoter activity.

**Figure 23. hNIS Functional Assay of HDACi Treatment**



Different HDACis (FK228 10ng/mL, Sodium-butyrate (SB) 10  $\mu\text{M}$ , Tricostatin A (TSA) 50 nM ) were tested using functional assay. FK 228 (10ng/mL) shows the most potent inductivity. (Baseline: PC3-CAR-NIS without treatment).

### 3.5 Single Clone Screening

In order to prepare for the animal study, the most highly expressing clone of PC3-CAR-NIS was chosen. To do this, 1, 5, 10 cells were plated in 12-well dishes, after about 10 days, the colonies of single clones started to form. Using a cloning cylinder (Bellco Biotech), single clones were selected and detached with 100  $\mu$ L trypsin and re-plated into 6-well dish. When the cells attain 90% confluence, mRNA was extracted and hNIS expression was quantified by RT-PCR using designed NIS primer (section 3.8). The housekeeping gene 18S served as an internal control. The NIS expression in each clone was determined by comparative  $\Delta$ CT methods. By doing this, expression of the target gene CAR-NIS in different clones of stable transfectants was compared at the transcription level. Fifteen clones were screened with RT-PCR and results showed there was no difference between clones at both transcriptional level and protein functional levels.

### 3.6 Animal Model Establishment

A subcutaneous human xenograft mouse model was set up as described in section 2.3, one side with PC3-Neo cells, the other with PC3-CAR-NIS cells. Though higher induction of CAR promoter activity was observed, TCC cells were not used because they do not form good tumors. Weekly tumor volume was measured 3-dimensionally by calipers. It took two to three weeks for tumors to grow to about 50 mm<sup>3</sup> in volume and mice bearing size matched tumors were chosen for reporter gene imaging studies.

### 3.7 *In Vivo* Reporter Gene Imaging

For "proof of principle", the CMV-hNIS expressing PC3 xenografts were established and

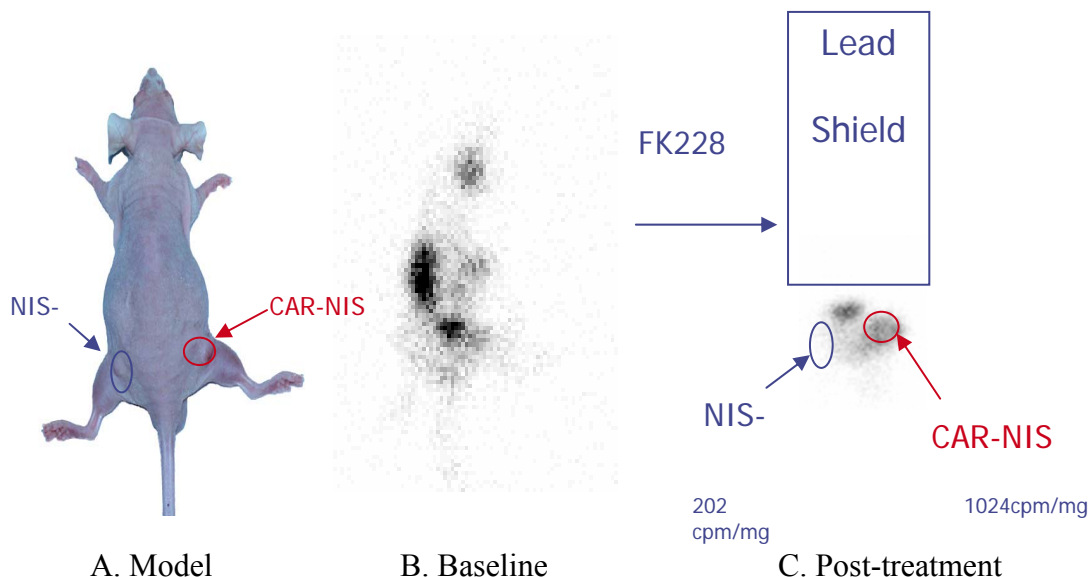
image was acquired using  $^{99m}\text{TcO}_4^-$  / hNIS system (Appendix C1). The radionuclide imaging techniques successfully imaged hNIS normal distribution in thyroid, stomach and PC3 expressing hNIS (Appendix C1). Next, the HDACi mediated CAR promoter activity was tested by the  $^{99m}\text{TcO}_4^-$  / hNIS reporter gene imaging system.

The reporter gene images were acquired based on hNIS function. Before the imaging procedure, a digital photograph of tumor-bearing mice was taken and the tumor size was measured for further reference. The mice were pre-treated with L-thyroxine (T4) 5mg/L supplemented water for 2 weeks. On the image day, the mice were anesthetized with Avertin<sup>®</sup> (Tribromoethanol) 4 mg /10 g and placed on a transparency with mice sketches on it. A thermal blanket could be used to maintain body temperature if necessary. The neck and the upper abdomen of each mouse were shielded with lead. For local administration, 10  $\mu\text{Ci}$   $^{99m}\text{TcO}_4^-$  was injected intratumorally. For systemic administration, 70  $\mu\text{Ci}$   $^{99m}\text{TcO}_4^-$  was injected through tail vein or orbital sinus. Planar imaging was performed on one head of a Toshiba 9300 triple head clinical gamma camera equipped with low energy high-resolution collimators for 10 minutes or until approximately 100,000 counts were acquired. Before acquiring baseline and post-treatment images, the difference in blood flow between both tumors in different individual mice was assessed as follows. Five tumor-bearing mice were injected with 1 mCi  $^{99m}\text{TcO}_4^-$  and dynamic images were acquired 3 frames per minute for 10 minutes. The acquired data showed that 5 mice exhibit same blood flow pattern in both tumor regions. The optimal imaging time point was determined using different time points 60, 120, 180 and 240 minutes after intravenous administration of  $^{99m}\text{TcO}_4^-$  by visually comparing target (tumor) / background (blood) ratio. Since the tumors were implanted on the thighs of

the body, the lowest possible pelvic background would be preferred. After the time point was determined (1 h delay for systemic  $^{99m}\text{TcO}_4^-$  administration, 4 h delay for local  $^{99m}\text{TcO}_4^-$  administration), the baseline images and post-treatment images were acquired by using the following protocol: a high resolution general purpose collimator, 20% window centered at 140 keV energy peak of  $^{99m}\text{TcO}_4^-$ , 256 by 256 matrix, appropriate zooming, and orientation were used for better images display. After the baseline images, the animals were treated with HDACi FK228 with different dosage (0.8, 1.6, 3.2 mg/kg) and different routes of injection. The animals were then subjected to further serial imaging studies at different time points to determine whether HDACi treatment induced CAR promoter activity. To treat the animals with HDACi, FK228 was diluted with 1:20 mixed 5% Glucose. Each dosage of FK228 was administered twice a week for up to 4 weeks. To quantify the results, the *in vivo* tumor average pixel intensity was determined by ROI analysis using software available on the clinical workstation. The ratios between CAR (+) and CAR (-) tumors were calculated based upon average pixel intensity in ROI. After the imaging sessions were completed, the tumors were excised, weighed and the *ex vivo* activity was counted using a gamma counter. The cpm per mg tumor tissue was calculated for further analysis and compared with *in vivo* average pixel intensity.



**Figure 24. Representative Image of Reporter Gene Imaging**



Panel A. Xenografts were established by implanting PC3-CAR-NIS tumor cells on one side while PC3-Neo cells (NIS-) were implanted on the other side. Panel B. Baseline image acquired 4h after local injection of  $10 \mu\text{Ci } ^{99\text{m}}\text{TcO}_4^-$ . Panel C. Post-treatment image acquired 4h after local injection of  $10 \mu\text{Ci } ^{99\text{m}}\text{TcO}_4^-$ . The upper body of the same mice was covered by a lead shield. The average pixel intensity for CAR-NIS expressing tumor was 1.5 while NIS- tumor was 0.6. The *ex vivo* counts were measured by a gamma counter after imaging.

Figure 24 shows representative images of CAR-NIS stable transfectant xenografts following  $^{99\text{m}}\text{TcO}_4^-$  administration. After the baseline image, acquired following local injection of  $10 \mu\text{Ci } ^{99\text{m}}\text{TcO}_4^-$  and a 4 h delay, the mouse was treated with FK228 3.2 mg/kg i.p. twice a week for 4 weeks and images were acquired weekly. On the imaging day,  $10 \mu\text{Ci } ^{99\text{m}}\text{TcO}_4^-$  was locally administered and 4 h later the post-treatment images were acquired. By doing this, the washout rate of  $^{99\text{m}}\text{TcO}_4^-$  was imaged *in vivo* and it turned out the NIS expressing tumor could retain  $^{99\text{m}}\text{TcO}_4^-$  longer after HDACi treatment (Figure 24). For NIS (-) tumor, the radioisotope washes in and washes out with the blood, what was visualized was the background activity in the blood. hNIS functions as a transporter for  $^{99\text{m}}\text{TcO}_4^-$ ; however, because of the lack of a fixation or organification mechanism for radioiodine in the tumor

cells, the accumulated  $^{99m}\text{TcO}_4^-$  is washed out after being transported into the cell. In the mean time, because of the 3D-structure of the tumor, the re-uptake of  $^{99m}\text{TcO}_4^-$  by NIS function is taking place which could prolong the retention time of  $^{99m}\text{TcO}_4^-$  for us to image [169, 170]. Another thing should be pointed out here is, for CAR-NIS expressing tumor, since CAR is a very weak promoter compared with CMV-hNIS used for "proof of principle" images (Appendix C1),  $^{99m}\text{TcO}_4^-$  accumulation on baseline images was not visualized.

Although HDACi FK228 successfully induces CAR promoter activity in culture, for *in vivo* studies, there was variability in response to FK228 treatment in terms of imaging of induction of CAR promoter activity. These may cause inconsistent results for imaging studies. To further find out the reason, mRNA was extracted from the same tumors for the imaging studies and measured using RT-PCR (addressed in section 3.8). However, most of these tumor samples' mRNA already degraded after *ex vivo* counting. In the future, a separate group of mice will be needed to address the *in vivo* induction of CAR promoter activity by FK228. The NIS expression at both transcriptional and translational level will be studied and compared with *in vivo* imaging and *ex vivo* counting studies. If the CAR-NIS expression was indeed induced at both mRNA and protein level while failed to be detected *in vivo*, high activity injections, amplification strategies (discussed in 5.2) and more dedicated imaging modalities such as small animal SPECT or PET should be used for this purpose.

In order to block the uptake of  $^{99m}\text{TcO}_4^-$  by unwanted organs such as thyroid and stomach, T4 was used and lower activity in thyroid was acquired. T4 could negatively feedback the release of TSH whose suppression inhibits the hNIS at both transcriptional and translational levels [171]. Since our reporter gene hNIS was driven by a CAR promoter, it won't be

affected by suppression of TSH. However, the inhibitory effect on thyroid of pretreatment was not as good as that of shielding. More studies will be needed to address the high background on the image caused by nonspecific uptake. In addition, about 10 mg/kg of sodium perchlorate ( $\text{NaClO}_4$ ) could be injected intraperitoneally 30 minutes prior to  $^{99\text{m}}\text{TcO}_4^-$  administration to assess the inhibition of  $^{99\text{m}}\text{TcO}_4^-$  uptake if necessary.

Another alternative way to image the HDACi effect using gamma camera imaging is to use series of "difference" images based upon exactly same positioning of imaging subjects. By definition, the "difference" image is made by subtracting the baseline image from the post-HDACi-treatment images. The differences in tumors are the HDACi induction of CAR promoter effects. These effects could be further compared with ROI analyses and *ex vivo* counting.

### **3.8 *In Vitro* Validation of Reporter Gene Imaging**

The tumors were excised and subjected to *in vitro* studies to confirm *in vivo* imaging findings. Western blot was used to detect the hNIS protein expression. Total or membrane protein from tumors or cells were prepared based on Pierce protocol (Mem-PER<sup>®</sup>). RT-PCR was used to test hNIS mRNA level.

For western blot, tumors, thyroid and muscle tissue were frozen in liquid nitrogen. The frozen tissue sample were homogenized and extracted in lysis buffer containing detergent (usually NP40). Glycoproteins could be enriched using affinity chromatography by incubating with wheat germ agglutinin (WGA) (EY labs) beads [172]. The protein concentration was determined by Bradford Assay methods. About 20  $\mu\text{g}$  of total protein (or membrane protein) lysate were subjected to SDS-PAGE using 10% polyacrylamide gels and

then transferred to nitrocellulose membrane. Immunodetection was carried out subsequently using mouse anti-hNIS monoclonal antibody (1:5,000, Chemicon International). Anti-mouse  $\beta$ -actin was used as the loading control. Bio-Image Intelligent Quantifier software (Bio Image) was used for quantifying the intensity of each protein band. To determine the relative protein levels, the intensity of the protein band was normalized with the intensity of the  $\beta$ -actin protein band from each sample. hNIS detection by western blot failed (data not shown) because lack of a good anti-NIS antibody.

For RT-PCR, 1-2  $\mu$ g of total cellular RNA from each cell line was reverse transcribed into first strand cDNA. The primer was designed (sense: 5' TGG GAC TAC GGG GTC TTT GC 3' antisense: CAG GCA CAT CCA GAG GAA CTT) and synthesized by Integrated DNA Technologies ([www.idtdna.com](http://www.idtdna.com)). About 4  $\mu$ L cDNA were subjected to a 25  $\mu$ L PCR (35 cycles of 94°C (30s), 54°C (30s) and 72°C (30s) using the NIS primer set (1 ng/ $\mu$ L each), the 18S rRNA primer set (0.5  $\mu$ g/ $\mu$ L) and Taq polymerase (Invitrogen)). The final PCR products (10  $\mu$ L) were electrophoresed in a 2% NuSieve agarose gel (3:1, FMC Bioproducts, Rockland, ME) and quantified with BioMax 1D image analysis software (Eastman Kodak, Rochester, NY). The relative level of NIS mRNA from each sample as normalized to 18S transcript from the same reaction. Also, a RT-PCR (Bio-Rad) was run using SYBR green for comparative  $\Delta$ Ct method. The relative mRNA level was determined before and after HDACi treatment compared with control groups. A representative RT-PCR result is shown in Appendix C2.

## CHAPTER FOUR

### TARGETED RADIONUCLIDE IMAGING OF ADENOVIRUS DELIVERY (TRIAD)

The above two models were both cell-based models. From the clinical research point of view, how to monitor the adenoviral gene delivery and adenoviral delivered transgene expression at real time are important questions to be answered. Instead of using CAR expression to predict potential adenoviral gene delivery efficiency, an *in vivo* molecular imaging approach was proposed to monitor the fate of adenoviral delivered transgene. To address this, in the absence of direct labeling of the virus, a reporter gene needs to be delivered by the adenovirus for imaging purposes. The hypothesis tested targeted radionuclide imaging could be used to monitor the recombinant adenovirus (Ad-CAR-NIS) delivered transgene expression *in vivo*.

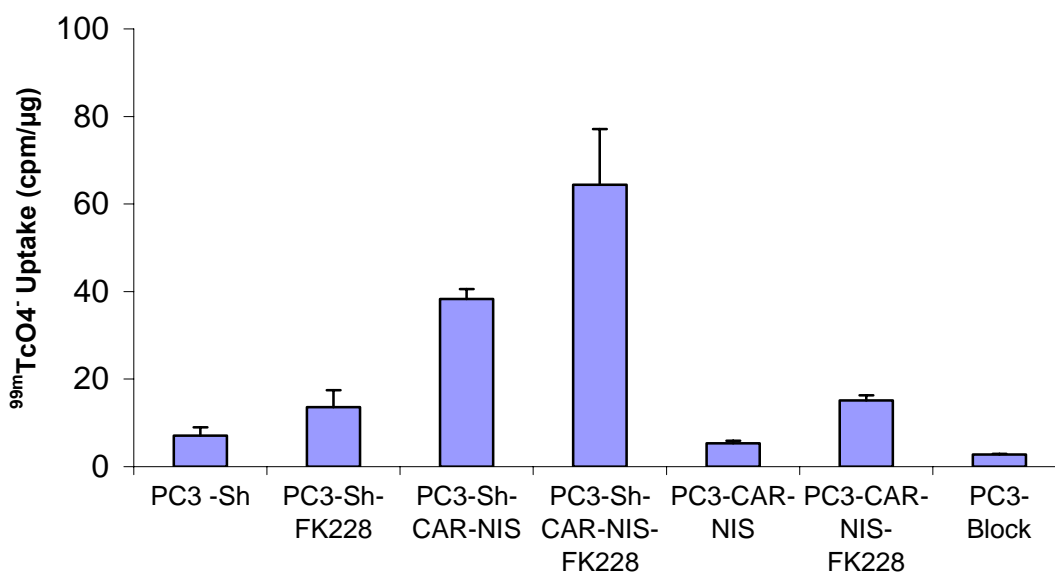
#### 4.1 Construction of Recombinant Adenovirus

##### 4.1.1 Clone CAR-NIS into Shuttle Vector

The ultimate goal of this project is to effectively deliver a novel construct for diagnostic, therapeutic and prognostic purposes. A replication deficient recombinant adenovirus was used to deliver CAR-NIS in this project. To construct a replication deficient recombinant adenovirus, the plasmid CAR-NIS was released from pcDNA 3 vector by cutting with Kpn I and Not I and then cloned into shuttle vector pCMV/PA [173] in which the CMV promoter has been removed. pCMV/PA is a shuttle vector that allows DNA to replicate and to be

transferred in two different species (eukaryotes and prokaryotes) . Because of the limitation of suitable digestion enzymes, a low efficiency blunt end ligation was performed (If this failed, a linker would be put in the shuttle vector and ligate with target DNA). Thirty to forty clones were screened by diagnostic enzyme digestion. Only one clone showed the correct pattern by using diagnostic enzyme digestion (Hpa I and Stu I). This clone, C3, was further confirmed by DNA sequence using primer 5' - CTACTTCGGGGTTGCTATG - 3'. A large-scale plasmid DNA purification was performed as in section **3.1** to amplify and purify the positive clone C3. The final concentration of C3 was around 0.35 µg/µL, and  $A_{260} / A_{280} = 1.94$ .

After C3 was confirmed by diagnostic enzyme digestion and DNA sequencing, a transient functional assay was performed by using transiently transfected PC3 cell with C3 DNA. One µg C3 DNA, serum-free-T medium and Lipofectamine Plus<sup>®</sup> reagent were used for transient transfection. The CAR-NIS function was tested by using NIS functional assay described in section **3.3**. PC3 cells transfected with empty shuttle vector were used as a negative control while PC3-CAR-NIS cells were used as a positive control. HDACi (FK228 10 ng/mL) mediated induction of CAR promoter activity was also tested by NIS functional assay. All counts per minute (cpm) were normalized by protein concentration. Based on the results of both sequence and transient expression assay (Figure 25), it was confirmed that the construct CAR-NIS had been successfully cloned into an adenovirus shuttle vector.

**Figure 25. Transient Expression Assay**

PC3 cells were transiently transfected with empty shuttle vector (PC3-Sh), CAR-NIS in vector (PC3-Sh-CAR-NIS) and then treated with HDACi FK228. The PC3 stable transfectant PC3-CAR-NIS was used as “+” control. For PC3-Block, 10  $\mu$ M NaClO<sub>4</sub> was added to block NIS function during incubation. Cells were lysed, activity and protein concentration measured then expressed as a ratio cpm/ $\mu$ g.

#### 4.1.2 Recombinant Adenovirus Construction

All recombinant adenoviruses were propagated in human embryonic kidney (HEK) 293 cells [174] and purified using conventional methods. In detail, 293 cells are maintained in Dubelco’s Modified Eagle’s Medium (DMEM) supplemented with 10% FBS. The recombinant adenovirus was generated by homologous DNA recombination. In detail, the CAR-NIS in a shuttle vector (C3) and pJM 17 [175] containing the entire Ad5 genome with an insert in the E1 region that exceeds the packaging constraints of the adenovirus capsid were used to co-transfect HEK 293 cells. Ten P-60 mm Petri dishes’ 293 cells were transfected with 1.2  $\mu$ g C3 and 0.8  $\mu$ g pJM17 using Lipofectamine Plus<sup>®</sup> agent (Invitrogen).

At Day 7, the viral plaque started to form and the medium were collected for DNA extraction and further virus amplification.

#### **4.1.3 Recombinants Identification by PCR**

Five hundred  $\mu$ L of supernatant from the infected 293 cell plate was used to extract DNA by a phenol- chloroform-isoamylethanol (PCI) mixture. The DNA products were subjected to a series of PCR based identifications to verify 1) The recombinant adenovirus contains adenoviral genome; 2) The recombinant adenovirus has a deletion in E1A region so it is replication deficient; and 3) The recombinant adenovirus encodes the CAR-NIS gene. Specifically, the A3/A4 primer was used for test adenovirus genome which was provided by pJM17. Wild type virus was used as a positive control. A5/A6 was used to verify the E1A region absence; the positive control was wild type virus since it contains E1A region. NIS primer was used to verify the CAR-NIS insert and the plasmid CAR-NIS was used as a positive control (Sequence A3: TCGTTTCTCAGCAGCTGTTG; A4: CATCTGAACTCAAAGCG-TGG; A5: ATTACCGAAGAAATGGCCGC; A6: CCCATTTAACACGCCATGCA). One representative example is shown in Appendix D1, clone V1 was identified as a positive clone for further amplification.

#### **4.2 Virus Amplification and Purification**

Being confirmed as a positive clone, the virus was used to re-infect the 293 cells and purified by cesium chloride (CsCl). To do this, 20 p-150 dishes of 80% confluent 293 cells and about 300  $\mu$ L virus medium per plate were used to initiate infection. 28h after infection, 90% CPE was observed and cells were harvested for CsCl purification. A discontinuous CsCl gradient (1.25 g/mL; 1.35 g/mL and 1.5 g/mL) was used to centrifuge (Beckman Optima™ XL-100K

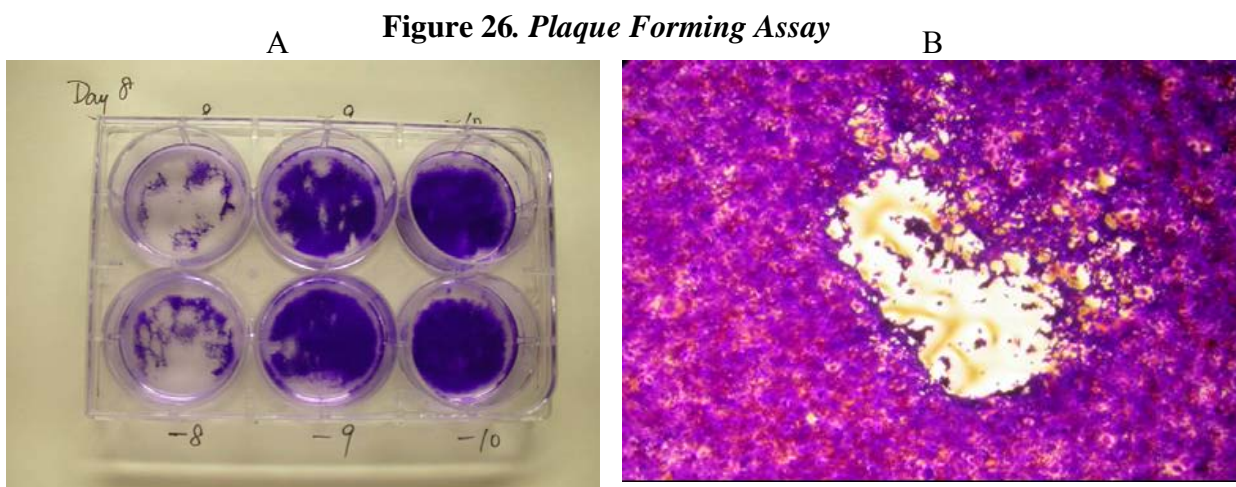


ultracentrifuge) for 35,000 rpm, 1 h to remove the majority of cellular contaminants. Subsequently a continuous CsCl gradient (1.35 g/mL) was used to centrifuge for 35,000 rpm, 18 h to completely separate infectious and defective viral particles. The CsCl solution was later removed by dialysis in a sterile buffer containing 1 mM MgCl<sub>2</sub>, 10 mM Tris-HCL (pH 7.5) and 10% glycerol. The A<sub>260</sub> was measured for virus particles. Ratio between A<sub>260</sub> and A<sub>280</sub> was used for estimation of virus quality (range: 1.3-1.4). The final virus particles were around  $3.8 \times 10^{11}$ /mL, A<sub>260</sub> / A<sub>280</sub> = 1.39.

### 4.3 Plaque Forming Assay

Due to variations in virus preparations the ratio of live/dead varies significantly and therefore, viral particles do not reflect the amount of active virus in the preparation. More accurate titration of virus relies on the plaque-forming assay which represents the titer of the infectious or functional virus in the preparation. The viral titers were determined by plaque assay and expressed in plaque-forming units (PFU) / mL. To do this, serial 1:10 dilutions of the virus stock were tested in a six-well plate dish containing 293 cells at 100% confluence. From several experiments, 1:10<sup>7</sup>-10<sup>10</sup> were used for titration. 1:10<sup>3</sup> was used as a positive control. After 2 h infection, the cells were washed by PBS and then 3 mL of 0.75% low melting point agar (Invitrogen) in 20% DMEM were overlaid to limit the movement of virus. Cells were fed with 10% DMEM every 3-5 days. At Day 7, virus plaques started to form. This is the cytopathic effect (CPE). For the plaque-forming assay, the plaque was fixed with formalin, stained with crystal violet and counted under microscope (Figure 26). The final titer of Ad-CAR-NIS was around  $2 \times 10^{10}$  pfu/mL. A single virus plaque (usually from 1:10<sup>8</sup> well) was chosen and collected into 1 mL 10% DMEM with an end-cut 200 µL tip and stored

in  $-80^{\circ}\text{C}$  for future virus amplification.



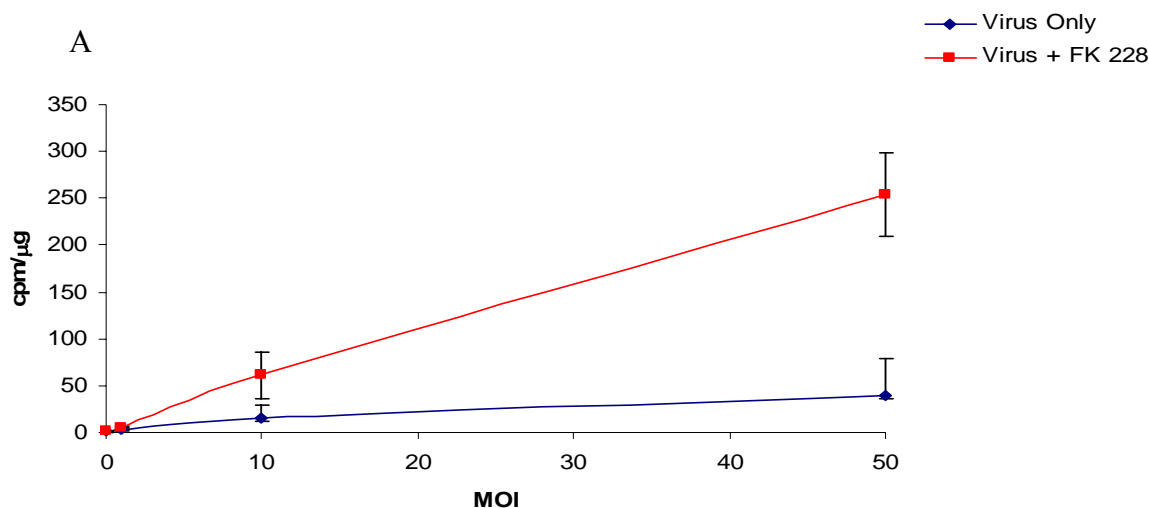
Panel A.  $1:10^{8-10}$  dilutions of Ad-CAR-NIS ( $3.8 \times 10^{10}$  viral particles /mL) were used to infect a monolayer of 293 cells. After 8 days infection, plaques were formed and live cells were stained with crystal violet. Panel B. A close-up ( $100 \times$ ) of cytopathic effect shown by unstained formed plaque.

#### 4.4 Functional Assay after Adenoviral Gene Delivery

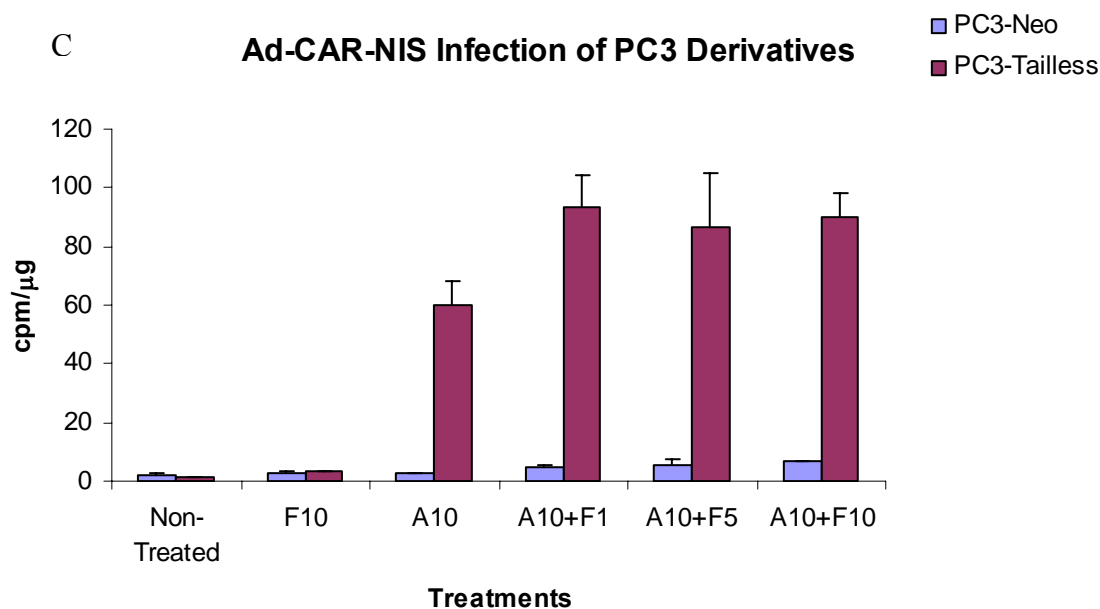
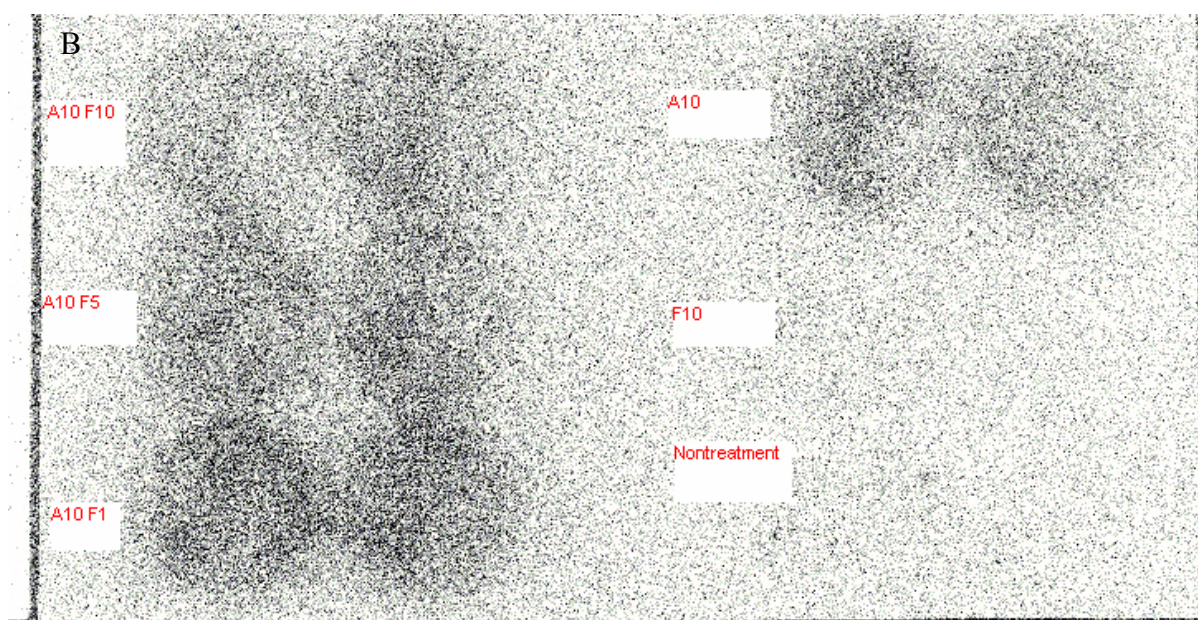
An *in vitro* functional assay of prostate cancer cells infected by Ad-CAR-NIS was done using prostate cell lines and their derivatives. For this project, PC3, PC3-Tailless, PC3-Neo, DU 145 cells were chosen for *in vitro* studies. The reason to choose these cell lines was because they express CAR protein at different levels. Higher uptake of  $^{99\text{m}}\text{TcO}_4^-$  in Ad-CAR-NIS infected high CAR expression cells than low CAR expression cells after 24 h or 48 h infection was expected and  $^{99\text{m}}\text{TcO}_4^-$  accumulation could be increased by HDACi FK228 treatment in a dose-dependent manner. Different strategies of FK228 treatment (i.e. simultaneously or sequentially with Ad-CAR-NIS infection, before or after infection) were tested by cell studies. Sodium perchlorate ( $10\text{-}50\ \mu\text{M}$ ) is known as a hNIS inhibitor and was used to further prove the radioisotope accumulation was due to hNIS function. Varying dose of Ad-CAR-NIS (different MOI starting with 0, 1, 10, and 50) and varying dose of FK228

were used to determine optimal dose for radioisotope uptake. In detail,  $1.25 \times 10^5$  cells were plated in six-well dish one day before infection. 0, 1, 5, 10, 50 MOI adenoviruses were used to infect cell for 24 or 48 h and 0, 1, 2, 5, 10 ng/mL FK228 were used pre- or post- virus infection. The radioisotope uptake was initiated by incubating cells with  $^{99m}\text{TcO}_4^-$  diluted in 5% culture medium in concentration of  $2 \mu\text{Ci/mL}/10^5$  cells for 2 h. After incubation, cells were immediately washed three times with ice-cold 10 mM PBS and then lysed with 0.5 N NaOH. The cell lysate was collected for activity counting. The activity was normalized to protein concentration (cpm/ $\mu\text{g}$ ). Ad- $\beta$ -Gal was used as virus control. Ethanol was used as solvent control. The autoradiography was performed as stated in 3.3 and the relative light output (DLU/ $\text{mm}^2$ ) were correlated with cpm/ $\mu\text{g}$ . Representative results are shown in Figure 27 A, B, C.

**Figure 27. Ad-CAR-NIS Infection (DU-145)**



Panel A. Du-145 cells were infected with Ad-CAR-NIS for 24h and then treated with FK228 at 10 ng/mL for another 24h. The functional assay was initiated by incubation with  $^{99m}\text{TcO}_4^-$ . Activity of  $^{99m}\text{TcO}_4^-$  was counted by gamma counter and normalized with protein concentration.



Panel B. Autoradiograph of Ad-CAR-NIS delivery to PC3-Tailless cells. Equal numbers of PC3-Tailless cells were treated with virus only, drug only or different combinations. Each sample was in duplicate, sample ID is marked beside wells. Phosphor plates were used for exposure for 60m. Panel C. Ad-CAR-NIS delivery in culture. Equal numbers of PC3-Tailless or PC3-Neo cells were infected with Ad-CAR-NIS for 48h. Subsequently, the cells were treated with different doses of FK228 for another 24h and then a functional assay was performed. Non-infected cells and cells treated with drug only served as controls. A10: Ad-CAR-NIS 10MOI; F1, F5, F10: FK228 1, 5 or 10 ng/mL.

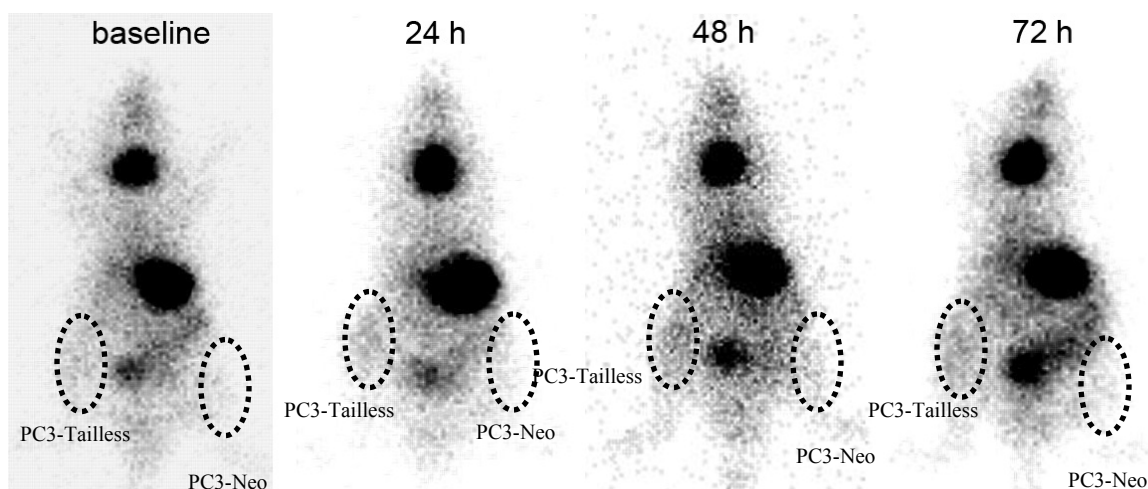
Based on *in vitro* NIS functional assay, it was proved that Ad-CAR-NIS could successfully deliver the CAR-NIS gene into target cells in a dose dependent manner. The endogenous expression of CAR could affect the adenoviral gene delivery efficiency which was the reason why positive results were found in DU-145 cells (Figure 27A) and PC3-Tailless cells (both high CAR expression) while not in PC3-Neo cells (Figure 27B and C). The transgene CAR-NIS was expressed and functioned properly as shown by accumulation of  $^{99m}\text{TcO}_4^-$ . The expression level of the transgene could be induced by low dose of HDACi (1 ng/mL) in culture, 60 cpm/ $\mu\text{g}$  for virus only vs. 90.1 cpm/ $\mu\text{g}$  for virus infected plus 1 ng/mL FK228 treatment (Figure 27C). The *in vitro* studies made preparations for *in vivo* imaging studies in terms of determination of dosage, infection time of virus and treatment with FK228.

#### 4.5 Molecular Imaging of Adenoviral Delivery *In Vivo*

Established tumors in both flanks of nu/nu mice were infected by intratumoral injection of Ad-CAR-NIS  $2 \times 10^9$ ,  $5 \times 10^8$  and  $2 \times 10^8$  pfu in 50  $\mu\text{L}$  10 mM PBS solution. The infection was allowed to proceed for 24, 48 and 72 h before functional testing. For systemic administration,  $2 \times 10^9$  pfu Ad-CAR-NIS were intraorbitally injected into mouse. Before acquiring imaging data, 70  $\mu\text{Ci}$   $^{99m}\text{TcO}_4^-$  were injected intravenously (i.v.). After one-hour-delay, images were acquired by using one head of a Toshiba 9300 triple head clinical gamma camera equipped with a high resolution general-purpose low energy collimator. This one-hour-delay time point was determined from a preliminary imaging study of 5 mice at 1, 2, 3, 4 h after intravenous injection of 70  $\mu\text{Ci}$   $^{99m}\text{TcO}_4^-$  each and visually comparing the contrast between target and background. Because of high activity in the lower abdomen on 2, 3, and 4

h delay images, the earlier time point (1 h delay) was chosen for TRIAD studies. A 20% window was centered at 140 keV energy peak. Data were collected in a 256 by 256 matrix. Appropriate zooming and rotations were used for better image display. Images were acquired for 5 minutes without shielding or for 100,000 counts with shielding the upper body of the mice. Tumor regions of interest (ROI) were identified and average pixel intensity was determined using software available on the clinical workstation. In the mean time, the activity from the thyroid and the ipsilateral muscle were determined for control. The ratios between tumor and above regions were calculated and compared. Representative images of local Ad-CAR-NIS delivery were shown in Figure 28.

**Figure 28. Representative Radionuclide Images of Local Ad-CAR-NIS Delivery**



$5 \times 10^8$  pfu Ad-CAR-hNIS were used to infect PC3-Tailless and PC3-Neo xenografts. Planar images were acquired for 5 minutes after 24, 48 and 72h of infection. Only PC3-Tailless tumors were visualized.

As shown in Figure 28, the function of CAR-NIS transgene product could be imaged for at least 72 h after local administration of Ad-CAR-NIS. The infected CAR (+) PC3-Tailless tumor started to show up after 24 h injection, the activity in CAR (+) tumor persisted for 72 h

and gradually diminished. After 144 h of infection ( $5 \times 10^8$  pfu), CAR (+) (PC3-Tailless) could not be distinguished from CAR (-) (PC3-Neo) tumors (data not shown). Using the same imaging protocols, less dose of Ad-CAR-NIS ( $2 \times 10^8$  pfu ( $3 \times 10^9$  vps)) delivery was not detectable *in vivo*.

In order to quantify the imaging data and evaluate the magnitude of adenovirus delivered transgene expression, ROI analysis was performed using software available on clinical gamma camera workstation. The ratios between infected PC3-Tailless tumors and PC3-Neo tumors(R/L) were calculated (Table 5). For all PC3-Tailless tumors, the average pixel intensity was higher in infected PC3-Tailless tumors than PC3-Neo tumors after 24, 48 and 72 h ( $p < 0.02$ ); the ratios of R/L in infected PC3-Tailless tumors were significantly higher than baseline images ( $p < 0.05$ ).

**Table 5. ROI of Ad-CAR-NIS Delivery**

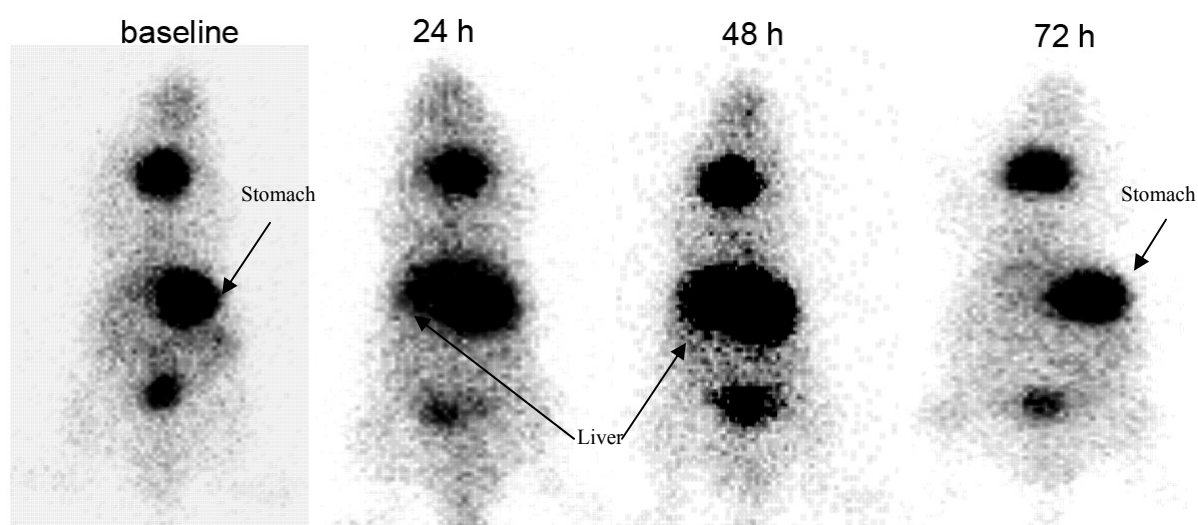
* ROI of Local Ad-CAR-NIS Delivery (n=3)			
Infection Time	Average Pixel Intensity		Ratio (+ vs. -)
	PC3-Tailless	PC3-Neo	R/L
Baseline	2.9±0.1	2.2±0.2	1.3±0.2
24 h	5.2±0.3	1.8±0.1	2.9±0.3
48 h	4.1±0.1	1.6±0.1	2.2±0.2
72 h	4.9±0.9	2.2±0.5	2.2±0.1

Based upon above results, the location and persistence of local adenoviral delivery could be monitored by imaging the transgene expression using simple gamma camera scintigraphy techniques. The quantification aspect of this approach could be further improved if using small animal SPECT, SPECT-CT, PET or PET-CT.



The systemic administration of adenovirus was tested through intraorbital injection here. Interestingly, though tumors were not confidently identified, imaging findings showed the adenovirus delivered transgene expressed in liver region of the mice when administered intraorbitally. Representative images of systemic Ad-CAR-NIS adenoviral delivery are shown in Figure 29.

**Figure 29. Representative Radionuclide Imaging of Systemic Ad-CAR-NIS Delivery**



$2 \times 10^9$  pfu Ad-CAR-NIS were used to systemically infect PC3-Tailless and PC3-Neo xenografts. Planar images were acquired for 5 minutes after 24, 48 and 72h of infection. Liver regions were visualized after infection.

As shown in Figure 29, the fate of intraorbital administration of Ad-CAR-NIS delivery could be tracked *in vivo* ( $2 \times 10^9$  pfu). The transgene CAR-NIS expression ended up in mouse liver region when compared with locally administered adenovirus (Figure 28). The episomal expression of transgene ended around 72 h post-infection ( $2 \times 10^9$  pfu). Tumors were not confidently recognizable on these images even infected with  $2 \times 10^9$  pfu of adenovirus.

Next, the induction of transgene CAR-NIS was monitored *in vivo* using imaging approaches. Two experimental designs were proposed: 1) To infect animals with Ad-CAR-NIS first and

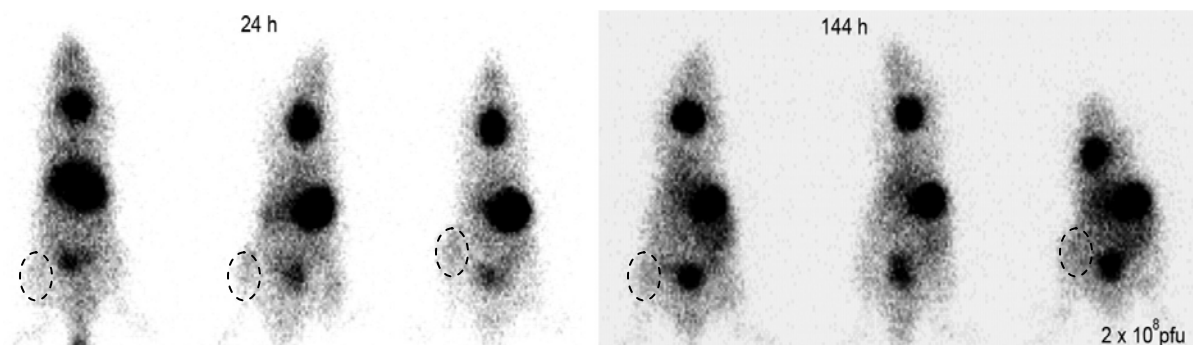


then treat with FK228; 2) To treat mice with FK 228 first and then infect with Ad-CAR-NIS.

To test Design 1, three tumor-bearing mice were infected with  $5 \times 10^8$  pfu for 24 h first and then treated with FK 2 mg/kg twice a week for two weeks and imaged weekly. A difference between CAR (+) and CAR (-) tumors was not detectable (data not shown). A real-time PCR analysis for tumor lysate was performed to determine if the CAR promoter activity was induced afterwards (Section 4.6).

To test Design 2, an additional 3 mice were treated with FK228 (2 mg/kg) twice a week for 2 weeks first and then locally infected with Ad-CAR-NIS. 24 h after infection, 70  $\mu\text{Ci}$   $^{99\text{m}}\text{TcO}_4^-$  were i.v. administered and an hour later, a five-minute image was acquired. Instead of enhancement of the magnitude of CAR-NIS expression, the infection dosage of Ad-CAR-NIS could be reduced to  $2 \times 10^8$  pfu for visualization of tumors. The images of combination of FK228 treatment and Ad-CAR-NIS delivery are shown in Figure 30. The CAR (+) tumors (encircled) were always visualized after 24 h infection. The ratio for CAR (+) tumor / CAR (-) tumor at 24 h post-infection was  $2.0 \pm 0.4$ . This was close to the ratio when using with  $5 \times 10^8$  pfu infection but without FK228 treatment; additionally, the visualization of transgene CAR-NIS expression persisted longer (until 144 h) after infection ( $\text{CAR (+) / CAR (-)} = 1.5 \pm 0.2$ ). This could be caused by FK228 induction of CAR expression in CAR (+) tumors which in turn leads to enhancement the efficiency of delivery of recombinant adenovirus.

**Figure 30. Images of Ad-CAR-NIS Delivery to HDACi Pretreated Tumor Bearing Mice**



Three mice were pretreated with HDACi FK228 2mg/kg twice a week for 2 weeks. Subsequently,  $2 \times 10^8$  pfu Ad-CAR-NIS were used to locally infect PC3-Tailless and PC3-Neo xenografts. Planar images were acquired for 5 minutes after 24, and 144h infection. Encircled are visualized PC3-Tailless tumors.

After all the imaging sessions were completed, the tumors were excised immediately for *ex vivo* gamma counting followed by freezing in liquid nitrogen and storage in  $-80^{\circ}\text{C}$  for *in vitro* studies. One mouse sacrificed after 96 h infection showed 2 fold greater activity (cpm/mg) in the PC3-Tailless tumor compared with PC3-Neo tumor. The rest of the animals were sacrificed after 144 h and failed to show any clearly difference in activity between PC3-Tailless and PC3-Neo tumors. Clearly more animals are needed to address the *in vivo* imaging of Ad-CAR-NIS delivery using radionuclide imaging, especially HDACi induction of adenoviral delivered transgene expression *in vivo*. Additionally, all the upper body of all animals should be shielded so the activity measured is emitted mainly from the tumors.

#### 4.6 *In Vitro* Validation of TRIAD

In order to address the causes of the failure of imaging FK228 induction *in vivo*, two mice were locally infected with Ad-CAR-NIS for 72 h and then treated with FK228 2mg/kg twice a week for 2 weeks. The tumors were excised and mRNA was extracted for a real-time PCR

study using protocol as in section **4.8**. Comparative  $\Delta\text{Ct}$  methods showed 8 fold higher hNIS mRNA level in FK228 treated Ad-CAR-NIS infected PC3-Tailless tumor compared with non-treated but infected PC3-Tailless tumor. Based on these results, it can be inferred 1) FK228 treatment induced adenoviral delivered transgene CAR-NIS expression *in vivo* at the transcriptional level; and 2) Current clinical gamma scintigraphy failed to detect an 8-fold difference of mRNA *in vivo*. Using more dedicated modalities could possibly improve the detection limit. In addition, with the comparisons between ROI analyses, *ex vivo* gamma counting and assessment of mRNA and protein levels, it is feasible to quantitatively correlate targeted molecular imaging of adenoviral delivery with molecular biology studies.

In the future, a dynamic study should be performed to decide the radioisotope washout rate in this adenoviral gene delivery model. For dynamic studies, a relatively (compared with  $^{99\text{m}}\text{TcO}_4^-$ ) longer half life radioiodine  $^{123}\text{I}$  will be used because kinetics and biodistribution of  $^{99\text{m}}\text{TcO}_4^-$  and  $^{123}\text{I}$  in NIS expressing tissues are remarkably similar [169]. A higher dose of Ad-CAR-NIS ( $2 \times 10^9$  pfu) may be intratumorally injected to initiate the infection. A high dose of  $^{123}\text{I}$ , about 1-2 mCi, should be injected 6 h before imaging. 24 h after infection, the  $^{123}\text{I}$  imaging should be acquired every 24 h until signal could not be detected. A block study could be performed by i.p. sodium perchlorate (10 mg/kg), 30 minutes before injection of  $^{123}\text{I}$  at one or two time points during the serial imaging study. The signal intensity from the positive tumor will be compared with the negative ones. The decay of the isotope will be corrected by software available at clinical workstation. Alternatively, a small animal micro-PET ( $^{124}\text{I}$ ) and the phosphor system could be used to further address the quantitative aspect of TRIAD study.

#### **4.7 *In Vitro* Combination Therapy**

In order to further explore the therapeutic potential for the combination of chemotherapy, adenoviral gene delivery and radioiodine therapy, a series of experiments were performed in culture. Though the mechanisms could be many factors such as enhanced radiosensitization and additive anti-tumor effects, the combination of different therapeutic regimens could exert more therapeutic effect than monotherapy [21, 176-182]. Different regimens could target different phases of the cell cycle. Irradiation mostly targets the M and G2 phase, gene therapy targets the S phase while most chemotherapy targets M phase or S phase [10, 21, 179]. The Ad-CAR-NIS approaches have potential to be used for combination of adenoviral gene delivery, chemotherapy and radionuclide therapy since hNIS can accumulate different radioisotopes. Of those isotopes, radioiodine and rhenium are both beta emitters and have the potential to be used for treatment of advanced prostate cancer complications such as bone metastases [183-185]. Astatine-211 ( $^{211}\text{At}$ ) is suitable for targeted alpha therapy [114, 186].

I tested combination of HDACi and  $^{131}\text{I}$  treatment in CAR-NIS expressing PC3 or TCC stable transfectants. For radioiodine treatment, a time-course treatment was used to simulate clinical situation. In detail, about 10,000 cells (TCC-Neo and TCC-CAR-NIS) were plated into 24 –well dishes. After 24 h, cells were treated with FK228 (1 ng/mL) and another 24 h later, the medium was replaced by fresh medium containing 30  $\mu\text{Ci/mL}$   $^{131}\text{I}$ . At 48, 72 or 96 h of incubation with radioisotope containing medium, the therapeutic reaction was terminated by washing the cells with ice-cold PBS and then the plates were stained with crystal violet and subjected to optical density measurement using Titertek Multiscan at 560 nm. The untreated cells were used as a control. The therapeutic effect was expressed as the percentage

of control cells. Since FK228 is a cytotoxic drug, the  $IC_{50}$  for 24 h is less than 1 ng/mL, lower doses (<1 ng/mL) was used for the combination therapy. Data (Appendix D2) from different dose combination provided the rational for the future studies.

The combination of different doses of FK228 and radioiodine did not show any significant synergistic effect ( $p>0.05$ ) from the preliminary studies (Appendix D2). No further combination therapeutic studies were performed because of the following reasons: 1) In contrast to previous functional assay in which 10 ng/mL FK228 was usually used, less than 1 ng/mL was used for combination therapy study, the inductivity of CAR-NIS was not obtained; 2) Radioiodine has a range of 2.2 mm, when dealing with monolayer cells, most of the energy was likely deposited outside the cells which cause very low cell killing efficiency. This could be improved in 3-D structural tumor models; and 3) Replication deficient recombinant adenovirus is not good for therapeutic purposes because the transgene has not been incorporated into the genome so the expression is transient.

## CHAPTER FIVE

### SUMMARY, CONCLUSIONS AND FUTURE DIRECTIONS

#### 5.1 Imaging CAR Protein Expression

$^{123}\text{I}$  labeled anti-CAR F(ab')<sub>2</sub> successfully localized the CAR expressing tumors *in vivo*. The *in vivo* approach proves that radionuclide based molecular imaging shows qualitatively the same pattern that is shown by *ex vivo* molecular biology techniques. Imaging findings have the potential to predict efficiency of adenoviral gene delivery. Targeted molecular imaging can be used to provide useful information before the initiation of adenoviral gene therapy. Anti-CAR imaging is a generalizable approach for different tumors because of availability of different imaging agents (radiolabel, magnetic particles, quantum dots and organic dyes). Since CAR expression enhancement was observed in both metastatic prostate cancer patients [46] and invasive mammary adenocarcinoma mouse models [187], anti-CAR imaging approach could also be a unique approach for those CAR expressing tumors, especially for inoperable CAR expressing refractory tumors. Anti-CAR imaging could also be used for exploiting the functional role of differential CAR expression in cancer with the help of highly-sensitive and spatially segregating imaging modalities such as SPECT and PET. Some of the technical limitations and possible solutions have been addressed in context. In order to achieve high tumor / non-tumor ratio and potentially avoid the dehalogenation observed with anti-CAR imaging, pre-targeting strategy could play an important role in both radioimmunodetection and radioimmunotherapy [129, 188]. Another important aspect needs to be improved is the quantitative potential of this approach. Both animal SPECT and PET

have great potential in quantitative aspects. In the future, quantitative imaging would finally be correlated with gene copy number of particular targets for quantitative prediction of adenoviral gene delivery efficiency.

## **5.2 Imaging CAR Promoter Activity**

Reporter gene imaging shows the potential to differentiate HDACi mediated induction of CAR-NIS expressing tumors after local administration of radioisotopes. This approach provides rationale to evaluate CAR promoter activity *in vivo* for the first time and it has potential to be used to screen appropriate drug candidates with the premise the drug can epigenetically regulate CAR promoter activity. More small animal imaging studies are needed to address the sensitivity of inducible CAR promoter imaging approaches, to optimize imaging studies and to correlate the quantitative imaging parameters such as average pixel intensity, cpm/mg with the HDACi up-regulation of CAR promoter activity and CAR protein expression. Different approaches have been proposed to amplify the reporter gene expression and coupled one reporter gene with others in the past couple of years, such as two-step transcriptional amplification (TSTA), internal ribosome entry site (IRES), gene fusion or dual promoter approaches [189, 190]. These amplification approaches could help to overcome the weakness of CAR promoter. To summarize, the CAR promoter has its own beauty in terms of its inducibility and has potential to be used as an indicator for both chemotherapy and adenoviral gene delivery efficiency.

### 5.3 Targeted Molecular Imaging of Adenoviral Delivery

For the TRIAD study, the idea of using radionuclide imaging to monitor the location, magnitude and duration of adenoviral delivery was tested in proof of principle experiments. Combination therapy of adenoviral gene therapy, chemotherapy and radionuclide therapies were tested in culture. A new replication deficient recombinant adenovirus was constructed to deliver reporter gene hNIS driven by the CAR promoter, whose activity could be induced by chemotherapeutic agent HDACi. Since hNIS can accumulate both alpha emitters such as  $^{211}\text{At}$  and beta emitters such as  $^{131}\text{I}$ , a potential combination of chemotherapeutic agent (HDACi), radiation therapy (either alpha or beta emitter) and adenoviral gene delivery could exert more therapeutic effect than single regimen when dealing with refractory cancers.

The detectability of hNIS based imaging is determined by the number of NIS expressing cells, the protein expression level, the function of hNIS and the sensitivity of imaging modality. In current TRIAD studies, an inducible adenoviral gene delivery model was established while CAR (+) tumors that were locally injected  $2 \times 10^8$  pfu of Ad-CAR-NIS could not be visualized *in vivo* by gamma camera scintigraphy. More sophisticated imaging modalities such as SPECT-CT or PET-CT will highly improve TRIAD approach as discussed in section 4.6. Such studies may allow more definitive quantification of transgene activity or viral delivery if the virus is labeled. Functional images combined with anatomic images from CT will further allow more definitive localization of the virus or functioning transgene expression. Finally, the numbers of NIS expressing cells and level of NIS expression will be determined by correlating the imaging signal with the *in vitro* cell and molecular biology studies using current model.



The duration of the episomal transgene expression could be monitored *in vivo* by using radionuclide imaging approaches which provides a reference to direct any recombinant adenoviral delivery *in vivo*. In the future, a self-inactivating recombinant lentivirus could be used to replace adenovirus and attain stable expression of transgene since the lentivirus could stably integrate the delivered gene into the host genome [191, 192]. Alternatively, conditional replication adenoviral vectors (CRAd) could be used to exert more therapeutic effects on specific cancers [193-195]. Also, the utilization of TSTA and other DNA recombination approaches [189, 190] could be helpful in enhancing the CAR promoter activity and thereby increasing the expression of the reporter gene hNIS. In addition, therapeutic genes could be coupled with the reporter gene for both diagnostic and therapeutic purposes.

For viral vector administration, catheter based delivery approaches could play an important role in terms of minimizing potential systemic side-effects and improving the target gene delivery efficiency [196]. Compared with local administration, systemic administration of adenovirus is predominantly liver uptake *in vivo*. Some intra-arterial administration has been proposed to bypass the liver uptake [197, 198]. This could be further addressed in the future studies.

In order to evaluate the therapeutic effect, an alternative is to use a classic *in vitro* clonogenic assay [90, 199]. This assay could be implemented as follows. About  $4 \times 10^5$  PC3 cells could be plated in a six-well dish, which will provide about 70% confluence, after 24 h treatment (with FK228 1 ng/mL) the cells will be incubated for 6-7 h at 37°C with 3 mL serum free T medium containing 1 mCi/10 mL Na<sup>131</sup>I. The reaction will be terminated by removing the

radioisotope-containing medium and washing the cells three times with ice-cold PBS. The cells will then be trypsinized, counted, and plated at densities of 250 cells (PC3) per well with T medium in 6-well plates. Detached cells are re-grown for 10 days, fixed with glutaraldehyde, and stained with crystal violet. The number of macroscopic colonies will be counted (>20 cells will be counted as 1 clone). The survival rate will be calculated as the killing percentage of colony numbers in a plate with treatment compared with the control plate (Non treatment vs. treatment, single treatment vs. combination treatment.) If synergistic effects could be found in above experiments, another experiment could be performed by using Ad-CAR-NIS to deliver the specific genes into target cells. In detail, wild type PC3 cells will be divided into 6 groups and therapeutic effect of each group will be compared. Group 1 will be treated with Ad-CAR-NIS only to exclude the toxicity of recombinant adenovirus (100 MOI 24 h). Group 2 will be treated with HDACi (FK228 1ng/mL 24 h) only to see the single chemotherapeutic drug effect on PC3 cells. Group 3 will be treated with  $^{131}\text{I}$  30  $\mu\text{Ci/mL}$  only to see the single irradiation effect. Group 4 will be treated with combination of HDACi and  $^{131}\text{I}$ . Group 5 will be treated with combination of adenovirus and  $^{131}\text{I}$ . Group 6 will be treated with combination of all three. The treatment effect will be compared with a non-treatment control group. The final dose and time will be subjected to change. The cell number will be determined as discussed in section 4.7.

In summary, TRIAD studies show the combination of adenoviral gene delivery and chemotherapeutic agent could make adenoviral gene delivery more efficient with potentially less toxicity since fewer doses or lower amounts of virus could be used via monitoring by a

real-time radionuclide imaging approach. In combination with chemotherapy, irradiation and adenoviral gene delivery, the cancer cells may be killed in largest extent.

Based upon the above studies, a potential targeted molecular imaging approach is feasible to monitor the CAR expression and evaluate drug induction on CAR promoter activity *in vivo* using gamma camera scintigraphy. With the help of combined anatomical and functional imaging modalities and the imaging/therapy construct CAR-NIS, targeted molecular imaging could become a potent *in vivo* approach to guide the combination therapy.

## APPENDIX A ABBREVIATIONS

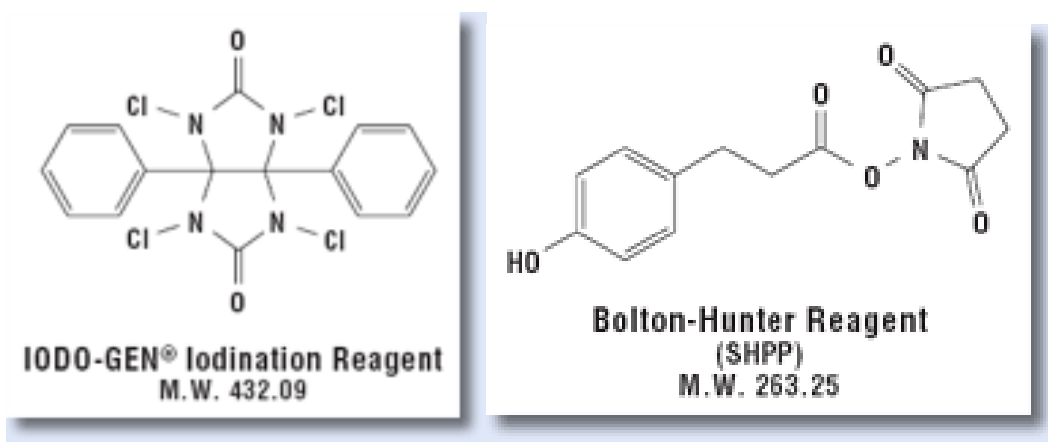
99m-TcO <sub>4</sub> <sup>-</sup>	metastable technetium 99 pertechnetate
%ID/g	percentage of the injected dose per gram
Ad	Adenovirus
ANOVA	Analysis of Variance
BSA	Bovine Serum Albumin
CAR	Coxsackie and Adenovirus' Receptor
PCa	Prostate Cancer
CEA	Carcinomaembryonic Antigen
CMV	Cytomegalovirus
CT	Computed Tomography
CPM	Counts Per Minute
CRAAd	Conditional Replication Adenovirus
CsCl	Cesium Chloride
EC	Electron Capture
FACS	Fluorescence Activated Cell Sorting
FDA	Food and Drug Administration
FITC	Fluorescein Isothiocyanate
GFP	Green Fluorescent Protein
GI	Gastrointestinal
HAMA	Human Anti Mouse Antibodies
HAT	Histone acetyltransferases
hD <sub>2</sub> R	Human Dopamine 2 Receptor
HDAC	Histone Deacetylases
HDACi	Histone Deacetylases Inhibitor
HNIS	Human Sodium Iodine Symporter
HPLC	High Performance Liquid Chromatography
HRP	Horseradish Peroxidase

HSV1-TK	Herpes Simplex Virus type one Thymidine Kinase
IC <sub>50</sub>	half maximal inhibitory concentration
IRES	Internal Ribosome Entry Site
ITLC	Instant Thin Layer Chromatography
LUC	Luciferase
MCS	Multi-Cloning Site
MRI	Magnetic Resonance Imaging
MOI	Multiplicity of Infection
MW	Molecular Weight
OD	Optical Density
PBS	Phosphate Buffer Solution
PCI	Phenol/Chloroform/Isoamyl alcohol
PET	Positron Emission Tomography
PMT	Photomultiplier Tube
PFU	Plaque Forming Unit
PSA	Prostate Specific Antigen
PSMA	Prostate Specific Membrane Antigen
RPM	Revolutions Per Minute
RT	Room Temperature
RT-PCR	Real-Time Polymerase Chain Reaction
SDS-PAGE	Sodium Dodecyl Sulfate Polyacrylamide Gel Electrophoresis
SE	Size Exclusion
SPECT	Single Photon Emission Computed Tomography
TCC	Transitional Cell Carcinoma
TRIAD	Targeted Radionuclide Imaging of Adenoviral Delivery
TSTA	Two-Step Transcriptional Activation
WGA	Wheat Germ Agglutinin

## APPENDIX B

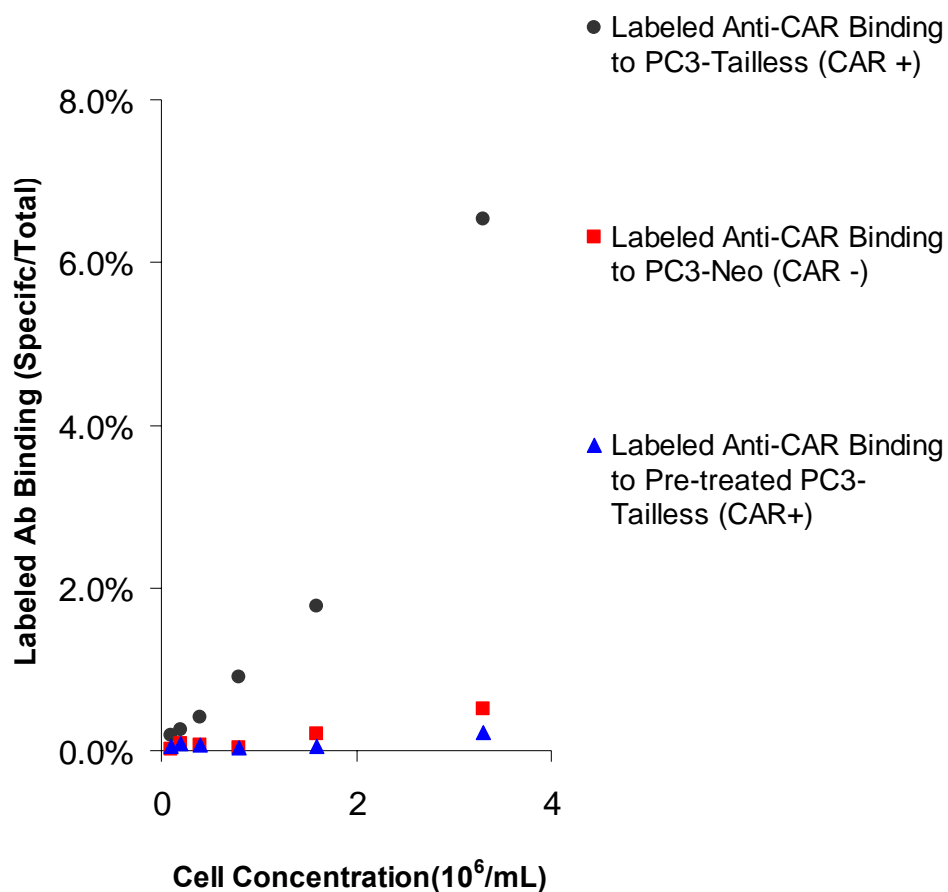
### Additional Data for Imaging CAR Protein Expression

#### B1. Structures of Commonly Used Oxidizing Agent for Radioiodination



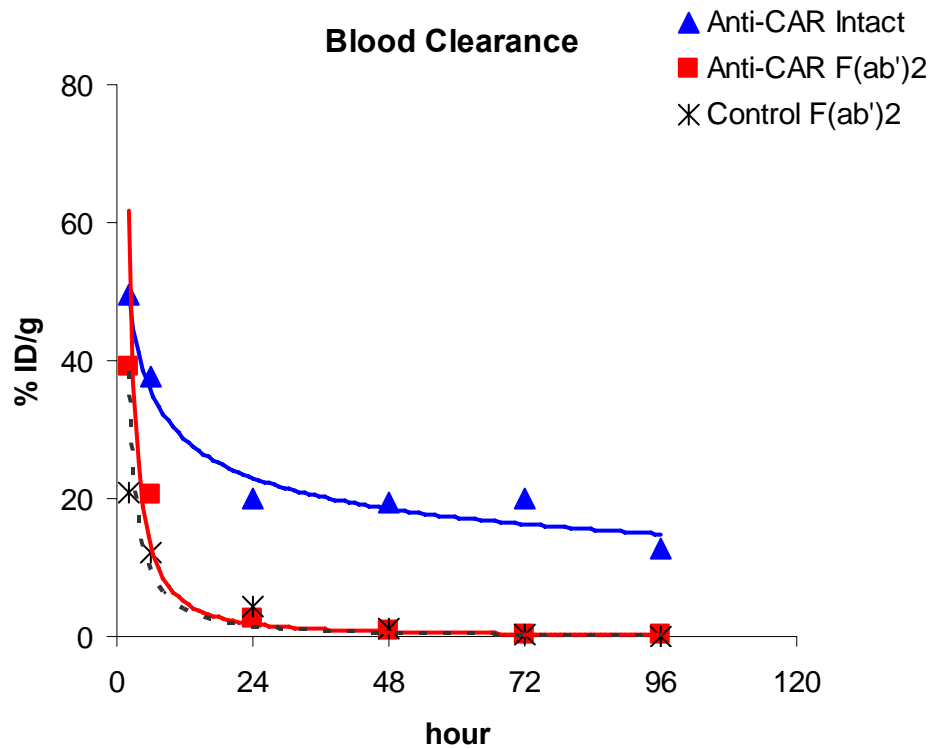
Adapted from [www.piercenet.com](http://www.piercenet.com)

## B2. Binding of Labeled Anti-CAR F (ab')<sub>2</sub> to PC3 cells



Up to  $3.3 \times 10^6$  PC3-Tailless cells or PC3-Neo cells were incubated with radiolabeled anti-CAR F(ab')<sub>2</sub> and/ or unlabeled anti-CAR antibody under room temperature for 1h and then washed with PBS 3 times. Cell pellets were collected and counted to determine the ratio between total applied (T) and specific binding (B). Data were then plotted as specific binding (B/T) vs. concentration (10<sup>6</sup>/mL).

### B3. Blood Clearance of Radiolabeled Antibodies



Blood clearance of different antibody preparations. Using %ID/g, the activity in blood was plotted as a function of time for each form of radiolabeled antibody. Anti-CAR F(ab')<sub>2</sub> and control F(ab')<sub>2</sub> both showed faster blood clearance compared with anti-CAR intact antibody.



#### B4. Statistical Analyses of Tumor Targeting As a Function of Time

%ID/g (mean $\pm$ SD)									
CAR (+) Tumor <sup>+</sup>					CAR (-) Tumor <sup>+</sup>				
Time (hr)	Intact	F(ab') <sub>2</sub>	# Control	Intact vs.F(ab') <sub>2</sub>	*p-value Control vs.Intact	Control vs.F(ab') <sub>2</sub>	Intact	F(ab') <sub>2</sub>	#Control
2	5.4 $\pm$ 2.0	9.9 $\pm$ 1.4	4.4 $\pm$ 0.6	0.007	0.60	0.001	3.0 $\pm$ 2.8	9.4 $\pm$ 1.2	2.5 $\pm$ 1.2
6	8.2 $\pm$ 1.4	10.6 $\pm$ 2.6	5.8 $\pm$ 0.7	0.32	0.23	0.02	9.5 $\pm$ 3.3	10.5 $\pm$ 3.7	5.8 $\pm$ 2.6
24	16.9 $\pm$ 7.1	9.2 $\pm$ 2.1	1.8 $\pm$ 0.5	0.03	<0.0001	<0.0001	12.1 $\pm$ 8.0	3.0 $\pm$ 1.9	3.3 $\pm$ 2.3
48	19.0 $\pm$ 3.8	4.7 $\pm$ 1.0	2.2 $\pm$ 0.9	<0.0001	<0.0001	0.002	10.3 $\pm$ 1.2	1.5 $\pm$ 0.4	2.1 $\pm$ 1.4
72	26.0 $\pm$ 17.5	2.8 $\pm$ 2.0	0.2 $\pm$ 0.1	<0.0001	<0.0001	<0.0001	9.1 $\pm$ 3.7	0.8 $\pm$ 0.2	0.2 $\pm$ 0.1
96	11.5 $\pm$ 4.4	1.0 $\pm$ 0.3	0.1 $\pm$ 0.1	<0.0001	<0.0001	<0.0001	7.2 $\pm$ 6.0	0.7 $\pm$ 0.4	0.1 $\pm$ 0.0

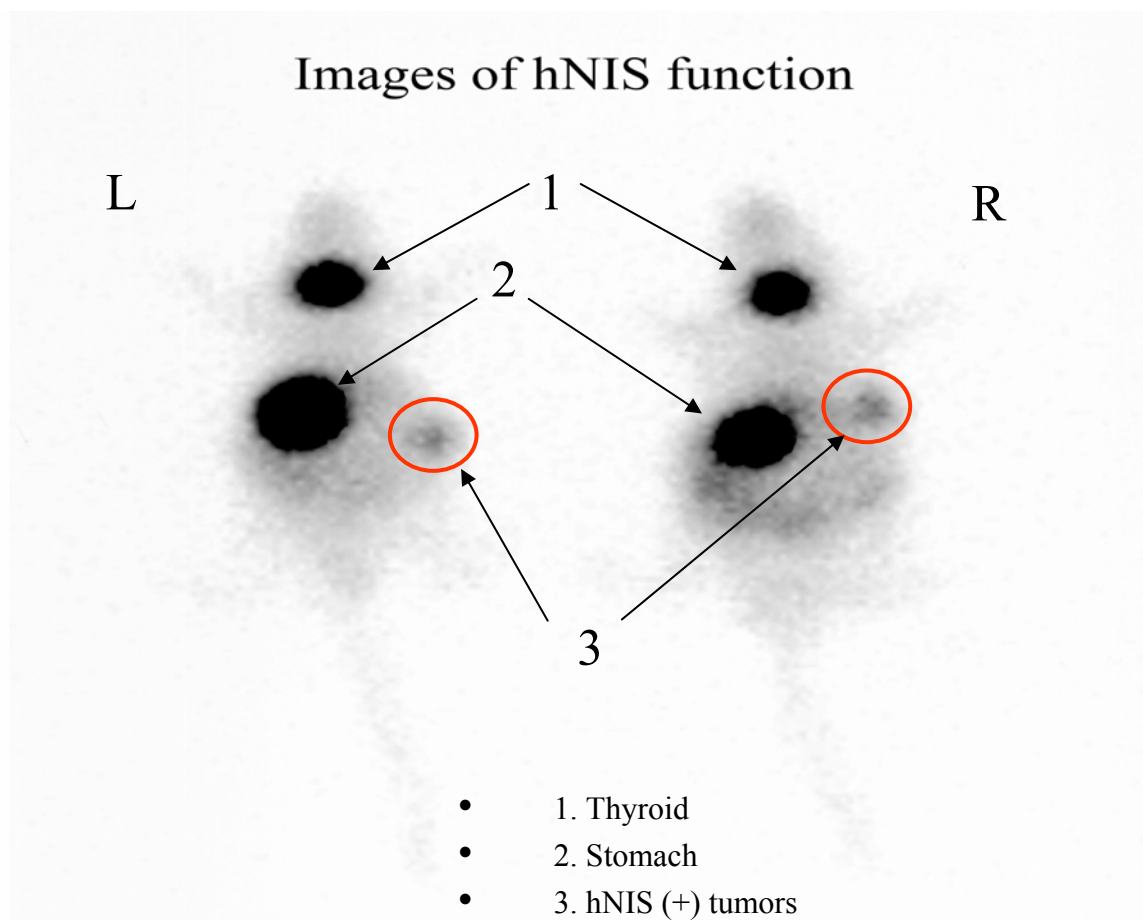
\*p determined with analysis of variance model after log transformation.

<sup>+</sup>n=5-6; # n=4

## APPENDIX C

### Additional Data for Imaging CAR Promoter Activity

#### C1. hNIS Proof of Principle Images



Two tumor bearing nu/nu mice, one side with PC3-hNIS (CMV promoter), the other side with PC3-Neo, were i.v. injected with 40  $\mu\text{Ci}$   $^{99\text{m}}\text{TcO}_4^-$ . 4h later, planar images were acquired for 5 minutes. Only the hNIS expressing tumors (right side) were seen. Organs with normal expression of hNIS (thyroid, stomach) were also visualized on above images.

## C2. Relative Ct Value by RT-PCR of TCC Stable Transfectants

Cells	GOI Ct	HKG Ct	Delta Ct	Ddelta Ct	Relative Value
TCC-Neo	31	11	20	0	1
TCC-Neo FK228	29	9	20	0	1
TCC-CAR-NIS	24	9.5	14.5	-5.5	45
TCC-CAR-NIS FK228	22	10.5	11.5	-8.5	360

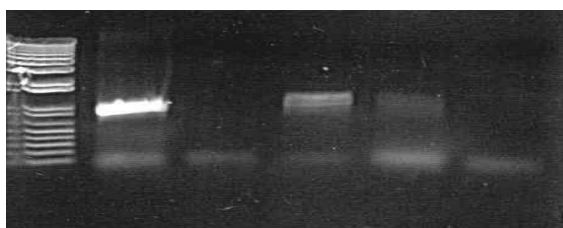
- FK228 dose =10 ng/mL
- GOI: Gene of Interest
- HKG: Housekeeping Gene
- Ct: Cycle of Threshold
- Delta Ct: Ct difference between GOI and HKG.
- Ddelta Ct: Ct difference between sample and control.
- Relative value: Fold of difference calculated by  $2^{-\text{Ddelta Ct}}$

## APPENDIX D

### Additional Data for TRIAD

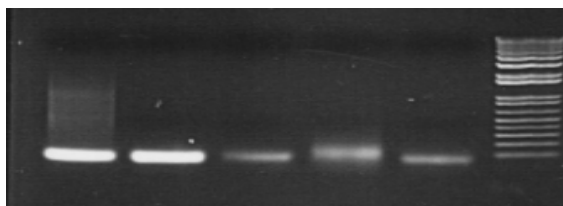
#### D1. PCR Identification of Replication Deficient Recombinant Ad-CAR-NIS

a. A3/A4 primer.



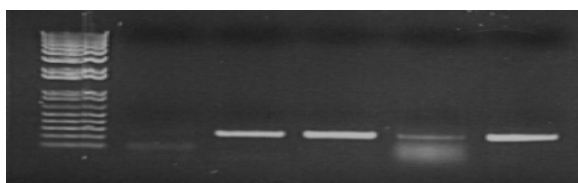
M      +      -      V1      V2      V4

b. A5/A6 primer.



+      -      V1      V2      V4      M

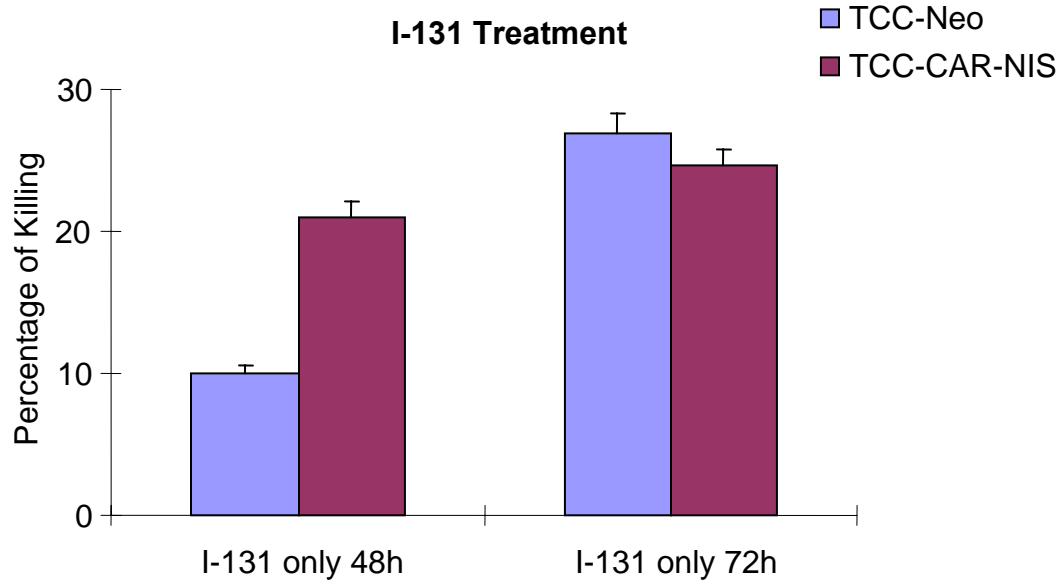
c. hNIS primer.



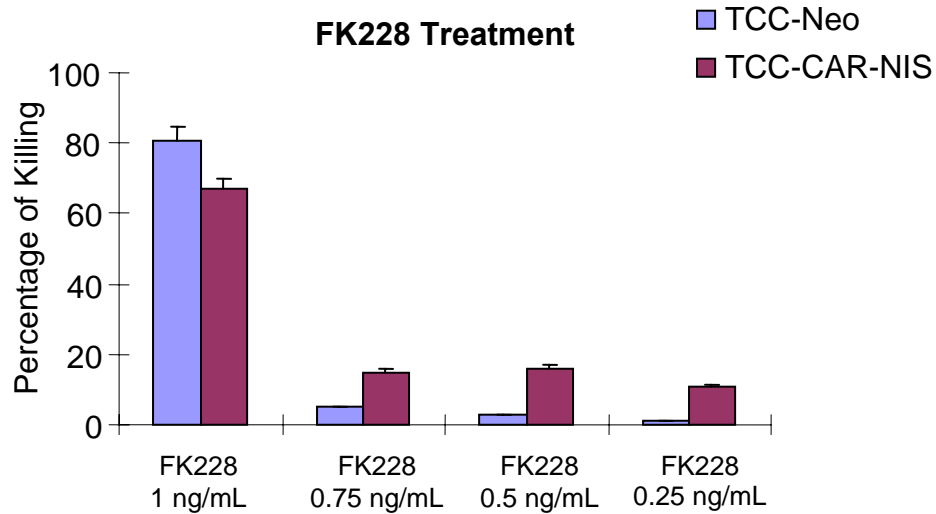
M      -      +      V1      V2      V4

M: Molecular Marker; +: Positive control; - Negative control; V1-4 different clones.

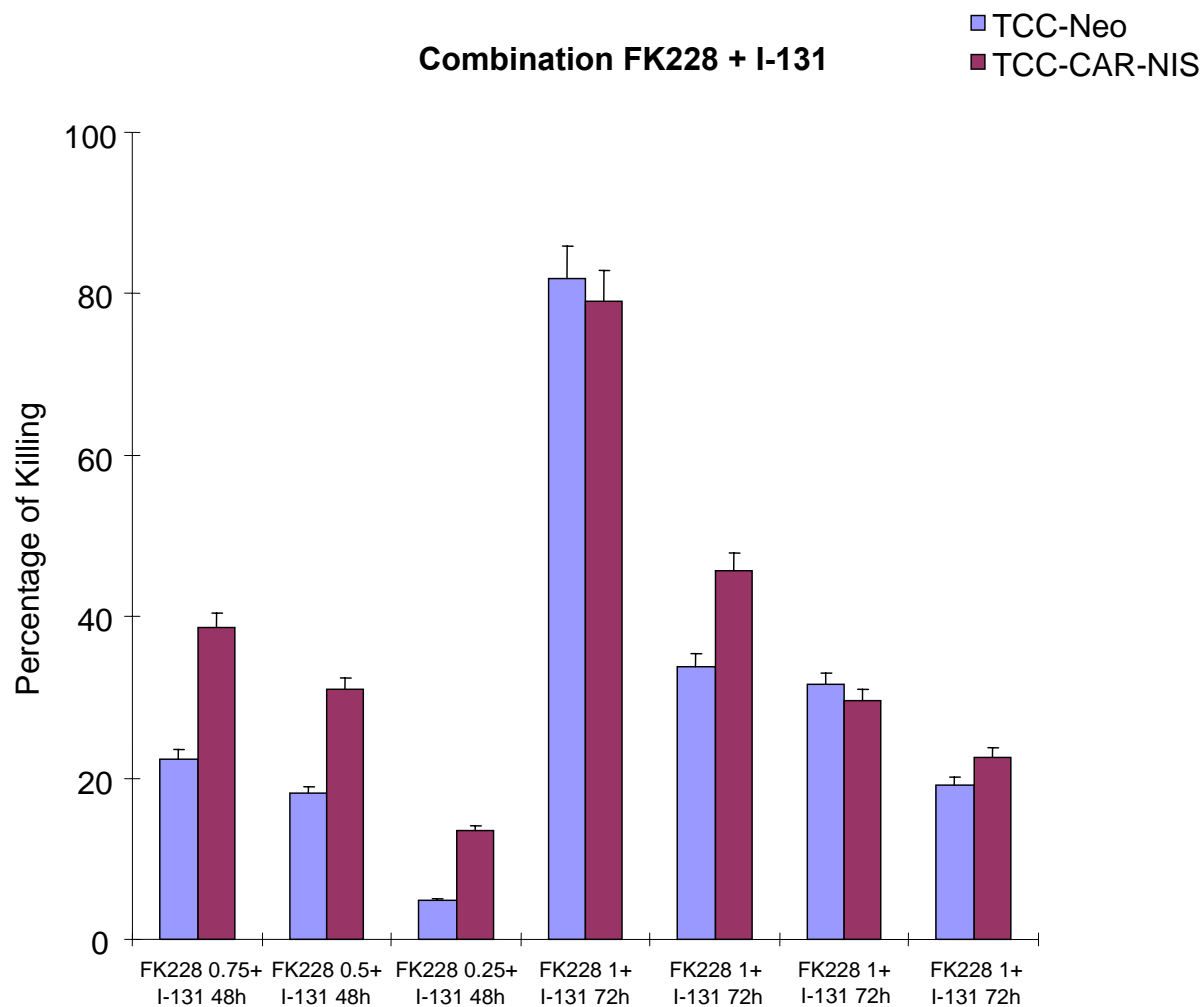
## D2. Single or Combination Treatment on TCC Derivatives



10,000 TCC-Neo or TCC-CAR-NIS cells were plated and treated with 30  $\mu\text{Ci}$  of  $^{131}\text{I}$  in 1mL medium for 48h or 72h. Cells without treatment were used as control. Cells were stained with crystal violet and counted.



10,000 TCC-Neo or TCC-CAR-NIS cells were plated and treated with 0.25-1 ng/mL FK228 for 24h. Cells without treatment were used as control. Cells were stained with crystal violet and then counted.



10,000 TCC-Neo or TCC-CAR-NIS cells were plated and treated with FK228 first and then treated with 30  $\mu$ Ci of  $^{131}\text{I}$  in 1mL medium for 48h or 72h. Cells without treatment were used as control. Cells were stained with crystal violet and then counted by measuring OD at 405 nm.

## BIBLIOGRAPHY

1. Jemal, A., T. Murray, E. Ward, et al., *Cancer statistics, 2005*. CA Cancer J Clin, 2005. **55**(1): p. 10-30.
2. Jemal, A., R. Siegel, E. Ward, et al., *Cancer statistics, 2006*. CA Cancer J Clin, 2006. **56**(2): p. 106-30.
3. Ryan, C.J. and E.J. Small, *Prostate cancer update: 2005*. Curr Opin Oncol, 2006. **18**(3): p. 284-8.
4. Nelson, W.G., A.M. De Marzo, and W.B. Isaacs, *Prostate cancer*. N Engl J Med, 2003. **349**(4): p. 366-81.
5. Klein, E.A., *Chemoprevention of prostate cancer*. Crit Rev Oncol Hematol, 2005. **54**(1): p. 1-10.
6. de Braud, F., M. Maffezzini, V. Vitale, et al., *Bladder cancer*. Crit Rev Oncol Hematol, 2002. **41**(1): p. 89-106.
7. Borden, L.S., Jr., P.E. Clark, and M.C. Hall, *Bladder cancer*. Curr Opin Oncol, 2005. **17**(3): p. 275-80.
8. Gwynn, E.S. and P.E. Clark, *Bladder cancer*. Curr Opin Oncol, 2006. **18**(3): p. 277-83.
9. Majeesh, N.J., H. Zhong, and J.W. Simons, *Gene therapy of prostate cancer: current and future directions*. Endocr Relat Cancer, 2002. **9**(2): p. 115-39.
10. Simons, J.W. and F.F. Marshall, *The future of gene therapy in the treatment of urologic malignancies*. Urol Clin North Am, 1998. **25**(1): p. 23-38.
11. Kaliberov, S.A. and D.J. Buchsbaum, *Gene delivery and gene therapy of prostate cancer*. Expert Opin Drug Deliv, 2006. **3**(1): p. 37-51.
12. Essand, M., *Gene therapy and immunotherapy of prostate cancer: adenoviral-based strategies*. Acta Oncol, 2005. **44**(6): p. 610-27.
13. Irie, A., *Advances in gene therapy for bladder cancer*. Curr Gene Ther, 2003. **3**(1): p. 1-11.
14. Kubo, H., T.A. Gardner, Y. Wada, et al., *Phase I dose escalation clinical trial of adenovirus vector carrying osteocalcin promoter-driven herpes simplex virus thymidine kinase in localized and metastatic hormone-refractory prostate cancer*. Hum Gene Ther, 2003. **14**(3): p. 227-41.
15. Pinski, J. and T.B. Dorff, *Prostate cancer metastases to bone: pathophysiology, pain management, and the promise of targeted therapy*. Eur J Cancer, 2005. **41**(6): p. 932-40.
16. Logothetis, C.J. and S.H. Lin, *Osteoblasts in prostate cancer metastasis to bone*. Nat Rev Cancer, 2005. **5**(1): p. 21-8.
17. Chester, J.D., G.D. Hall, M. Forster, and A.S. Protheroe, *Systemic chemotherapy for patients with bladder cancer--current controversies and future directions*. Cancer Treat Rev, 2004. **30**(4): p. 343-58.
18. Pienta, K.J. and D.C. Smith, *Advances in prostate cancer chemotherapy: a new era begins*. CA Cancer J Clin, 2005. **55**(5): p. 300-18; quiz 323-5.

19. Pollera, C.F. and F. Nelli, *Developing innovative strategies for advanced transitional cell carcinoma of the bladder*. Expert Rev Anticancer Ther, 2006. **6**(1): p. 83-92.
20. Fujimoto, N., M. Nomura, and T. Matsumoto, *Current and future status of prostate cancer chemoprevention*. Expert Rev Anticancer Ther, 2006. **6**(1): p. 59-71.
21. Teh, B.S., E. Aguilar-Cordova, M.T. Vlachaki, et al., *Combining radiotherapy with gene therapy (from the bench to the bedside): a novel treatment strategy for prostate cancer*. Oncologist, 2002. **7**(5): p. 458-66.
22. Tsao, A.S., E.S. Kim, and W.K. Hong, *Chemoprevention of cancer*. CA Cancer J Clin, 2004. **54**(3): p. 150-80.
23. O'Connor, K.M. and J.M. Fitzpatrick, *Side-effects of treatments for locally advanced prostate cancer*. BJU Int, 2006. **97**(1): p. 22-8.
24. Rubanyi, G.M., *The future of human gene therapy*. Mol Aspects Med, 2001. **22**(3): p. 113-42.
25. Verma, I.M. and M.D. Weitzman, *Gene Therapy: Twenty-First Century Medicine*. Annu Rev Biochem, 2004.
26. McCormick, F., *Cancer gene therapy: fringe or cutting edge?* Nat Rev Cancer, 2001. **1**(2): p. 130-41.
27. Raper, S.E., *Gene therapy: the good, the bad, and the ugly*. Surgery, 2005. **137**(5): p. 487-92.
28. Young, L.S., P.F. Searle, D. Onion, and V. Mautner, *Viral gene therapy strategies: from basic science to clinical application*. J Pathol, 2006. **208**(2): p. 299-318.
29. MacRae, E.J., A. Giannoudis, R. Ryan, et al., *Gene therapy for prostate cancer: current strategies and new cell-based approaches*. Prostate, 2006. **66**(5): p. 470-94.
30. Zhang, Y. and J.M. Bergelson, *Adenovirus receptors*. J Virol, 2005. **79**(19): p. 12125-31.
31. Kanerva, A. and A. Hemminki, *Adenoviruses for treatment of cancer*. Ann Med, 2005. **37**(1): p. 33-43.
32. Vorburger, S.A. and K.K. Hunt, *Adenoviral gene therapy*. Oncologist, 2002. **7**(1): p. 46-59.
33. Dannull, J. and A.S. Belldegrun, *Development of gene therapy for prostate cancer using a novel promoter of prostate-specific antigen*. Br J Urol, 1997. **79 Suppl 1**: p. 97-103.
34. Chester, J.D., W. Kennedy, G.D. Hall, P.J. Selby, and M.A. Knowles, *Adenovirus-mediated gene therapy for bladder cancer: efficient gene delivery to normal and malignant human urothelial cells in vitro and ex vivo*. Gene Ther, 2003. **10**(2): p. 172-9.
35. Pisters, L.L., C.A. Pettaway, P. Troncso, et al., *Evidence that transfer of functional p53 protein results in increased apoptosis in prostate cancer*. Clin Cancer Res, 2004. **10**(8): p. 2587-93.



36. DeWeese, T.L., H. van der Poel, S. Li, et al., *A phase I trial of CV706, a replication-competent, PSA selective oncolytic adenovirus, for the treatment of locally recurrent prostate cancer following radiation therapy*. Cancer Res, 2001. **61**(20): p. 7464-72.
37. Barton, K.N., D. Paielli, Y. Zhang, et al., *Second-generation replication-competent oncolytic adenovirus armed with improved suicide genes and ADP gene demonstrates greater efficacy without increased toxicity*. Mol Ther, 2006. **13**(2): p. 347-56.
38. Dwyer, R.M., S.M. Schatz, E.R. Bergert, et al., *A preclinical large animal model of adenovirus-mediated expression of the sodium-iodide symporter for radioiodide imaging and therapy of locally recurrent prostate cancer*. Mol Ther, 2005. **12**(5): p. 835-41.
39. Barton, K.N., D. Tyson, H. Stricker, et al., *GENIS: gene expression of sodium iodide symporter for noninvasive imaging of gene therapy vectors and quantification of gene expression in vivo*. Mol Ther, 2003. **8**(3): p. 508-18.
40. Excoffon, K.J., G.L. Traver, and J. Zabner, *The role of the extracellular domain in the biology of the coxsackievirus and adenovirus receptor*. Am J Respir Cell Mol Biol, 2005. **32**(6): p. 498-503.
41. Philipson, L. and R.F. Pettersson, *The coxsackie-adenovirus receptor--a new receptor in the immunoglobulin family involved in cell adhesion*. Curr Top Microbiol Immunol, 2004. **273**: p. 87-111.
42. Coyne, C.B. and J.M. Bergelson, *CAR: a virus receptor within the tight junction*. Adv Drug Deliv Rev, 2005. **57**(6): p. 869-82.
43. Wang, X. and J.M. Bergelson, *Coxsackievirus and adenovirus receptor cytoplasmic and transmembrane domains are not essential for coxsackievirus and adenovirus infection*. J Virol, 1999. **73**(3): p. 2559-62.
44. Bergelson, J.M., J.A. Cunningham, G. Droguett, et al., *Isolation of a common receptor for Coxsackie B viruses and adenoviruses 2 and 5*. Science, 1997. **275**(5304): p. 1320-3.
45. Tomko, R.P., R. Xu, and L. Philipson, *HCAR and MCAR: the human and mouse cellular receptors for subgroup C adenoviruses and group B coxsackieviruses*. Proc Natl Acad Sci U S A, 1997. **94**(7): p. 3352-6.
46. Rauen, K.A., D. Sudilovsky, J.L. Le, et al., *Expression of the coxsackie adenovirus receptor in normal prostate and in primary and metastatic prostate carcinoma: potential relevance to gene therapy*. Cancer Res, 2002. **62**(13): p. 3812-8.
47. Okegawa, T., R.C. Pong, Y. Li, J.M. Bergelson, A.I. Sagalowsky, and J.T. Hsieh, *The mechanism of the growth-inhibitory effect of coxsackie and adenovirus receptor (CAR) on human bladder cancer: a functional analysis of car protein structure*. Cancer Res, 2001. **61**(17): p. 6592-600.
48. Mizuguchi, H. and T. Hayakawa, *Targeted adenovirus vectors*. Hum Gene Ther, 2004. **15**(11): p. 1034-44.

49. Matsumoto, K., S.F. Shariat, G.E. Ayala, K.A. Rauen, and S.P. Lerner, *Loss of coxsackie and adenovirus receptor expression is associated with features of aggressive bladder cancer*. Urology, 2005. **66**(2): p. 441-6.
50. Bao, Y., W. Peng, A. Verbitsky, et al., *Human coxsackie adenovirus receptor (CAR) expression in transgenic mouse prostate tumors enhances adenoviral delivery of genes*. Prostate, 2005. **64**(4): p. 401-7.
51. Hemminki, A., A. Kanerva, B. Liu, et al., *Modulation of coxsackie-adenovirus receptor expression for increased adenoviral transgene expression*. Cancer Res, 2003. **63**(4): p. 847-53.
52. Goldsmith, M.E., M. Kitazono, P. Fok, T. Aikou, S. Bates, and T. Fojo, *The histone deacetylase inhibitor FK228 preferentially enhances adenovirus transgene expression in malignant cells*. Clin Cancer Res, 2003. **9**(14): p. 5394-401.
53. Pong, R.C., R. Roark, J.Y. Ou, et al., *Mechanism of increased coxsackie and adenovirus receptor gene expression and adenovirus uptake by phytoestrogen and histone deacetylase inhibitor in human bladder cancer cells and the potential clinical application*. Cancer Res, 2006. **66**(17): p. 8822-8.
54. Kitazono, M., M.E. Goldsmith, T. Aikou, S. Bates, and T. Fojo, *Enhanced adenovirus transgene expression in malignant cells treated with the histone deacetylase inhibitor FR901228*. Cancer Res, 2001. **61**(17): p. 6328-30.
55. Sachs, M.D., M. Ramamurthy, H. Poel Hv, et al., *Histone deacetylase inhibitors upregulate expression of the coxsackie adenovirus receptor (CAR) preferentially in bladder cancer cells*. Cancer Gene Ther, 2004.
56. Jaenisch, R. and A. Bird, *Epigenetic regulation of gene expression: how the genome integrates intrinsic and environmental signals*. Nat Genet, 2003. **33 Suppl**: p. 245-54.
57. Egger, G., G. Liang, A. Aparicio, and P.A. Jones, *Epigenetics in human disease and prospects for epigenetic therapy*. Nature, 2004. **429**(6990): p. 457-63.
58. Kornberg, R.D. and Y. Lorch, *Chromatin structure and transcription*. Annu Rev Cell Biol, 1992. **8**: p. 563-87.
59. Hsieh, J. and F.H. Gage, *Epigenetic control of neural stem cell fate*. Curr Opin Genet Dev, 2004. **14**(5): p. 461-9.
60. Maggio, S.C., R.R. Rosato, L.B. Kramer, et al., *The histone deacetylase inhibitor MS-275 interacts synergistically with fludarabine to induce apoptosis in human leukemia cells*. Cancer Res, 2004. **64**(7): p. 2590-600.
61. Saito, A., T. Yamashita, Y. Mariko, et al., *A synthetic inhibitor of histone deacetylase, MS-27-275, with marked in vivo antitumor activity against human tumors*. Proc Natl Acad Sci U S A, 1999. **96**(8): p. 4592-7.
62. Minucci, S. and P.G. Pelicci, *Histone deacetylase inhibitors and the promise of epigenetic (and more) treatments for cancer*. Nat Rev Cancer, 2006. **6**(1): p. 38-51.
63. Takai, N., T. Ueda, M. Nishida, K. Nasu, and H. Narahara, *A novel histone deacetylase inhibitor, Scriptaid, induces growth inhibition, cell cycle arrest and*

- apoptosis in human endometrial cancer and ovarian cancer cells*. Int J Mol Med, 2006. **17**(2): p. 323-9.
64. Kwon, H.J., M.S. Kim, M.J. Kim, H. Nakajima, and K.W. Kim, *Histone deacetylase inhibitor FK228 inhibits tumor angiogenesis*. Int J Cancer, 2002. **97**(3): p. 290-6.
  65. Mie Lee, Y., S.H. Kim, H.S. Kim, et al., *Inhibition of hypoxia-induced angiogenesis by FK228, a specific histone deacetylase inhibitor, via suppression of HIF-1 $\alpha$  activity*. Biochem Biophys Res Commun, 2003. **300**(1): p. 241-6.
  66. Zhang, Z., J. Karam, E. Frenkel, A. Sagalowsky, and J.T. Hsieh, *The application of epigenetic modifiers on the treatment of prostate and bladder cancer*. Urol Oncol, 2006. **24**(2): p. 152-60.
  67. Ueda, H., T. Manda, S. Matsumoto, et al., *FR901228, a novel antitumor bicyclic depsipeptide produced by Chromobacterium violaceum No. 968. III. Antitumor activities on experimental tumors in mice*. J Antibiot (Tokyo), 1994. **47**(3): p. 315-23.
  68. Sasakawa, Y., Y. Naoe, T. Inoue, et al., *Effects of FK228, a novel histone deacetylase inhibitor, on tumor growth and expression of p21 and c-myc genes in vivo*. Cancer Lett, 2003. **195**(2): p. 161-8.
  69. Baylin, S.B. and J.E. Ohm, *Epigenetic gene silencing in cancer - a mechanism for early oncogenic pathway addiction?* Nat Rev Cancer, 2006. **6**(2): p. 107-16.
  70. Li, L.C., P.R. Carroll, and R. Dahiya, *Epigenetic changes in prostate cancer: implication for diagnosis and treatment*. J Natl Cancer Inst, 2005. **97**(2): p. 103-15.
  71. Pong, R.C., Y.J. Lai, H. Chen, et al., *Epigenetic regulation of coxsackie and adenovirus receptor (CAR) gene promoter in urogenital cancer cells*. Cancer Res, 2003. **63**(24): p. 8680-6.
  72. Massoud, T.F. and S.S. Gambhir, *Molecular imaging in living subjects: seeing fundamental biological processes in a new light*. Genes Dev, 2003. **17**(5): p. 545-80.
  73. Hogemann, D., J.P. Babilion, and R. Weissleder, *[Molecular imaging in magnetic resonance tomography and nuclear medicine]*. Radiologe, 2001. **41**(2): p. 116-20.
  74. Jaffer, F.A. and R. Weissleder, *Molecular imaging in the clinical arena*. JAMA, 2005. **293**(7): p. 855-62.
  75. Weissleder, R. and U. Mahmood, *Molecular imaging*. Radiology, 2001. **219**(2): p. 316-33.
  76. Blasberg, R., *Imaging gene expression and endogenous molecular processes: molecular imaging*. J Cereb Blood Flow Metab, 2002. **22**(10): p. 1157-64.
  77. Gross, S. and D. Piwnicka-Worms, *Spying on cancer: molecular imaging in vivo with genetically encoded reporters*. Cancer Cell, 2005. **7**(1): p. 5-15.
  78. Ottobriini, L., P. Ciana, A. Biserni, G. Lucignani, and A. Maggi, *Molecular imaging: A new way to study molecular processes in vivo*. Mol Cell Endocrinol, 2006. **246**(1-2): p. 69-75.
  79. Czernin, J., W.A. Weber, and H.R. Herschman, *Molecular imaging in the development of cancer therapeutics*. Annu Rev Med, 2006. **57**: p. 99-118.

80. Price, P., *Molecular imaging to improve radiotherapy*. Radiother Oncol, 2006. **78**(3): p. 233-5.
81. Yang, D.J., E.E. Kim, and T. Inoue, *Targeted molecular imaging in oncology*. Ann Nucl Med, 2006. **20**(1): p. 1-11.
82. Weissleder, R., *Molecular imaging in cancer*. Science, 2006. **312**(5777): p. 1168-71.
83. Nichol, C. and E.E. Kim, *Molecular imaging and gene therapy*. J Nucl Med, 2001. **42**(9): p. 1368-74.
84. Shah, K., A. Jacobs, X.O. Breakefield, and R. Weissleder, *Molecular imaging of gene therapy for cancer*. Gene Ther, 2004. **11**(15): p. 1175-87.
85. Feeley, B.T., A.H. Conduah, O. Sugiyama, L. Krennek, I.S. Chen, and J.R. Lieberman, *In vivo molecular imaging of adenoviral versus lentiviral gene therapy in two bone formation models*. J Orthop Res, 2006. **24**(8): p. 1709-21.
86. Dwyer, R.M., E.R. Bergert, M.K. O'Connor, S.J. Gendler, and J.C. Morris, *Sodium iodide symporter-mediated radioiodide imaging and therapy of ovarian tumor xenografts in mice*. Gene Ther, 2006. **13**(1): p. 60-6.
87. Weissleder, R., *Molecular imaging: exploring the next frontier*. Radiology, 1999. **212**(3): p. 609-14.
88. Serganova, I. and R. Blasberg, *Reporter gene imaging: potential impact on therapy*. Nucl Med Biol, 2005. **32**(7): p. 763-80.
89. Chung, J.K., *Sodium iodide symporter: its role in nuclear medicine*. J Nucl Med, 2002. **43**(9): p. 1188-200.
90. Scholz, I.V., N. Cengic, C.H. Baker, et al., *Radioiodine therapy of colon cancer following tissue-specific sodium iodide symporter gene transfer*. Gene Ther, 2005. **12**(3): p. 272-80.
91. Spitzweg, C., M.K. O'Connor, E.R. Bergert, D.J. Tindall, C.Y. Young, and J.C. Morris, *Treatment of prostate cancer by radioiodine therapy after tissue-specific expression of the sodium iodide symporter*. Cancer Res, 2000. **60**(22): p. 6526-30.
92. Spitzweg, C., A.B. Dietz, M.K. O'Connor, et al., *In vivo sodium iodide symporter gene therapy of prostate cancer*. Gene Ther, 2001. **8**(20): p. 1524-31.
93. Spitzweg, C., S. Zhang, E.R. Bergert, et al., *Prostate-specific antigen (PSA) promoter-driven androgen-inducible expression of sodium iodide symporter in prostate cancer cell lines*. Cancer Res, 1999. **59**(9): p. 2136-41.
94. Smanik, P.A., Q. Liu, T.L. Furminger, et al., *Cloning of the human sodium iodide symporter*. Biochem Biophys Res Commun, 1996. **226**(2): p. 339-45.
95. Filetti, S., J.M. Bidart, F. Arturi, B. Caillou, D. Russo, and M. Schlumberger, *Sodium/iodide symporter: a key transport system in thyroid cancer cell metabolism*. Eur J Endocrinol, 1999. **141**(5): p. 443-57.
96. Spitzweg, C., *[The sodium-iodide symporter. Pathophysiologic, diagnostic and therapeutic significance]*. Internist (Berl), 2003. **44**(4): p. 396-402, 404-8, 410-1.
97. Spitzweg, C. and J.C. Morris, *The sodium iodide symporter: its pathophysiological and therapeutic implications*. Clin Endocrinol (Oxf), 2002. **57**(5): p. 559-74.

98. Levy, O., A. De la Vieja, and N. Carrasco, *The Na<sup>+</sup>/I<sup>-</sup> symporter (NIS): recent advances*. J Bioenerg Biomembr, 1998. **30**(2): p. 195-206.
99. Dai, G., O. Levy, and N. Carrasco, *Cloning and characterization of the thyroid iodide transporter*. Nature, 1996. **379**(6564): p. 458-60.
100. Groot-Wassink, T., E.O. Aboagye, Y. Wang, N.R. Lemoine, W.N. Keith, and G. Vassaux, *Noninvasive imaging of the transcriptional activities of human telomerase promoter fragments in mice*. Cancer Res, 2004. **64**(14): p. 4906-11.
101. Kim, K.I., J.K. Chung, J.H. Kang, et al., *Visualization of endogenous p53-mediated transcription in vivo using sodium iodide symporter*. Clin Cancer Res, 2005. **11**(1): p. 123-8.
102. Kang, J.H., D.S. Lee, J.C. Paeng, et al., *Development of a sodium/iodide symporter (NIS)-transgenic mouse for imaging of cardiomyocyte-specific reporter gene expression*. J Nucl Med, 2005. **46**(3): p. 479-83.
103. Kim, Y.H., D.S. Lee, J.H. Kang, et al., *Reversing the silencing of reporter sodium/iodide symporter transgene for stem cell tracking*. J Nucl Med, 2005. **46**(2): p. 305-11.
104. Mandell, R.B., L.Z. Mandell, and C.J. Link, Jr., *Radioisotope concentrator gene therapy using the sodium/iodide symporter gene*. Cancer Res, 1999. **59**(3): p. 661-8.
105. Joba, W., C. Spitzweg, K. Schriever, and A.E. Heufelder, *Analysis of human sodium/iodide symporter, thyroid transcription factor-1, and paired-box-protein-8 gene expression in benign thyroid diseases*. Thyroid, 1999. **9**(5): p. 455-66.
106. Boland, A., M. Ricard, P. Opolon, et al., *Adenovirus-mediated transfer of the thyroid sodium/iodide symporter gene into tumors for a targeted radiotherapy*. Cancer Res, 2000. **60**(13): p. 3484-92.
107. Haberkorn, U., *Gene therapy with sodium/iodide symporter in hepatocarcinoma*. Exp Clin Endocrinol Diabetes, 2001. **109**(1): p. 60-2.
108. Pinke, L.A., D.S. Dean, E.R. Bergert, C. Spitzweg, C.M. Dutton, and J.C. Morris, *Cloning of the mouse sodium iodide symporter*. Thyroid, 2001. **11**(10): p. 935-9.
109. Dwyer, R.M., E.R. Bergert, M.K. O'Connor, S.J. Gendler, and J.C. Morris, *Sodium iodide symporter-mediated radioiodide imaging and therapy of ovarian tumor xenografts in mice*. 2005.
110. Dwyer, R.M., E.R. Bergert, K. O'Connor M, S.J. Gendler, and J.C. Morris, *In vivo radioiodide imaging and treatment of breast cancer xenografts after MUC1-driven expression of the sodium iodide symporter*. Clin Cancer Res, 2005. **11**(4): p. 1483-9.
111. Vadysirisack, D.D., D.H. Shen, and S.M. Jhiang, *Correlation of Na<sup>+</sup>/I<sup>-</sup> Symporter Expression and Activity: Implications of Na<sup>+</sup>/I<sup>-</sup> Symporter as an Imaging Reporter Gene*. J Nucl Med, 2006. **47**(1): p. 182-190.
112. Marsee, D.K., D.H. Shen, L.R. MacDonald, et al., *Imaging of metastatic pulmonary tumors following NIS gene transfer using single photon emission computed tomography*. Cancer Gene Ther, 2004. **11**(2): p. 121-7.
113. Hasegawa, K., L. Pham, M.K. O'Connor, M.J. Federspiel, S.J. Russell, and K.W. Peng, *Dual therapy of ovarian cancer using measles viruses expressing*

- carcinoembryonic antigen and sodium iodide symporter*. Clin Cancer Res, 2006. **12**(6): p. 1868-75.
114. Petrich, T., L. Quintanilla-Martinez, Z. Korkmaz, et al., *Effective cancer therapy with the alpha-particle emitter [211At]astatine in a mouse model of genetically modified sodium/iodide symporter-expressing tumors*. Clin Cancer Res, 2006. **12**(4): p. 1342-8.
  115. Dwyer, R.M., E.R. Bergert, K. O'Connor M, S.J. Gendler, and J.C. Morris, *Adenovirus-Mediated and Targeted Expression of the Sodium-Iodide Symporter Permits In Vivo Radioiodide Imaging and Therapy of Pancreatic Tumors*. Hum Gene Ther, 2006.
  116. Chen, L., A. Altmann, W. Mier, et al., *Radioiodine therapy of hepatoma using targeted transfer of the human sodium/iodide symporter gene*. J Nucl Med, 2006. **47**(5): p. 854-62.
  117. Niu, G., R.D. Anderson, M.T. Madsen, M.M. Graham, L.W. Oberley, and F.E. Domann, *Dual-expressing adenoviral vectors encoding the sodium iodide symporter for use in noninvasive radiological imaging of therapeutic gene transfer*. Nucl Med Biol, 2006. **33**(3): p. 391-8.
  118. Van Den Bossche, B. and C. Van de Wiele, *Receptor imaging in oncology by means of nuclear medicine: current status*. J Clin Oncol, 2004. **22**(17): p. 3593-607.
  119. Goldenberg, D.M., *Perspectives on oncologic imaging with radiolabeled antibodies*. Cancer, 1997. **80**(12 Suppl): p. 2431-5.
  120. Maloney, D.G., A.J. Grillo-Lopez, C.A. White, et al., *IDEC-C2B8 (Rituximab) anti-CD20 monoclonal antibody therapy in patients with relapsed low-grade non-Hodgkin's lymphoma*. Blood, 1997. **90**(6): p. 2188-95.
  121. Graziano, C., *HER-2 breast assay, linked to Herceptin, wins FDA's okay*. CAP Today, 1998. **12**(10): p. 1, 14-6.
  122. Middleton, G. and D.V. Lapka, *Bevacizumab (Avastin)*. Clin J Oncol Nurs, 2004. **8**(6): p. 666-9.
  123. Ng, M. and D. Cunningham, *Cetuximab (Erbix)--an emerging targeted therapy for epidermal growth factor receptor-expressing tumours*. Int J Clin Pract, 2004. **58**(10): p. 970-6.
  124. Jana, S. and M.D. Blafox, *Nuclear medicine studies of the prostate, testes, and bladder*. Semin Nucl Med, 2006. **36**(1): p. 51-72.
  125. Bander, N.H., *Technology Insight: monoclonal antibody imaging of prostate cancer*. Nat Clin Pract Urol, 2006. **3**(4): p. 216-25.
  126. Rosenthal, S.A., M.K. Haseman, and T.J. Polascik, *Utility of capromab pendetide (ProstaScint) imaging in the management of prostate cancer*. Tech Urol, 2001. **7**(1): p. 27-37.
  127. Breitz, H.B., A. Tyler, M.J. Bjorn, T. Lesley, and P.L. Weiden, *Clinical experience with Tc-99m nofetumomab merpentan (Verluma) radioimmunoscinigraphy*. Clin Nucl Med, 1997. **22**(9): p. 615-20.
  128. Carter, P., *Improving the efficacy of antibody-based cancer therapies*. Nat Rev Cancer, 2001. **1**(2): p. 118-29.

129. Goldenberg, D.M., *Targeted therapy of cancer with radiolabeled antibodies*. J Nucl Med, 2002. **43**(5): p. 693-713.
130. Matzku, S., W. Tilgen, H. Kalthoff, W.H. Schmiegell, and E.B. Brocker, *Dynamics of antibody transport and internalization*. Int J Cancer Suppl, 1988. **2**: p. 11-4.
131. Hsu, K.H., K. Lonberg-Holm, B. Alstein, and R.L. Crowell, *A monoclonal antibody specific for the cellular receptor for the group B coxsackieviruses*. J Virol, 1988. **62**(5): p. 1647-52.
132. Klee, G.G., *Human anti-mouse antibodies*. Arch Pathol Lab Med, 2000. **124**(6): p. 921-3.
133. Hoffman, T., *Anticipating, recognizing, and preventing hazards associated with in vivo use of monoclonal antibodies: special considerations related to human anti-mouse antibodies*. Cancer Res, 1990. **50**(3 Suppl): p. 1049s-1050s.
134. Kashmiri, S.V., R. De Pascalis, N.R. Gonzales, and J. Schlom, *SDR grafting--a new approach to antibody humanization*. Methods, 2005. **36**(1): p. 25-34.
135. Mirick, G.R., B.M. Bradt, S.J. Denardo, and G.L. Denardo, *A review of human anti-globulin antibody (HAGA, HAMA, HACA, HABA) responses to monoclonal antibodies. Not four letter words*. Q J Nucl Med Mol Imaging, 2004. **48**(4): p. 251-7.
136. Aguillon, J.C., J. Contreras, A. Dotte, et al., *[New immunological weapons for medicine in the 21st Century: biological therapy based on the use of the latest generation monoclonal antibodies]*. Rev Med Chil, 2003. **131**(12): p. 1445-53.
137. Wu, A.M. and P.J. Yazaki, *Designer genes: recombinant antibody fragments for biological imaging*. Q J Nucl Med, 2000. **44**(3): p. 268-83.
138. Peehl, D.M., *Primary cell cultures as models of prostate cancer development*. Endocr Relat Cancer, 2005. **12**(1): p. 19-47.
139. Okegawa, T., Y. Li, R.C. Pong, J.M. Bergelson, J. Zhou, and J.T. Hsieh, *The dual impact of coxsackie and adenovirus receptor expression on human prostate cancer gene therapy*. Cancer Res, 2000. **60**(18): p. 5031-6.
140. Kanamaru, H. and O. Yoshida, *Assessment of in vitro lymphokine activated killer (LAK) cell activity against renal cancer cell lines and its suppression by serum factor using crystal violet assay*. Urol Res, 1989. **17**(4): p. 259-64.
141. Kleinman, H.K. and G.R. Martin, *Matrigel: basement membrane matrix with biological activity*. Semin Cancer Biol, 2005. **15**(5): p. 378-86.
142. Wilbur, D.S., *Radiohalogenation of proteins: an overview of radionuclides, labeling methods, and reagents for conjugate labeling*. Bioconjug Chem, 1992. **3**(6): p. 433-70.
143. Hiltunen, J.V., *Search for new and improved radiolabeling methods for monoclonal antibodies. A review of different methods*. Acta Oncol, 1993. **32**(7-8): p. 831-9.
144. Adam, M.J. and D.S. Wilbur, *Radiohalogens for imaging and therapy*. Chem Soc Rev, 2005. **34**(2): p. 153-63.
145. Behr, T.M., M. Gotthardt, W. Becker, and M. Behe, *Radioiodination of monoclonal antibodies, proteins and peptides for diagnosis and therapy. A review*

- of standardized, reliable and safe procedures for clinical grade levels kBq to GBq in the Gottingen/Marburg experience.* Nuklearmedizin, 2002. **41**(2): p. 71-9.
146. Bolton, A.E. and W.M. Hunter, *The labelling of proteins to high specific radioactivities by conjugation to a <sup>125</sup>I-containing acylating agent.* Biochem J, 1973. **133**(3): p. 529-39.
  147. Bailey, G.S., *Labeling of peptides and proteins by radioiodination.* Methods Mol Biol, 1994. **32**: p. 441-8.
  148. Russell, J., J.A. O'Donoghue, R. Finn, et al., *Iodination of annexin V for imaging apoptosis.* J Nucl Med, 2002. **43**(5): p. 671-7.
  149. Hnatowich, D.J., *Recent developments in the radiolabeling of antibodies with iodine, indium, and technetium.* Semin Nucl Med, 1990. **20**(1): p. 80-91.
  150. Liu, C.B., G.Z. Liu, N. Liu, et al., *Radiolabeling morpholinos with <sup>90</sup>Y, <sup>111</sup>In, <sup>188</sup>Re and <sup>99m</sup>Tc.* Nucl Med Biol, 2003. **30**(2): p. 207-14.
  151. Anderson, C.J. and M.J. Welch, *Radiometal-labeled agents (non-technetium) for diagnostic imaging.* Chem Rev, 1999. **99**(9): p. 2219-34.
  152. Novak-Hofer, I., R. Waibel, K. Zimmermann, et al., *Radiometal labeling of antibodies and antibody fragments for imaging and therapy.* Methods Mol Biol, 2004. **248**: p. 481-94.
  153. Krohn, K.A. and A.L. Jansholt, *Radiochemical quality control of short-lived radiopharmaceuticals.* Int J Appl Radiat Isot, 1977. **28**(1-2): p. 213-27.
  154. Lindmo, T., E. Boven, F. Cuttitta, J. Fedorko, and P.A. Bunn, Jr., *Determination of the immunoreactive fraction of radiolabeled monoclonal antibodies by linear extrapolation to binding at infinite antigen excess.* J Immunol Methods, 1984. **72**(1): p. 77-89.
  155. Dux, R., A. Kindler-Rohrborn, K. Lennartz, and M.F. Rajewsky, *Determination of immunoreactive fraction and kinetic parameters of a radiolabeled monoclonal antibody in the absence of antigen excess.* J Immunol Methods, 1991. **144**(2): p. 175-83.
  156. Konishi, S., K. Hamacher, S. Vallabhajosula, et al., *Determination of immunoreactive fraction of radiolabeled monoclonal antibodies: what is an appropriate method?* Cancer Biother Radiopharm, 2004. **19**(6): p. 706-15.
  157. Mattes, M.J., *Determination of antibody immunoreactive fraction.* Cancer Biother Radiopharm, 2004. **19**(6): p. 667-8.
  158. Glatting, G. and S.N. Reske, *Determination of the immunoreactivity of radiolabeled monoclonal antibodies: a theoretical analysis.* Cancer Biother Radiopharm, 2006. **21**(1): p. 15-21.
  159. Yokoyama, K., J.C. Reynolds, C.H. Paik, et al., *Immunoreactivity affects the biodistribution and tumor targeting of radiolabeled anti-P97 Fab fragment.* J Nucl Med, 1990. **31**(2): p. 202-10.
  160. Boskovitz, A., G.H. Akabani, C.N. Pegram, D.D. Bigner, and M.R. Zalutsky, *Human/murine chimeric 81C6 F(ab')(2) fragment: preclinical evaluation of a potential construct for the targeted radiotherapy of malignant glioma.* Nucl Med Biol, 2004. **31**(3): p. 345-55.



161. Wolff, J., I.L. Chaikoff, and et al., *The temporary nature of the inhibitory action of excess iodine on organic iodine synthesis in the normal thyroid*. Endocrinology, 1949. **45**(5): p. 504-13, illust.
162. Lamki, L.M., Y.Z. Patt, and J.L. Murray, *In-111 monoclonal antibody immunoscintigraphy of colorectal cancer*. Cancer Treat Res, 1990. **51**: p. 293-312.
163. Lai, Y.J., R.C. Pong, J.D. McConnell, and J.T. Hsieh, *Surrogate marker for predicting the virus binding of urogenital cancer cells during adenovirus-based gene therapy*. Biotechniques, 2003. **35**(1): p. 186-90, 192-4.
164. Dehecchi, M.C., A. Tamanini, A. Bonizzato, and G. Cabrini, *Heparan sulfate glycosaminoglycans are involved in adenovirus type 5 and 2-host cell interactions*. Virology, 2000. **268**(2): p. 382-90.
165. Dehecchi, M.C., P. Melotti, A. Bonizzato, M. Santacatterina, M. Chilosi, and G. Cabrini, *Heparan sulfate glycosaminoglycans are receptors sufficient to mediate the initial binding of adenovirus types 2 and 5*. J Virol, 2001. **75**(18): p. 8772-80.
166. Boshart, M., F. Weber, G. Jahn, K. Dorsch-Hasler, B. Fleckenstein, and W. Schaffner, *A very strong enhancer is located upstream of an immediate early gene of human cytomegalovirus*. Cell, 1985. **41**(2): p. 521-30.
167. Foecking, M.K. and H. Hofstetter, *Powerful and versatile enhancer-promoter unit for mammalian expression vectors*. Gene, 1986. **45**(1): p. 101-5.
168. Amemiya, Y. and J. Miyahara, *Imaging plate illuminates many fields*. Nature, 1988. **336**(6194): p. 89-90.
169. Zuckier, L.S., O. Dohan, Y. Li, C.J. Chang, N. Carrasco, and E. Dadachova, *Kinetics of perrhenate uptake and comparative biodistribution of perrhenate, pertechnetate, and iodide by NaI symporter-expressing tissues in vivo*. J Nucl Med, 2004. **45**(3): p. 500-7.
170. Dingli, D., E.R. Bergert, Z. Bajzer, K. O'Connor M, S.J. Russell, and J.C. Morris, *Dynamic iodide trapping by tumor cells expressing the thyroidal sodium iodide symporter*. Biochem Biophys Res Commun, 2004. **325**(1): p. 157-66.
171. Dohan, O., A. De la Vieja, V. Paroder, et al., *The sodium/iodide Symporter (NIS): characterization, regulation, and medical significance*. Endocr Rev, 2003. **24**(1): p. 48-77.
172. Ghosh, D., O. Krokhin, M. Antonovici, et al., *Lectin affinity as an approach to the proteomic analysis of membrane glycoproteins*. J Proteome Res, 2004. **3**(4): p. 841-50.
173. Serhan, F., N. Jourdan, S. Saleun, P. Moullier, and G. Duisit, *Characterization of producer cell-dependent restriction of murine leukemia virus replication*. J Virol, 2002. **76**(13): p. 6609-17.
174. Graham, F.L., J. Smiley, W.C. Russell, and R. Nairn, *Characteristics of a human cell line transformed by DNA from human adenovirus type 5*. J Gen Virol, 1977. **36**(1): p. 59-74.
175. McGrory, W.J., D.S. Bautista, and F.L. Graham, *A simple technique for the rescue of early region I mutations into infectious human adenovirus type 5*. Virology, 1988. **163**(2): p. 614-7.

176. Yamanaka, H., K. Ito, S. Naito, et al., *Effectiveness of adjuvant intermittent endocrine therapy following neoadjuvant endocrine therapy and external beam radiation therapy in men with locally advanced prostate cancer*. Prostate, 2005. **63**(1): p. 56-64.
177. Labrie, F., A. Belanger, J. Simard, C. Labrie, and A. Dupont, *Combination therapy for prostate cancer. Endocrine and biologic basis of its choice as new standard first-line therapy*. Cancer, 1993. **71**(3 Suppl): p. 1059-67.
178. Nicholson, B., K. Gulding, M. Conaway, S.R. Wedge, and D. Theodorescu, *Combination antiangiogenic and androgen deprivation therapy for prostate cancer: a promising therapeutic approach*. Clin Cancer Res, 2004. **10**(24): p. 8728-34.
179. Kim, J.J. and I.F. Tannock, *Repopulation of cancer cells during therapy: an important cause of treatment failure*. Nat Rev Cancer, 2005.
180. Li, X., S.P. Raikwar, Y.H. Liu, et al., *Combination therapy of androgen-independent prostate cancer using a prostate restricted replicative adenovirus and a replication-defective adenovirus encoding human endostatin-angiostatin fusion gene*. Mol Cancer Ther, 2006. **5**(3): p. 676-84.
181. Guo, W., H. Zhu, L. Zhang, et al., *Combination effect of oncolytic adenovirotherapy and TRAIL gene therapy in syngeneic murine breast cancer models*. Cancer Gene Ther, 2006. **13**(1): p. 82-90.
182. Nyati, M.K., M.A. Morgan, F.Y. Feng, and T.S. Lawrence, *Integration of EGFR inhibitors with radiochemotherapy*. Nat Rev Cancer, 2006. **6**(11): p. 876-85.
183. Buchsbaum, D.J., T.R. Chaudhuri, and K.R. Zinn, *Radiotargeted gene therapy*. J Nucl Med, 2005. **46 Suppl 1**: p. 179S-86S.
184. Kassis, A.I. and S.J. Adelstein, *Radiobiologic principles in radionuclide therapy*. J Nucl Med, 2005. **46 Suppl 1**: p. 4S-12S.
185. Suit, H.D., *Application of radiobiologic principles to radiation therapy*. Cancer, 1968. **22**(4): p. 809-15.
186. Mulford, D.A., D.A. Scheinberg, and J.G. Jurcic, *The promise of targeted {alpha}-particle therapy*. J Nucl Med, 2005. **46 Suppl 1**: p. 199S-204S.
187. Bruning, A., E. Stickeler, D. Diederich, et al., *Coxsackie and adenovirus receptor promotes adenocarcinoma cell survival and is expressionally activated after transition from preneoplastic precursor lesions to invasive adenocarcinomas*. Clin Cancer Res, 2005. **11**(12): p. 4316-20.
188. Wu, A.M. and P.D. Senter, *Arming antibodies: prospects and challenges for immunoconjugates*. Nat Biotechnol, 2005. **23**(9): p. 1137-46.
189. Iyer, M., L. Wu, M. Carey, Y. Wang, A. Smallwood, and S.S. Gambhir, *Two-step transcriptional amplification as a method for imaging reporter gene expression using weak promoters*. Proc Natl Acad Sci U S A, 2001. **98**(25): p. 14595-600.
190. Yu, Y., A.J. Annala, J.R. Barrio, et al., *Quantification of target gene expression by imaging reporter gene expression in living animals*. Nat Med, 2000. **6**(8): p. 933-7.

191. Cao, F., S. Lin, X. Xie, et al., *In vivo visualization of embryonic stem cell survival, proliferation, and migration after cardiac delivery*. Circulation, 2006. **113**(7): p. 1005-14.
192. Zufferey, R., T. Dull, R.J. Mandel, et al., *Self-inactivating lentivirus vector for safe and efficient in vivo gene delivery*. J Virol, 1998. **72**(12): p. 9873-80.
193. Gomez-Navarro, J. and D.T. Curiel, *Conditionally replicative adenoviral vectors for cancer gene therapy*. Lancet Oncol, 2000. **1**: p. 148-58.
194. Sonabend, A.M., I.V. Ulasov, and M.S. Lesniak, *Conditionally replicative adenoviral vectors for malignant glioma*. Rev Med Virol, 2006. **16**(2): p. 99-115.
195. Rots, M.G., D.T. Curiel, W.R. Gerritsen, and H.J. Haisma, *Targeted cancer gene therapy: the flexibility of adenoviral gene therapy vectors*. J Control Release, 2003. **87**(1-3): p. 159-65.
196. Yang, X., *Imaging of vascular gene therapy*. Radiology, 2003. **228**(1): p. 36-49.
197. Kim, Y.I., J.W. Chung, J.H. Park, J.K. Han, J.W. Hong, and H. Chung, *Intraarterial gene delivery in rabbit hepatic tumors: transfection with nonviral vector by using iodized oil emulsion*. Radiology, 2006. **240**(3): p. 771-7.
198. Reid, T., E. Galanis, J. Abbruzzese, et al., *Intra-arterial administration of a replication-selective adenovirus (dl1520) in patients with colorectal carcinoma metastatic to the liver: a phase I trial*. Gene Ther, 2001. **8**(21): p. 1618-26.
199. Kang, J.H., J.K. Chung, Y.J. Lee, et al., *Establishment of a human hepatocellular carcinoma cell line highly expressing sodium iodide symporter for radionuclide gene therapy*. J Nucl Med, 2004. **45**(9): p. 1571-6.

## **VITAE**

Gang Ren was born in Kunming, Yunnan Province, People's Republic of China, on March 3rd, 1974, the son of Zonghua Ren and Yuqiong Su. After completing his study at Tian Xiang High School, Kunming, Yunnan Province, China in 1991, he entered School of Medicine, Tongji University, Shanghai, China. He received his Medical Degree in June, 1996 and then attended the residency in Department of Radiology, Kunming Railway Hospital. He finished his residency in July, 2001. In August, 2001, he entered the Graduate Program in Radiological Sciences, Graduate School of Biomedical Sciences at the University of Texas Southwestern Medical Center at Dallas. He was awarded the doctoral degree of Philosophy of Science in December, 2006.

Permanent Address: #155 Southwest Forestry College  
Kunming, Yunnan Province 650224  
People's Republic of China